A LABORATORY STUDY OF HORNBLENDE AND TREMOLITE DISSOLUTION RATES

by

Joel Yutaka Narusawa

A Thesis Submitted to the Faculty of the

DEPARTMENT OF HYDROLOGY AND WATER RESOURCES

In Partial Fulfillment of the Requirements
For the Degree of

MASTER OF SCIENCE
WITH A MAJOR IN HYDROLOGY

In the Graduate College

THE UNIVERSITY OF ARIZONA

1 9 9 3

STATEMENT BY AUTHOR

This thesis has been submitted in partial fulfillment of requirements for an advanced degree at the University of Arizona and is deposited in the University Library to be made available to borrowers under rules of the library.

Brief quotations from this thesis are allowable without special permission, provided that accurate acknowledgement of source is made. Requests for permission for extended quotation from or reproduction of this manuscript in whole or in part may be granted by the head of the major department or the Dean of the Graduate College when in his or her judgement the proposed use of the material is in the interests of scholarship. In all other instances, however, permission must be obtained from the author.

SIGNED: 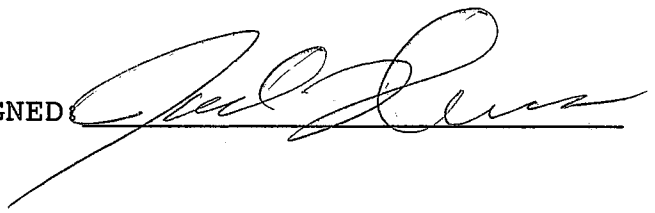

APPROVAL BY THESIS DIRECTOR

This thesis has been approved on the date shown below:

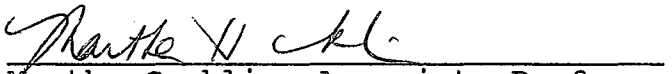

Martha Conklin, Associate Professor
of Hydrology and Water Resources

April 22, 1993
Date

ACKNOWLEDGEMENTS

I wish to thank my parents, without whose help and support this thesis would not have been possible.

I am grateful to Martha Conklin, my advisor, for allowing me the opportunity to do this research and for her patience in guiding me to its end. My thanks also to the other members of my committee, Roger Bales and Randy Bassett (both Associate Professors in the Hydrology Department of The University of Arizona), who took the time to share their knowledge and experience with me. Special thanks to Brent Hiskey (Professor of Material Science, The University of Arizona), Alisa Mast (USGS Water Resources Division, Denver, Colorado), David Braun (Principal Hydrologist, Arizona Department of Environmental Quality), and Tim Corley (Laboratory Supervisor, The University of Arizona) for their help which was invaluable to the progress of my research.

DEDICATION

I would like to dedicate this publication to my family, most notably my brother Leo, who taught me to cherish life and who unknowingly gave me the determination to finish this project.

TABLE OF CONTENTS

TABLE OF CONTENTS--Continued

TABLE OF CONTENTS--Continued

LIST OF ILLUSTRATIONS

LIST OF TABLES

ABSTRACT

Dissolution rates of hornblende and tremolite were studied using flow-through and batch reactor apparatuses to determine the effects of: (1) varying surface area by using different size fractions, < 600, 425-600, and 75-150 m; (2) varying pH (batch reactor: pH 4-6; flow-through reactor: pHs 9, 7, and 6); and (3) introducing organic ligands as 5 mg/l humic substances and 1 mM sodium oxalate at pH 7. No pH dependence of the dissolution rates could be found for either mineral. Organic enhancement was limited to certain cations. Mg or Si appeared to have the slowest release rates for both minerals. Measured weathering rates were very slow; hornblende batch reactor dissolution rates for Si release were 4.54×10^{-12}, 4.84×10^{-12}, and 3.20×10^{-11} mole/(m^2*sec), for pHs 4, 5, and 6 respectively. Dissolution of the < 600 m size range appeared to be adversely affected by the presence of ultra-fines. No correlation could be found between surface area and bulk dissolution rates.

CHAPTER 1

INTRODUCTION

1.1 Introduction

Acidic precipitation in the form of rain and snow can arise as a consequence of industrial combustion which produces acidic aerosols in the atmosphere. This acidity can severely disrupt ecosystems by killing not only fish but plants as well; changes in watersheds in the Adirondacks are such an example (Spencer, 1981). Mineral weathering is one important source of alkalinity in natural waters capable of neutralizing some of this acidic precipitation; the term for this potential is called acid neutralizing capacity (ANC). Mineral weathering and neutralization occurs as a result of an exchange of protons (H^+ ions) from the acidic precipitation with cations on mineral surfaces. This exchange affects the composition of the water that contacts the different minerals involved. These ANC properties are thought to be especially important in areas of sparse soil and vegetation such as alpine watersheds.

This thesis examines the weathering behavior of two minerals, hornblende and tremolite, to evaluate their potential contribution to the neutralization of acidic precipitation in alpine regions. Hornblende was chosen for this study because it is so widespread, while the tremolite allows comparison to results from other researchers.

Mineral weathering is especially important in alpine regions because there is usually little vegetation or other

effective contributors of ANC present. In alpine regions, conditions favor mineral weathering due to steep slopes continuously eroding and exposing new mineral surface, and topsoil usually does not build up more than a few inches deep (Mast and Drever, 1987). The Rocky Mountains of the western United States provide such an example where this weathering occurs. Hornblende is important because it is fairly common in the area and may be an important source of acid neutralizing capacity. To date, it has not been extensively studied. Hornblende can be found in many other places around the world also; in the United States, it can be found throughout California, Idaho, Utah, Colorado, Arizona, South Dakota, Pennsylvania, and New York, to name just a few (Roberts et al., 1974). Hornblende can be found as a constituent in igneous and metamorphic rocks and is an essential component of amphiboles, some schists, and gneisses. Although it is widespread, hornblende's weathering behavior is not well characterized.

1.2 Mineralogy

Tremolite and hornblende are both amphiboles, classified as inosilicates (Table 1.1). Both minerals are of interest, and 90% of the minerals in the Earth's crust are silicates. About 500 silicate minerals have been characterized to date. The silicates, compounds that include Si combined with O_2, make up about 1/3 of all known minerals. Moissanite (SiC),

Table 1.1 Silicates (a partial listing from Blackburn and Dennen, 1988)

A. Tectosilicates (Networks)

B. Phyllosilicates (Sheets)

C. Inosilicates (Chains and Rings)

Double Chains

Amphibole Group
- Anthophyllite
- Cummingtonite Series
- Tremolite Series $Ca_2(Mg,Fe)_5(Si_8O_{22})(OH)_2$
- Hornblende Series $Ca_2(Fe,Mg)_4Al(AlSi_7O_{22})(OH,F)_2$

Single Chains
- Pyroxene Family
- Pyroxenoids

D. Cyclosilicates (Rings)

E. Sorosilicates (Pairs)

F. Nesosilicates (Units)

G. Subsaturates

found in iron meteorites, is the only known case of silicon occurring without oxygen (Kostov, 1968).

Si typically forms a tetrahedral complex with four oxygen atoms, the SiO_4 group, which is the basic component of all silicate minerals. Most silicates incorporate large low-valent cations into their structure; for example, Ca^{2+}, Na^{+}, Mg^{2+}, K^{+}, Mn^{2+}, and Fe^{2+} (Kostov, 1968). These cations substitute for Si in the mineral. The anions can be impurities or substitutes for O_2 in the minerals; examples are OH^{-}, O^{2-}, F^{-}, Cl^{-}, S^{2-}, and can also include complexes such as PO_4^{3-}, SO_4^{2-}, and CO_3^{2-}.

There are six basic subgroups of silicate minerals that are classified primarily by the shapes of their individual tetrahedra. These silica-oxygen tetrahedra can form shapes such as long-extended chains, sheets, and rings (Figure 1.1). The silicate tetrahedra chains can consist of single- or double-chain structures and are called inosilicates (Table 1.1). Pyroxenes are an example of the single-chain type and amphiboles (for example, hornblende) the double-chain type.

The double-chain structures are of concern in this study because they include the amphibole group, of which the minerals hornblende and tremolite are a part. The double-chain structures are formed through the sharing of alternating tetrahedra from single chains. In amphiboles, cations such as Mg and Fe are incorporated into their structures to offset the

charge imbalance due to unsatisfied O_2 ions on the edges of the chains and the occasional substitution of Al^{3+} for Si^{4+}.

The amphibole minerals follow the formula:

$$(X,Y)_{7-8}[Z_4O_{11}]_2(OH)_2$$

where X = Na, K, or Ca; Y = Al, Fe^{3+}, Fe^{2+}, Mg, Mn, Ti, Cr, Li, or Zn (only the first four elements are important); and Z = Si or Al.

Amphiboles are further divided into two subgroups, orthorhombic and monoclinic. Orthorhombic minerals are "lime-free" (no CaO present), and monoclinic minerals are "lime-poor" calciferous and alkaline species. Hornblende and tremolite are both amphiboles of the monoclinic type and have a small amount of iron incorporated into their mineral matrix. This may be a notable characteristic because Siever and Woodford (1979) suggested that iron-rich minerals dissolve more quickly than do structural analogues with little or no iron, but little is known about iron-mineral dissolution mechanisms. Quartz is an example of a highly weather-resistant mineral; in contrast, calcite and dolomite are examples of non-resistant minerals.

Hornblende is a principal mineral found in igneous rocks such as diorites, syenites, and gabbros, as well as in metamorphic rocks such as amphibolites and hornblendic schists. It also occurs in pegmatites and volcanic rocks.

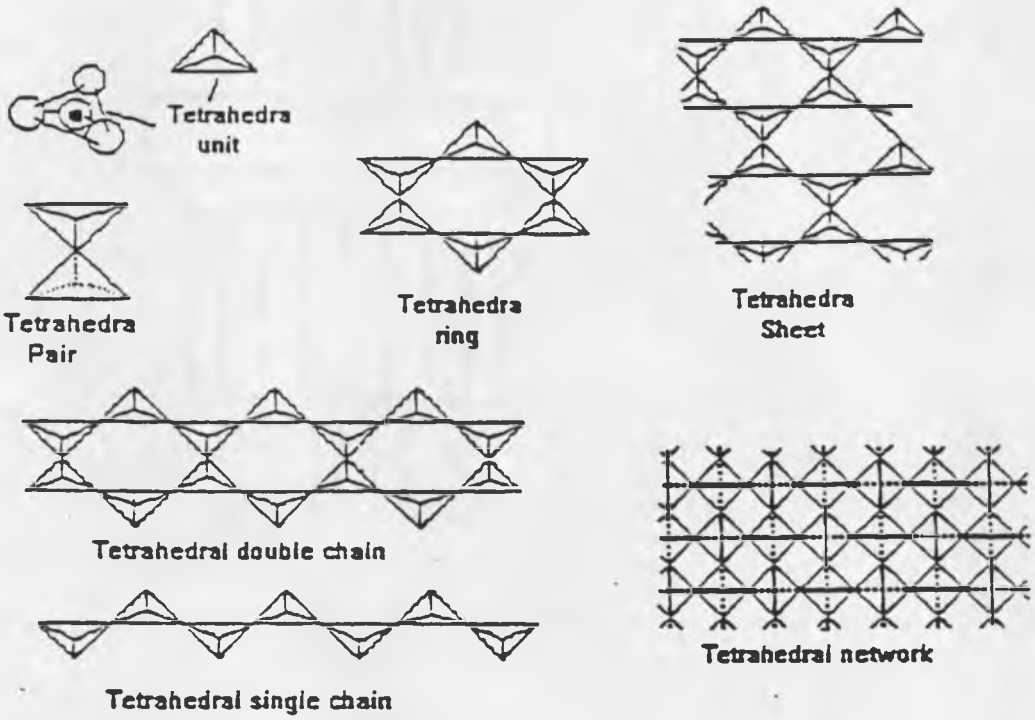

Figure 1.1 Silicate Configurations (adapted from Blackburn and Dennen, 1988)

The name hornblende derives from German and refers to the horn-like appearance of crystals when broken (Kostov, 1968). Common hornblende is a relatively stable mineral; however, under the influence of hydrothermal solutions, it can alter into minerals such as chlorite, epidote, calcite, and quartz. But under weathering conditions, it is converted to nontronite, opal, carbonates, and other minerals.

The mineral tremolite is named after the Tremola Valley (on the southern side of St. Gothard) in the Alps (Blackburn and Dennen, 1988). The fine fibrous varieties of this mineral are called asbestos, although some other amphiboles and fibrous minerals also are known by this name. Tremolites are metasomatic products of calcareous rocks and are also found with many serpentines where they are associated with anthophyllic and talc. The mineral is very similar to hornblende, except it has more Mg and less Al and Fe in its mineral formula, thus making the formation of secondary precipitates during dissolution less likely. In dissolution studies, this is important because the formation of a layer of oxides (Al and Fe) is suspected of negatively biasing bulk dissolution rates by inhibiting transport of ions through this oxide layer to and from the bulk solution.

1.3 Previous Studies

Some of the previous work done in the field of mineral dissolution will be discussed briefly in this section of the

thesis. The choices for the experimental work, such as temperature, pH, size fractions, buffers, etc. used in this study were based on these works.

The largest problem posed in dissolution studies is that mineral dissolution tends to be very slow even in the laboratory. As a result, it can take a great deal of time to sort out the effects of different variables on the dissolution process. Much effort has been put into trying to simplify the variables involved in dissolution studies, a slow-learning process for all involved in both field and laboratory studies. Factors such as seasonal exposure to different aqueous solutions, effective surface area, the effects of oxides, and aqueous solution composition are just a few examples of variables that complicate or mask the effective mineral dissolution rate.

Mineral weathering can be categorized into three types of rate-limiting processes: (1) reactions at the mineral surface; (2) diffusion through an inhibiting layer, which may be a leached or precipitated layer on the mineral surface; and (3) transport limitations to and from the mineral solution interface. Only the first two conditions are considered important at steady state (Drever, 1982).

In order to determine the buffering potential or ANC of minerals in nature, the different mineral dissolution rates must be known. Unfortunately, field estimates of dissolution rates tend to be as little as 0.1% of those derived in the

laboratory (Velbel, 1990). The effects of temperature may be one of the factors responsible for this discrepancy (Velbel, 1990). There is no simple solution to this problem but the reason for doing the laboratory experiments at 25°C in this study was to allow for analogies to work done by other researchers. The temperature at which rate constants are derived can contribute to a bias up to a factor of five for a 9°C temperature differential (e.g., mineral) in measured dissolution rates (Velbel, 1990).

Most previous laboratory dissolution studies have involved the use of batch reactors (BR) and flow-through columns (Chou and Wollast, 1985), but both pose problems for interpretation. The batch reactor method has the problem of concentrations changing with time so that reactor solutions can become saturated. In addition, mineral dissolution may release elements that compete for active mineral surface sites with those of interest in the weathering solutions. Flow-through columns, on the other hand, have the problem of preferential mineral weathering along the length of the column, which influences the aqueous solution concentrations. The variables that can be controlled in both of these experimental apparatuses are pH, temperature, pressure, ionic strength, and Eh. The pH can be fixed by the use of strong acids or buffered solutions. In both apparatuses, the effects of pH and complexation can complicate interpretations if solutions are not buffered. Finally, several studies have

used only aqueous silica concentration as the indicator of bulk mineral dissolution (Chou and Wollast, 1985). For these reasons, this study maintained pH through the use of titrators and buffered solutions, and six major cations were studied (Al, Ca, Fe, Mg, Na, and Si), not just Si.

The reason the BR was used in this study was to extend the work done by Hopkins (1989). The same pH conditions for both hornblende and tremolite were used along with different size fractions, stirrers, and the rates of Al, Ca, Fe, Mg, Na, and Si studied. In her research, Hopkins (1989) found no evidence for an inhibiting layer for either mineral (by use of X-ray diffraction), but she determined that there was non-linear pH dependence with the rate of dissolution being controlled by surface reactions.

Berner et al. (1979) also did laboratory dissolution studies (BR) with tremolite at pH 1 to 6. Their results were similar to Hopkins; they found initial dissolution to be incongruent, with preferential release of Ca and Mg relative to Si. Using X-ray photoelectron spectroscopy (XPS), they also found that there was evidence of a leached surface layer a few angstroms thick.

Chou and Wollast (1985) were among the pioneers in the use of flow-through bed reactors (FR). Such apparatuses have the advantage that mineral grains are suspended in a cone-shaped reactor. An aqueous solution is then allowed to percolate up through the mineral reactor in a semi-closed

system. The system is semi-closed due to fresh and old solutions being pumped in and out of the system at a balanced steady rate. Percolating solution up through the mineral eliminates the problem of preferential mineral weathering as encountered in flow-through columns. In addition, saturated conditions can also be prevented (Al and Fe oxides), thus avoiding secondary precipitation problems by use of fresh input and output solutions.

A great deal of information has accumulated over the years, indicating that organic ligands, such as natural organic matter, can enhance the dissolution of metal ions (Kittrick, 1986; Rashid and Leonard, 1973; Zinder et al., 1986). By doing so, the bulk dissolution rate in nature may be approximated. Part of this study attempted to determine if a rate-limiting element existed for hornblende or tremolite at the pH studied, and organic ligand enhancement was also attempted by the use of flow-through reactors (FR). This was done in separate experiments with hornblende and tremolite for pH's 9, 7, and 6, in which the influence of change in pH and exposure to organic ligands were examined. These results were to be compared to that of Mast and Drever (1987). In their experiments, Mast used a flow-through bed reactor (FR) apparatus to study the weathering of oligoclase and anthophyllite by varying pH and organic ligand exposure. She found no evidence of enhancement due to oxalate exposure and found that

the rate of dissolution of anthophyllite varied independently of pH, for the pH range from 2 to 5.

Exchange or dissolving mechanisms in nature are regulated by many factors (Velbel, 1990; Petrovich, 1981), many of which are still poorly understood. Transport of ions to and from the mineral surface to the bulk solution may be controlled by such factors as fluid flow in the interstitial pore spaces and the degree of solution saturation (Velbel, 1990). There are also limitations at the mineral surface, such as areas of preferential dissolution (for example, etch pits and micro-fractures and possible leached layers) through which ions moving to and from the bulk mineral must pass. Several years ago, many scientists (Siever and Woodford, 1979; Eggleton and Boland, 1982) proposed that the dissolution of iron-bearing silicates formed an inhibiting protective surface layer, but recent work does not seem to support this hypothesis (Hopkins, 1989; De Kimpe, et al., 1989; Berner and Schott, 1982).

Surface area effects are considered to be important in dissolution experiments because errors in the estimation of effective surface area can represent differences in laboratory and field rates of several orders of magnitude (Drever and Swoboda-Colberg, 1989 and 1992; Velbel 1990). For this reason, the effects of different size fractions were examined in this study.

Previous studies involving the grinding of mineral particles examined the effects of varying particle surface/-

mass ratios (Holdren and Speyer, 1985; Cremeens et al., 1988). The general conclusion has been that there seems to be a threshold below which grinding has no effect. This is due to the size of grains eventually approaching the size of surface defects (Petrovich, 1981; Holdren and Speyer, 1985; Velbel, 1990). Holdren and Speyer (1985) and Berner and Schott (1982) found that reaction rates vary with grain size for sufficiently large grain sizes; grain size, in turn, is related to the density of active weathering sites per surface area. These surface sites were confirmed in early studies by researchers such as Berner et al. (1979) and Kittrick (1986) by the use of instruments such as the scanning electron microscope (SEM). These studies have been followed up more recently by Cremeens et al. (1988), who examined methods to quantify effective surface area by techniques such as digital image analysis.

Other studies have implicated rate-limiting elements, such as Al and Fe, that can regulate the release of species from the mineral surface, thus restricting the rate at which other elements can be released from the mineral (Berner et al., 1979; Chou and Wollast, 1985).

1.4 Objectives of Study

This study seeks to further the knowledge of dissolution of hornblende and tremolite with regard to factors such as:

(1) Surface area effects, by varying size fractions;

(2) pH, by changing pH and noting its effects on the release rate of six major cations, Al, Ca, Fe, Mg, Na, and Si; and

(3) Enhancement due to the introduction of organic ligands such as oxalate and humic substances because it is common knowledge that organic ligands act as chelators in transport and distribution of metals such as Al and Fe in natural waters.

These variables were chosen because previous studies have shown that they all have potential to influence overall mineral dissolution rates, whereas the tremolite was used to provide an analogy to previous dissolution work done by Hopkins (1989) and Mast and Drever (1987).

CHAPTER 2

EXPERIMENTAL METHODS

2.1 Cleaning Methods

In this study, part per billion (ppb) concentrations (Al, Ca, Fe, Mg, Na, and Si) were routinely analyzed; hence, it was important that no contamination occurred. All plastic and glassware used were washed with Alconox soap, then rinsed well with Milli-Q (water cleaned by a Millipore ion-exchange system), followed by an acid bath (4 M HNO_3) for at least three hours. This was then followed by rinsing at least three times with Milli-Q and oven dried at 100°C.

2.1.1 Reagents and Standards

Standards for Al, Ca, Fe, Na, Mg, and Si used to calibrate the analytical instruments were made from 1000 mg/L Atomic Absorption Spectroscopy (AAS) stock solutions obtained from Alfa Chemicals. In addition, only American Chemical Society (ACS) reagent grade or better chemicals were used in this study. The standards were prepared as serial dilutions using class A glassware and calibrated Eppendorf Tip Ejector Microliter Pipetters. All standard dilutions were made with 1% nitric acid (HNO_3) to appropriate concentrations, except for Al. In this case, Milli-Q was used to prepare Al standards due to 1% ultra-pure (for metals) hydrochloric acid (HCl) having too high a background absorbance value when

running flow-through reactor (FR) samples for Al (by the UV-VIS method).

2.1.2 Flame Analysis

A Perkin Elmer 3100 Atomic Absorption Spectrometer (AAS) was used to quantify aqueous concentrations of Ca, Fe, Na, and Mg. The actual detection limits observed were greater than those cited in the operator's manual. Ca was cited to have a detection limit of 2 ppb, but was found to have an actual detection limit of 4 or 5 ppb. Fe was cited as having a detection limit of 4 ppb, but the actual detection limit was about 10 ppb. Mg was cited as having a detection limit of 0.01 ppb, but the actual detection limit was about 2 ppb; Na was cited as 0.2 ppb, but it was 50 ppb.

After running standards and several samples on a Perkin Elmer 3100, a Varian 375, a Varian 1475, and a Thermo Jarrel Ash AAS, it was found that the Perkin Elmer 3100 AAS performed as well, if not better than the other three instruments. It was also found that Ca was not a good standard to use when optimizing the burner and flame height for the Flame AA. Mg performed much better and yielded lower detection limit and less background noise.

2.1.3 Graphite Furnace Analysis

The Al, Si, and Fe analyses were attempted on a Perkin Elmer HGA-600 graphite furnace. The sample introduction was

done by hand and had such poor precision and accuracy that it was not used.

2.1.4 Spectrophotometric Analysis

A computer-controlled Shimadzu UV-2101PC UV-VIS Scanning Spectrophotometer and Beckman Spectrophotometer were used to analyze Al and Si. The analyses for Al and Si used the eriochrome cyanine R and heteropoly blue methods, respectively, as outlined in Standard Methods (Franson, 1985). Colorimetric analysis of Fe analysis was also attempted using the phenanthroline method (Franson, 1985), but was not sensitive enough for the concentrations that were being quantified. The observed detection limits for Al, Fe, and Si were 6, 50, and 50 ppb, respectively.

The Al colorimetric analysis presented a potential for negative bias when running samples with organic ligands present, such as in the FR experiments. This is due to competition of organic ligands and colorimetric reagents for aqueous Al species (Sposito, 1989), although none could be detected.

2.2 Mineral Characterization

Mineral characterization and preparation consisted of four steps: grinding/sieving, cleaning, microprobe analysis, and surface area analysis of mineral.

2.2.1 Grinding of Hornblende

The hornblende and tremolite samples used in this study were obtained from Ward's Natural Science Company. The tremolite was left over from a previous experiment (Hopkins, 1989) and did not need to be ground. It was prepared as was the hornblende, except where noted.

The hornblende came originally from the Faraday formation in Ontario, Canada. Hornblende is an amphibole containing many impurities such as quartz, olivine, and secondary iron oxide precipitates along the outer surface. The initial mineral preparation involved rinsing with Milli-Q and oven drying samples at 100°C for several hours. The mineral was then ground using a Braun Pulverizer type UA, manufactured by the Braun Corporation, Los Angeles, California. The grinder, plates, hopper, etc. were taken apart before and after grinding and cleaned with a sponge and water to reduce the possibility of sample contamination.

2.2.2 Cleaning of Mineral

After the initial grinding, the hornblende sample was visually sorted to remove any foreign matter using an American Optical Company Light and Stereoscope (X10). It was not possible to sort the tremolite sample for such inclusions as quartz, which is visually indistinguishable from tremolite.

In general, contaminant particles greater than 0.5 mm in diameter were removed. The samples were then separated into

three size fractions, U.S. Standard Sieve Series #30-40 (425-600 m dia.), #100-200 (75-150 m), and >#30 (< 600 m). The screens were also wire brushed before and after sieving and rinsed with distilled water to prevent sample contamination. At this time, the #30-40 size fraction was again visually sorted. The #100-200 size fraction was not sorted because it was too fine and would have taken too long a period of time to clean. It is also doubtful that the impurities, mainly quartz, would bias results (Mast and Drever, 1987). Finally, both size fractions were ultrasonically cleaned using Milli-Q as a solvent, for about half an hour, and oven dried at 100°C for several hours.

2.2.3 Microprobe Analysis

Prior to the microprobe analysis, the minerals had to be prepared. This was done by embedding the hornblende and tremolite mineral grains in 3.175 cm diameter epoxy plugs. A 1:6 ratio of Buehler Epoxide Hardener (20-8132-032) and Buehler Epoxide Resin (20-8130-128) was used. This was allowed to harden for eight hours, after which the epoxy plug mineral surface was exposed and ground flat using a Buehler Ecomet3 Variable Speed Grinder-Polisher and #600 Silica Carbide paper at a speed setting of 90 rpm. This step was followed by polishing with a Texmet cloth using a 5 m aluminum grinding compound and a speed of 130 rpm, which removed most of the grooves in the epoxy created in the first

step. A final polishing was then done with Mastermet cloth using 0.06 m silica compound and a speed of 130 rpm.

The microprobe analysis was done at the Space Science Center of The University of Arizona using a CAMECA SX-50. Prior to the microprobe examination, the sample mineral surface was lightly coated with carbon using a modified Varian/Vacuum Evaporator VE10; the sample sides were painted with colloidal carbon to help dissipate electrons generated from the sample surface by the X-ray beam.

The CAMECA SX-50 can focus its energizing beam down to a one to two micron diameter spot on the sample surface. The elemental weight fraction obtained is accurate to $\pm$1% at concentrations of 10-100 ppm. The standardization of the instrument for hornblende was done with a Sn-36 hornblende (Kakanui) standard. Twenty points on the sample were analyzed (three replicates were done at each point); ten each for the two size fractions of interest, #30-40 and #100-200. The results of the microprobe analysis are presented in Table 2.1. This technique was also used by Hopkins (1989) for hornblende and these are also included in Table 2.1.

The tremolite microprobe analysis was done with multiple standards: diopsite (Mg and Si); albite (Na); anorthite (Al and Ca); K-feldspar (K); rhodolite (Mn); and fayalite (Fe), because the tremolite standard turned out to be dolomite instead. Only the tremolite #100-200 size fraction was analyzed, using 20 points on the mineral surface (Table 2.2).

Table 2.1 Chemical Analysis And Surface Area Measurements of Hornblende Samples

Mineral		Hopkins (1989)		This study	
Chemical composition (% weight)	Na_2O	5.19	Na_2O	5.01	
	K_2O	1.70	K_2O	1.59	
	CaO	7.26	CaO	7.62	
	Al_2O_3	1.25	Al_2O_3		1.47
	SiO_2	56.58	SiO_2	55.91	
	MgO	20.23	MgO	20.43	
	MnO	0.36	MnO	-	
	FeO	6.16	FeO	5.87	
	TiO_2	0.24	TiO_2	0.19	
Total		98.97		98.09	
Surface Area[1]	>#30	0.409 m^2/g	#30-40	1.830 m^2/g	
			#100-200	1.278 m^2/g	
Specific Surface Area[2] (calculated)			#30-40	0.004 m^2/g	
			#100-200	0.017 m^2/g	

[1] No ultra-fines present in the #30-40 and #100-200 size fractions. These samples were ultrasonically cleaned.

[2] specific area = 6/(density*mean diameter)

Table 2.2 Chemical Analysis And Surface Area Measurements of Tremolite Samples

Mineral	Anthophyllite (Mast and Drever,1987)		This study	
Chemical composition (% by weight)	SiO_2	60.60	SiO_2	58.71
0.14	Al_2O_3	0.13	Al_2O_3	
	FeO	0.17	FeO	0.19
	Na_2O	0.16	Na_2O	0.52
	CaO	0.55	CaO	12.20
	MnO	3.78	MnO	0.46
	MgO	32.38	MgO	25.58
Total		97.77		97.90
Surface Area[1]	#100-200	0.057 m^2/g	#100-200	0.041 m^2/g

[1] specific area = 6/(density*mean diameter)

For comparison, results of Mast and Drever (1987) for anthophyllite are also given in Table 2.2.

An energy dispersive X-ray spectroscopy (EDXRF) analysis was later done with a TRACOR X-Ray Fluorescence Spectrophotometer model 5050 (at the Chemistry Department of The University of Arizona) in an attempt to establish the existence of a leached layer. Several hornblende samples, both freshly ground and leached mineral, were analyzed, but the results proved to be inconclusive.

2.2.4 Bet Analysis

A Brunauer-Emmett-Teller (BET) analysis was done on hornblende (#30-40 and #100-200) and tremolite (#100-200) samples to determine surface area (m^2/g) with a Micrometrics Accelerated Surface Area and Porosimetry 2000 System (ASAP 2000) at the Copper Center of The University of Arizona. The results are presented in Tables 2.1 and 2.2. The analysis is based on the amount of gas that sorbs to form a monolayer onto a solid surface. The instrument does this by measuring the change in thermal conductivity of a mixture of a sorbate gas and an inert carrier gas, usually nitrogen and helium.

The #30-40 size fraction of hornblende had a larger surface area per mass (m^2/g) than did the #100-200 size fraction, quite opposite to what was expected. This discrepancy may be due to micro-fractures in the mineral grains. It is not uncommon for minerals of this type to have micro-

fractures (Hiskey, personal communication, 1992). Assuming a perfect sphere with no micro-fractures, specific surface area (m^2/g) for the two size fractions, #30-40 and #100-200, should be about 0.2% of those obtained experimentally (Table 2.1), thus illustrating that micro-fractures do contribute significantly to the surface area.

2.3 Experiments

Dissolution experiments using hornblende and tremolite were carried out using both a batch reactor (BR) and a flow-through reactor (FR). The hornblende BR experiments were carried out at pHs 4 to 6, while the hornblende and tremolite FR experiments were carried out at pHs 9, 7, and 6. Both types of experiments were carried out at one common pH, pH 6. The pH values were chosen to correspond with that used by Hopkins (1989) and Mast and Drever (1987) and are in the range found in natural waters. Tremolite BR experiments were only carried out at pHs 4 and 6.

Two different methods for calculating aqueous concentrations were used (Table 2.3). The methods involved using different time and volume parameters for the BR and FR experiments. Total elapsed time and BR volume were used for the BR experiments, whereas elapsed time between samples and sample volume were used for the FR. The different approach for calculating aqueous concentrations was due to the inherent properties of each experimental apparatus. The BR volume

Table 2.3 Sample Calculations

Sample#	Time[A] (hr)	Volume[B] (ml)	Ca[C] (mg/l)	moles[D]	mole[E] m^2	mole[F] (m^2*sec)
1	10.00	5.0	4.65	$5.80x10^{-7}$	$5.67x10^{-7}$	$1.58x10^{-11}$

Notes

A Data from PHSTAT output
Total elapsed time (ET) of experiment for BR
Elapsed time between sampling (ST) for FR

B Previous volume - volume of sample removed
(for BR experiments)

or

Volume of each daily sample (for FR experiments)

C Analytical data

D C mg/L*(g/1000mg)*(1/molecular wt)*B mg/L*(L/1000ml) = moles

E D moles*(g/m^2)*(1/g mineral in reactor) = mole/m^2

F mole/m^2 * 1/ET * (hr/3600 sec) = mole/(m^2*sec)
(for BR experiment)

or

mole/m^2 * 1/ST * (hr/3600 sec) = mole/(m^2*sec)
(for FR experiment)

SAMPLE CALCULATIONS for FR

D $(4.65mg/l)*\left(\frac{g}{1000mg}\right)*\left(\frac{mole}{40.078g}\right)*(5ml)*(L/1000ml) = 5.80x10^{-7}$ mole

E $(mole)*(g/.409m^2)/(2.5g) = 5.67x10^{-7}$ mole/(m^2)

F $\left(\frac{5.67\ x10^{-7}\ mole/m^2}{10\ hr}\right)*\left(\frac{hr}{3600\ sec}\right) = 1.58x10^{-11}$ mole/(m^2*sec)

decreases with each sample that is extracted, and the aqueous concentrations in the reactor change with time because it is a closed system. The FR volume, however, remains more or less constant, although the aqueous solution concentrations may change with time.

2.3.1 Batch Reactor

Twenty-seven dissolution experiments were done with the BR using the setup represented in Figure 2.1. The approach used here is a modification of that used by Hopkins (1989). This system consisted of a 500 ml beaker with a water jacket, which maintained an environmental temperature of approximately 25°C; a mixer, a Nuova II stir plate and a CAFRAMO stirrer type RZR1 (at the lowest setting) were used; a computer, IBM compatible and an Apple compatible, which used a PHSTAT program to monitor and maintain a set pH; an acid titrator, a modified motorized Gilmont digital syringe (2.5 ml) and a Metrohm 665 Dosimat; and a Fisher Accumet 925 pH meter. Several BR experiments were carried out to compare the Dosimat and Gilmont titrators; no difference could be detected. In addition, all BR experiments were done under a nitrogen atmosphere to minimize formation of Fe (III) precipitate on the mineral surface which might have complicated interpretation of data.

2.3.1.1 Batch reactor (BR) methods. Approximately 2.5 g of hornblende was added to 250 ml of 0.1 M KNO_3 for each BR

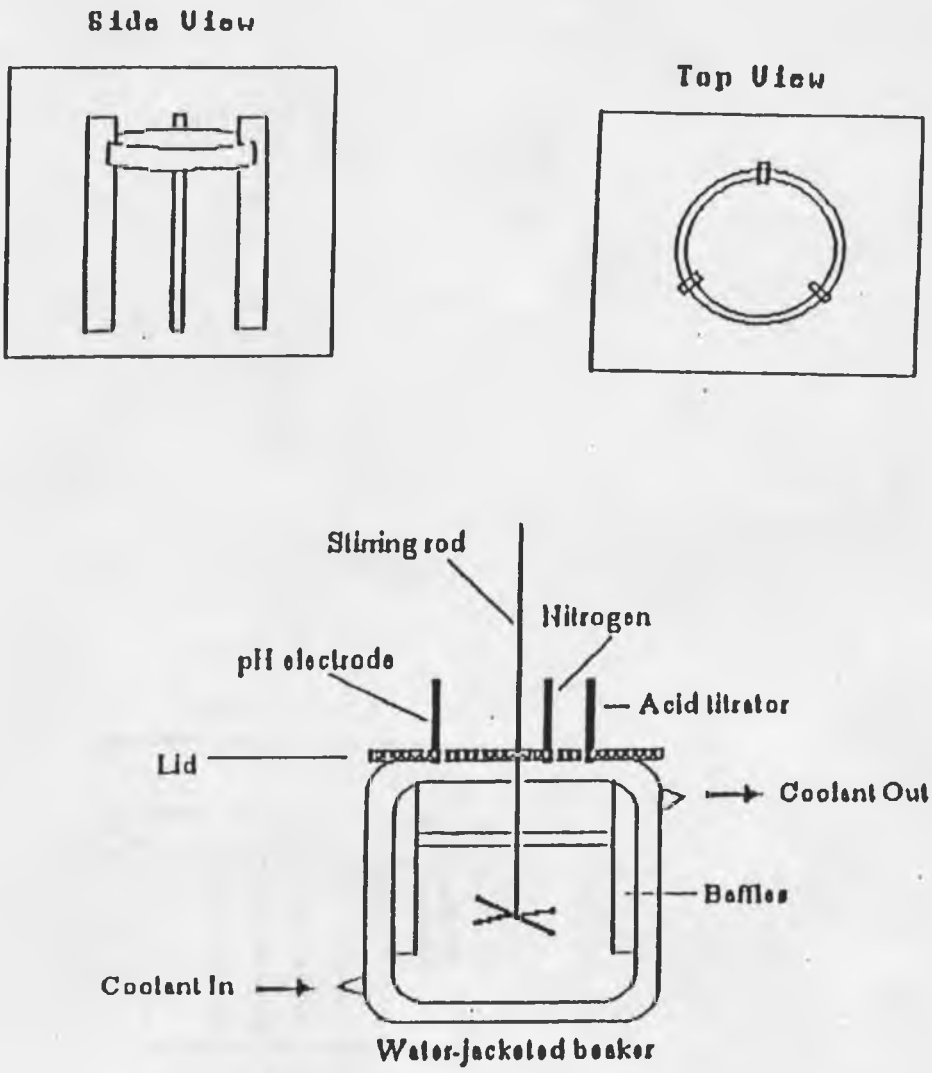

Figure 2.1 Batch reactor illustration

experiment, each of which ran 60-140 hr. Separate experiments were done at pHs 4, 5, and 6 with pH maintained by titrating with 0.1 M and 0.01 M HCl. Each sample (5-7 ml) was periodically removed from the reactor using a plastic syringe, which was rinsed with Milli-Q after each use. It was assumed that the solid-to-liquid ratio remained constant throughout the experiment. The samples were then filtered directly into sample bottles through 0.45 μm Millipore acetate filters that were changed, and the filter holders were acid-washed after each sample was taken. The filtered samples were acidified to pH $\leq$1 with 4 M HNO_3 and refrigerated until the analysis could be done.

Two BR calibration experiments were run to check for transport limitations; one used a stir plate, the other a drill type mixer. It was found that the stir plate could not agitate the solution sufficiently to eliminate transport limitations. The drill mixer, however, did not interfere with transport at any speed.

2.3.1.2 Gilmont versus Dosimat. Two titrators were used during the course of this study due to mechanical problems with the Gilmont titrator. During this period (BR 11-16), it was found that the Dosimat leaked acid. The problem was addressed with five possible solutions by: (1) diluting the titrant two orders of magnitude, 0.1 M HCl to 0.001 M HCl; (2) trying smaller diameter titrant tubing; (3) adding base; (4) changing the elevation of the titrator with respect to the

reactor; and (5) finally, removing the titrator tube from the reactor vessel for varying periods of time. However, none of these solutions worked well. It was later found that there is an anti-diffusion tip available from Metrohm which helps remedy this problem.

2.3.2 Flow-Through Reactor (FR)

The FR experimental setup used was as shown in Figure 2.2. The components of the system were the flow-through reactor, a slow pump, a fast pump, tubing, and a Fisher Accumet 665 pH meter to monitor and adjust outflow and inflow solutions. The mineral was placed into the reactor cone, and fluid volume in the reactor was maintained at 25 ml. This was accomplished by calibrating both pumps to the correct flow rates; a three-way valve was used to reduce the reservoir level when needed.

Two FR experiments were done, one using hornblende (FRH) and the other using tremolite (FRT). Both experiments were run for 78 days each, changing pH from 9 to 7, and then to 6. Organic ligands were introduced to the FR for two periods at pH 7. 1 mM sodium oxalate was used in the FRH experiment, and 5 ppm (as calculated from total carbon) humic substances (HS) extracted from Orange County groundwater (Mariner, 1991) was used in the FRT experiment. Samples were taken daily with volume and pH for both inflow and outflow solutions recorded.

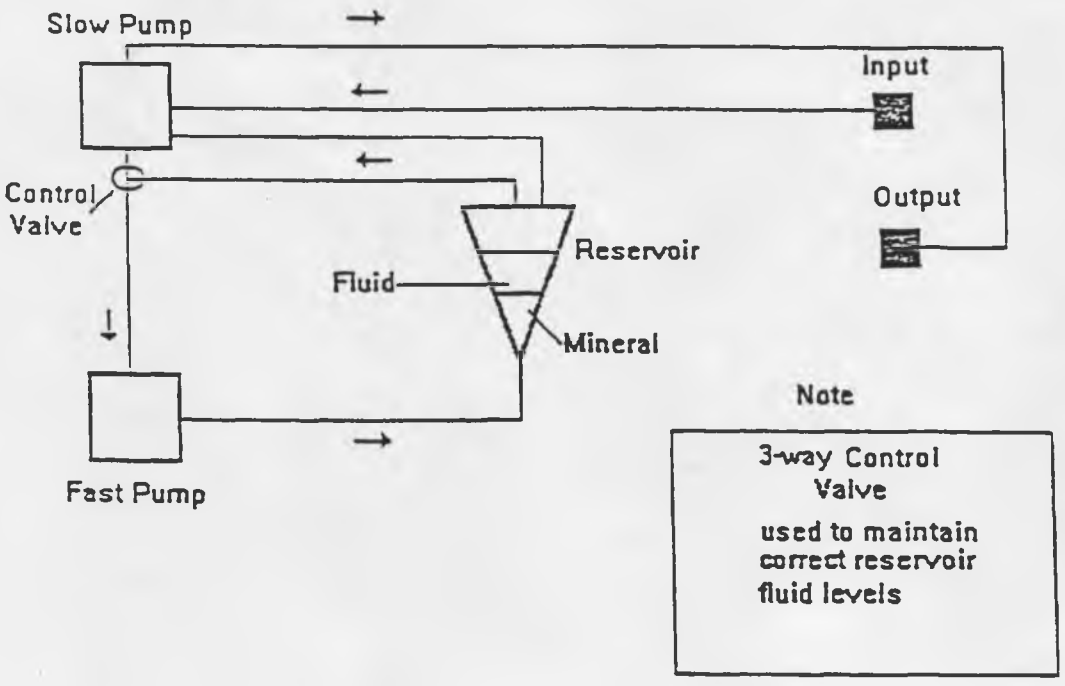

Figure 2.2 Flow-through bed reactor illustration

During the length of the experiments, nitrogen was bubbled through the input solution.

2.3.2.1 Flow-through reactor components. A Rainin Rabbit peristaltic pump calibrated to yield approximately 0.2 ml/min regulated flow into and out of the system to prevent saturated solutions. A Cole-Parmer Masterflex peristaltic pump calibrated to yield 2 ml/min simulated groundwater flow through a porous medium. #13 Cole-Parmer Norprene tubing (L-06485-13) and Rabbit polyvinyl chloride tubing (#39-621 0.38 ID) were used for pump leads; Teflon® tubing was used for the rest of the system. The Cole-Parmer tubing was found to last longer.

2.3.2.2 Flow-through reactor (FR) methods. The FR experiments were run using three different buffers to aid in maintaining pH; 5 mM 4-morpholine ethane sulfonic acid (MES) for solutions at pH 6, 5 mM 4-(2-hydroxyethyl)-1 piperazine ethane sulfonic acid (HEPES) for pH 7, and 5 mM boric acid for pH 9. In addition, two microbial inhibitors were used to eliminate the possibility of mineral degradation due to microbial activity, sodium azide (1 mM and 5 mM) for FRH and 1 mM potassium cyanide (KCN) FRT. All inflow solutions were under nitrogen atmosphere.

No background concentrations (all cations) of input solutions were measured during the course of both FR experiments. This has the potential to introduce experimental bias to the results. Factors such as precipitation, sorption, and differences in input solution background concentrations can

vary from batch to batch. Eight sets, with three replicates each, of blank solutions were run after the experiments were finished to check for the magnitude of introduced bias (Table 2.4). After correcting the data with mean blank concentrations, some exhibited negative values (FRH Fe and Si; FRT Ca, Fe, and Si), thus suggesting that the blanks represent an upper limit. The use of blanks did not change any of the experimental trends for the cations studied. Because of this, all data used here are not corrected with blanks to allow the data to be represented consistently and to permit the use of RRR curves. Mg was the only cation which did not have any change in background concentration due to blank corrections.

2.3.2.3 Flow-through reactor pump lead problems. The pump leads posed some problems in that they had to be replaced about every week. As a result, it was difficult to calibrate both inflow and outflow rates to maintain exactly 25 ml in the FR for the duration of the experiment. The effects could be seen for several samples after the problem was resolved as stray peaks. The biased sample points were not included in the rate calculations for this study.

Table 2.4. Average Flow-Through Reactor Blank Solutions (mg/l)

Set of Blanks	Blank Solutions[1] Al	Ca	Fe	Mg	Na	Si
1	5 mM MES + 1 mM Na Azide					
Mean	0.0302	0.000	0.005	0.000	--	0.046
2	5 mM MES + 1 mM Na Azide + 1 mM Na Oxalate					
Mean	0.0289	0.030	0.021	0.000	--	0.026
3	5 mM MES + 5 ppm HS + 1 mM KCN					
Mean	0.0258	0.010	0.263	0.000	0.19	0.117
4	5 mM MES + 1 mM KCN					
Mean	0.0284	0.000	0.014	0.000	0.19	0.029
5	5 mM HEPES + 1 mM KCN					
Mean	0.0167	0.030	0.001	0.000	0.18	0.018
6	5 mM HEPES + 1 mM Na Azide					
Mean	0.0204	0.010	0.000	0.000	--	0.017
7	5 mM Boric Acid + 1 mM KCN					
Mean	0.0145	0.010	0.010	0.000	0.17	0.035
8	5 mM Boric Acid+ 1 mM Na Azide					
Mean	0.0210	0.010	0.010	0.000	--	0.024

[1] FRH blank solutions = #1, 2, 6, 8
FRT blank solutions = #3, 4, 5, 7

CHAPTER 3

RESULTS

This chapter presents the results of the study in three sections. The first section (3.1) deals with the batch reactor results. The second section (3.2) then presents flow-through reactor results which is followed by the third section (3.3) dealing with chemical equilibrium model results.

3.1 Batch Reactor (BR)

Twenty-seven batch experiments (BR) were run at pHs 4 to 6 with both hornblende (BRH) and tremolite (BRT). The experiments differed in: (1) mixing method and speed, (2) mineral size fraction, (3) mass of mineral added to the reactor, (4) titrating device, and (5) length of experiment. The BR experiment schedule is shown in Table 3.1. BRH acid consumption rates and dissolution rates for Al, Ca, Fe, Mg, Na, and Si (mole/(m^2*sec)) using three mineral size ranges were studied. The dissolution rates for all of the cations studied appeared linear after 20-40 hr. After this time, rate calculations were made using the linear portion of each curve to accurately represent the behavior of each cation.

Early in this study, it was found that the stir plate method used by Hopkins (1989) did not agitate the solution sufficiently to reduce the diffuse layer enough to eliminate transport limitations (this issue is discussed in Section 3.1.1). In addition, experimental data for BR acid consump-

Table 3.1 Batch Reactor Experiment Schedule[1,2]

Experiment#	Size	Comments	pH	Titrator
1	> #30	Aborted	6	Gilmont
2	> #30	Hornblende + stir plate	6	Gilmont
3	> #30	Hornblende + stir plate/ calibration	6	Gilmont
4	> #30	Hornblende + mixer	6	Gilmont
5	> #30	Hornblende + mixer/calibration	6	Gilmont
6	> #30	Hornblende	4	Gilmont
7	> #30	Hornblende	4	Gilmont
8	> #30	Hornblende	5	Gilmont
9	> #30	Hornblende	5	Gilmont
10	> #30	Hornblende	6	Gilmont
11	#30-40	Hornblende	4	Dosimat
12	#30-40	Hornblende	5	Dosimat
13	#30-40	Hornblende	6	Dosimat
14	#100-200	Hornblende	4	Dosimat
15	#100-200	Hornblende	5	Dosimat
16	#100-200	Hornblende	6	Dosimat
17	#100-200	Aborted	5	Gilmont
18	#100-200	Tremolite	6	Gilmont
19	#30-40	Hornblende	4	Gilmont
20	#100-200	Hornblende	4	Gilmont
21	#100-200	Hornblende	5	Gilmont
22	#100-200	Hornblende	5	Gilmont
23	#100-200	Hornblende	6	Gilmont
24	_	Blank to check ionic strength	3.5	Gilmont
25	#100-200	Tremolite	4	Gilmont
26	#100-200	Tremolite	4	Gilmont
27	#100-200	Tremolite	4	Gilmont

[1] All experiments $\geq$ #6 were done with drill mixer

[2] BR experiments #3,5,11,12,14,15 and 16 were not used in the data analysis due to problems

tion rates and cation release rates were screened using the t-distribution method for data analysis with 90% confidence intervals (CI); the experiments used are indicated in Table 3.1.

3.1.1 Hornblende Batch Reactor (BRH) Acid Consumption Rates

No linear pH dependence of mineral dissolution rate could be demonstrated for the hornblende BR experiments at the pH studied, pHs 4 to 6. Figures 3.1 and 3.2 and Table 3.2 illustrate the acid consumption rates (moles of H^+/m^2 versus time) for hornblende at pHs 4, 5, and 6 (at 25°C under nitrogen atmosphere). In each figure, multiple experiments are plotted in which two distinct trends can be seen. One depicts an initial high nonlinear dissolution rate which is followed by a more gradual linear dissolution rate (after about 20-30 hr). The second group of data exhibits linear dissolution on the scale used.

The general effects of all the variables used in the BRH experiments are illustrated in Figure 3.2. The two groupings of experimental data are apparent and are associated with different size fractions, the > #30 (BR# 2, 4, 10) group and a group for #100-200 and #30-40 (BR# 13, 23). The rapid initial acid consumption rate for the > #30 size fraction appears to be due to initial dissolving of ultra-fine particles; the > #30 sample did not have the ultra-fines removed. After this early period, the rates of acid consumption for >

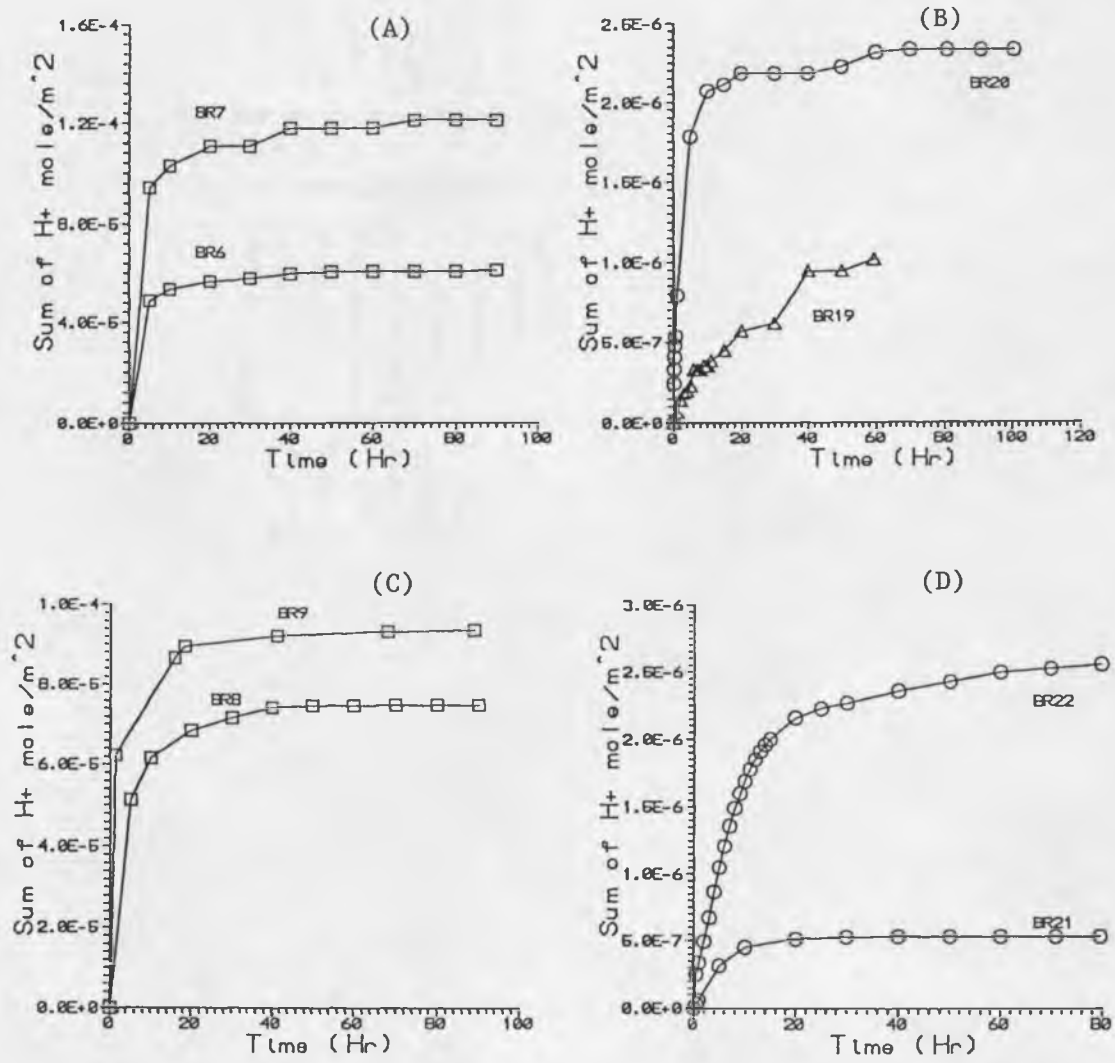

Figure 3.1 Hornblende batch reactor experiment acid consumption rates for pH 4 (A and B) and pH 5 (C and D) (□=>#30, ▲=#30-40, ○=#100-200)

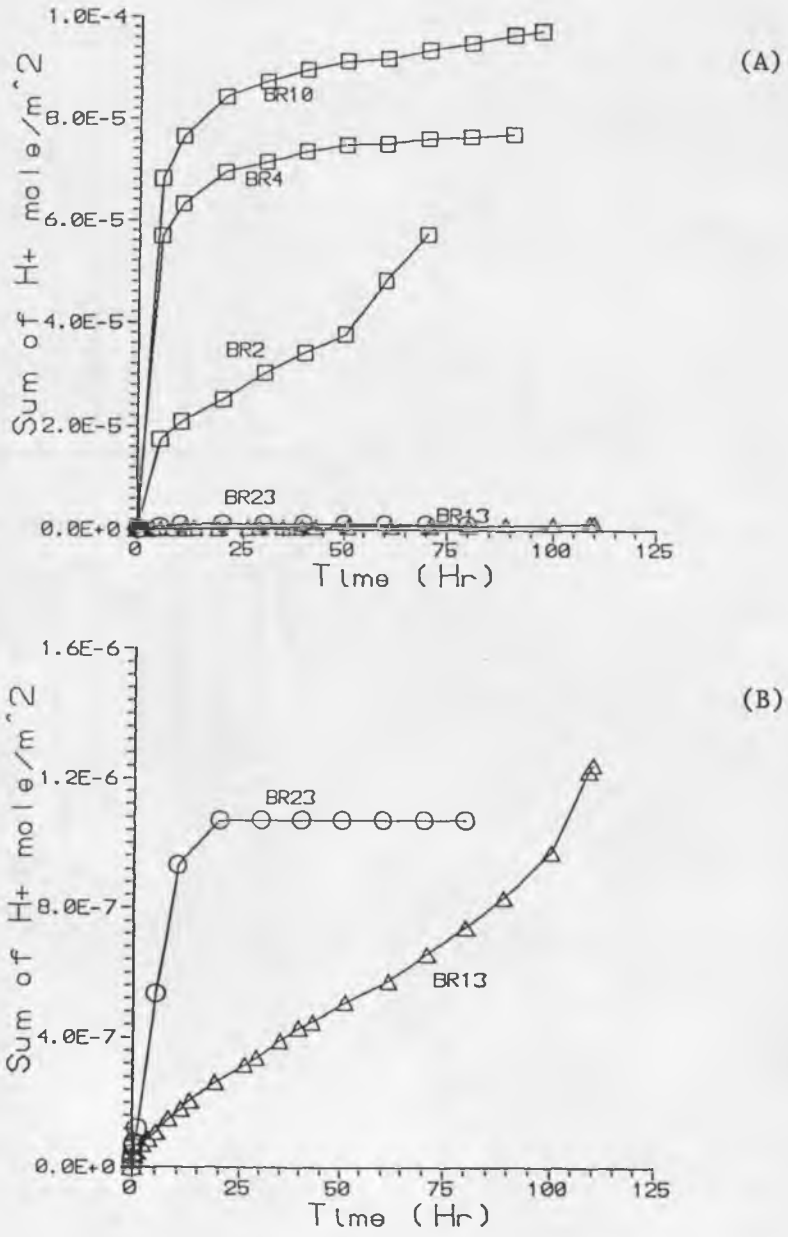

Figure 3.2 Acid consumption rates for pH 6 (A and B) hornblende batch reactor experiments (□=>#30, ▲=#30-40, ○=#100-200)

Table 3.2 Hornblende Average Acid Consumption Rates (mole/(m^2*sec))

pH	This study (Mean) ± (90% CI)[1]	Hopkins (1989) (Mean) ± (90% CI)
4	$4.51 \pm 2.54 \times 10^{-12}$	$5.51 \pm 4.26 \times 10^{-10}$
5	$2.28 \pm 1.88 \times 10^{-12}$	$4.28 \pm 3.12 \times 10^{-10}$
6	$3.31 \pm 2.03 \times 10^{-11}$	$2.56 \pm 2.45 \times 10^{-10}$

[1] CI calculated by using rate data between experiments

#30 experiments started to taper off to slower, linear rates. The BRH acid consumption rates for the linear portion of the curves are summarized in Table 3.2.

Another experimental variable which seemed to have a discernible effect on mineral dissolution was mixing rate. For example, in Figure 3.2, the slope of the line for BR2 suddenly increases at 51.6 hr. At this time, the speed of the stir plate was increased, thus indicating a probable effect of transport limitations due to a thick diffuse layer. The ions thus had to move a greater distance to and from the mineral surface to reach the bulk solution. This transport problem was determined early on, and a drill type mixer and baffles were used in subsequent experiments to hold mixing effects constant.

3.1.1.1 Hornblende batch reactor (BRH) dissolution rates. Figure 3.3 has been chosen as a representative illustration for the cation release results in the BRH experiments (data for other elements are in Appendix 1). The Mg data are illustrated because they showed the most consistent results for the widest range of experimental conditions.

Figure 3.3 shows that the release rate data for Mg at pH 5 exhibits two groups of experimental results similar to those discussed in the preceding section. The initial steep dissolution rate in the > #30 size fraction is again apparent, thus helping to support the hypothesis that ultra-fines were responsible. All the cation concentrations (Al^{3+}, Ca^{2+}, Fe^{2+},

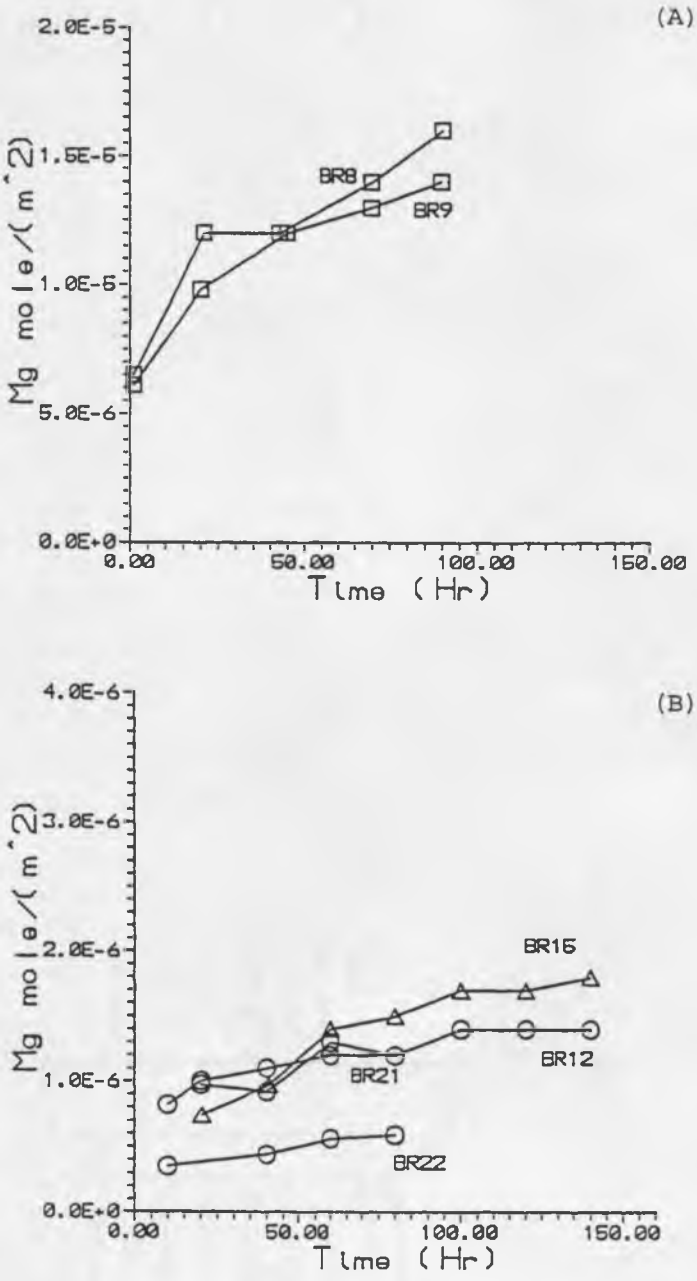

Figure 3.3 Mg dissolution rates for pH 5 (A and B) hornblende batch reactor experiments (□=>#30,▲=#30-40,○=#100-200)

Mg^{2+}, Na^{+}, and Si^{4+}) have been corrected for the mineral mass and surface area (mole/m^2). Here, titrator type and different added mineral mass did not exhibit any significant effect on Mg release rates. Three size fractions were used: BR12 #30-40; BR8 and 9 > #30; BR15, 21 and 22 #100-200. In addition, 5 g of mineral was used for BR21 and 2.5 g for BR8, 9, 12, 15, and 22. Two different titrators were also used, a Gilmont (BR8, 9, 21, and 22) and a Dosimat 665 (BR12 and 15).

The cation release rates for BRH experiments are summarized in Table 3.3, and the raw data are given in Appendix 1. Here, only the Al and Fe exhibited negative release rates (pH 5 and 6 and pH 5, respectively); this was not unexpected considering equilibrium calculations indicate that both Fe and Al were oversaturated under the experimental conditions. However, the positive Fe release rate for pH 6 is not as easily explained. Based on equilibrium considerations, Fe should have a negative release rate. It is believed that this effect is an artifact created by the variability in the experimental data. The 95% confidence interval (CI) for the cation is large and does not rule out the possibility that the release rate is positive. The large ranges in confidence intervals for cation release rates at pH 6 are probably linked to the experimental difficulty in maintaining the pH for those experiments.

3.1.1.2 BRH stoichiometric ratio. Relative release rates (RRR) were calculated by determining the ratio of cation

Table 3.3. Hornblende BR Cation Release Rate (mole/(m^2*sec))

	This study[1] (Mean) ± (90% CI)	Hopkins (1989) (Mean)
pH 4		
Al	$4.47 \pm -- \times 10^{-13}$	--
Ca	$2.54 \pm 0.21 \times 10^{-12}$	3.02×10^{-11}
Fe	$2.09 \pm 0.50 \times 10^{-12}$	--
Mg	$1.73 \pm 0.65 \times 10^{-12}$	1.58×10^{-10}
Na	$2.78 \pm -- \times 10^{-12}$	8.13×10^{-11}
Si	$4.54 \pm 1.84 \times 10^{-12}$	2.75×10^{-10}
pH 5		
Al	$-3.60 \pm -- \times 10^{-13}$	--
Ca	$5.72 \pm 5.17 \times 10^{-12}$	2.57×10^{-11}
Fe	$-1.80 \pm 2.39 \times 10^{-13}$	--
Mg	$1.20 \pm 0.35 \times 10^{-12}$	1.12×10^{-10}
Na	$1.64 \pm 0.21 \times 10^{-12}$	5.62×10^{-11}
Si	$4.84 \pm 0.64 \times 10^{-12}$	2.51×10^{-10}
pH 6		
Al	$-2.40 \pm 1.56 \times 10^{-12}$	--
Ca	$9.73 \pm 1.05 \times 10^{-12}$	2.24×10^{-11}
Fe	$9.48 \pm -- \times 10^{-13}$	--
Mg	$7.42 \pm -- \times 10^{-12}$	8.71×10^{-11}
Na	$1.72 \pm -- \times 10^{-12}$	3.80×10^{-11}
Si	$3.20 \pm 3.01 \times 10^{-11}$	2.23×10^{-10}

[1] 90% CI could not be calculated for cations with only one data set

release rate relative to Si release rate and comparing this ratio to the stoichiometric ratio of this cation to Si in the raw mineral. The RRR curves were used to determine if minerals are dissolving stoichiometrically. An RRR value less than one indicates that the ratio of a particular dissolved cation to aqueous silica concentration is less than the stoichiometric ratio of the two in the mineral solid. An RRR greater than one, on the other hand, indicates preferential dissolution, i.e., a greater concentration of dissolved cation relative to aqueous silica than expected from mineral stoichiometry. Stoichiometric dissolution would result in an RRR of one. RRR values are commonly expressed in logarithmic form (Log(RRR)), with a value of 0.00 indicating stoichiometric dissolution. The method for calculating Log(RRR) is:

$$\text{Log(RRR)} = \text{Log}\left[(X/Si)_{aq}/(X/Si)_{solid}\right]$$

where X is a base cation concentration.

The pH 4 batch reactor Log(RRR) data for hornblende are shown in Figures 3.4-3.5. Cation relative release rate curves (RRR) for all the base cations are mostly positive and generally seem to first experience a high preferential release which was followed by an approach to stoichiometric dissolution, although Log values of 0.00 were not reached during the length of these experiments, up to 140 hr. The preferential release of cations followed this order (high to low)

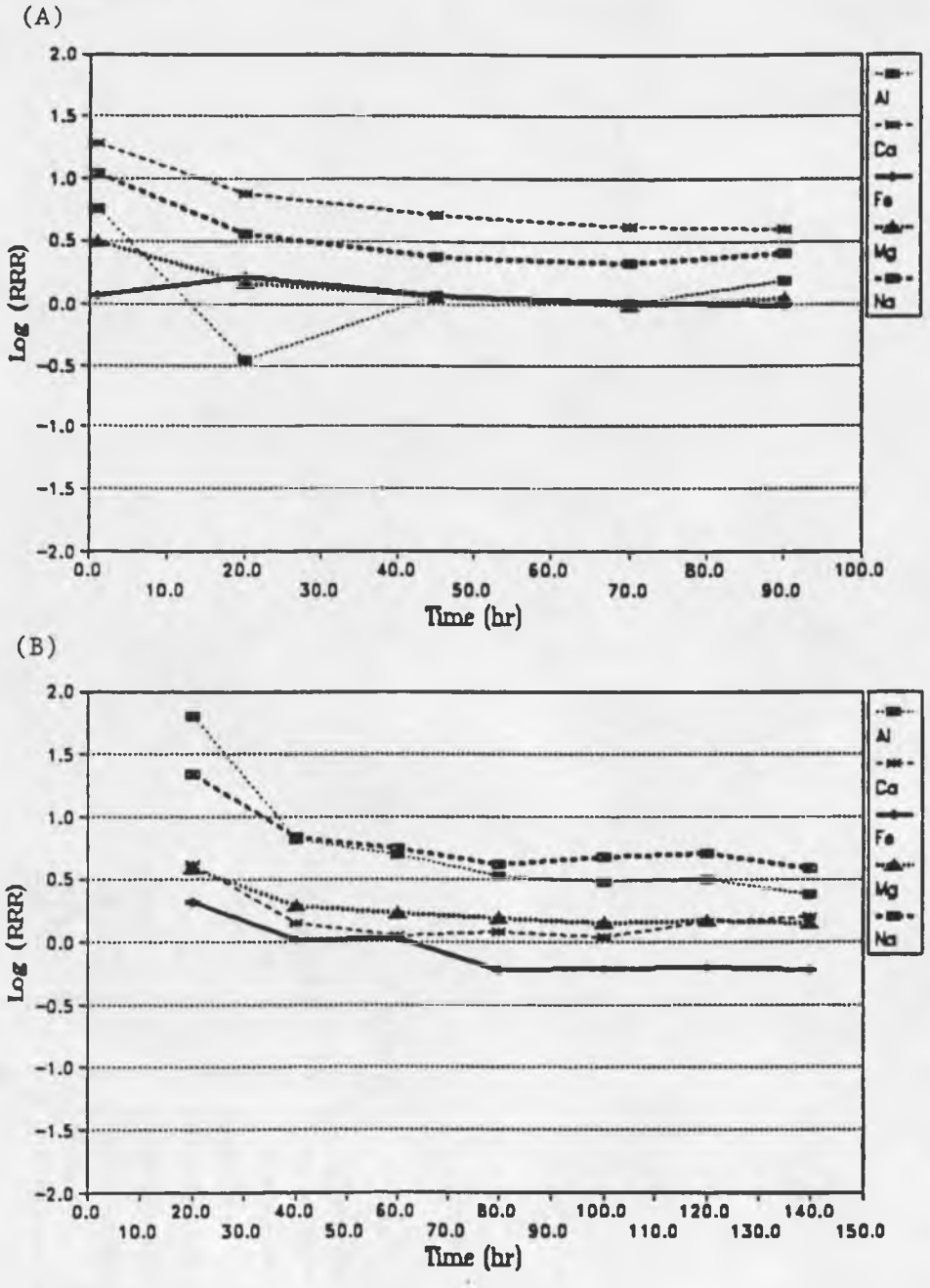

Figure 3.4 Relative release rate curves at pH 4 for hornblende batch reactor experiments (A) BR7 and (B) BR11

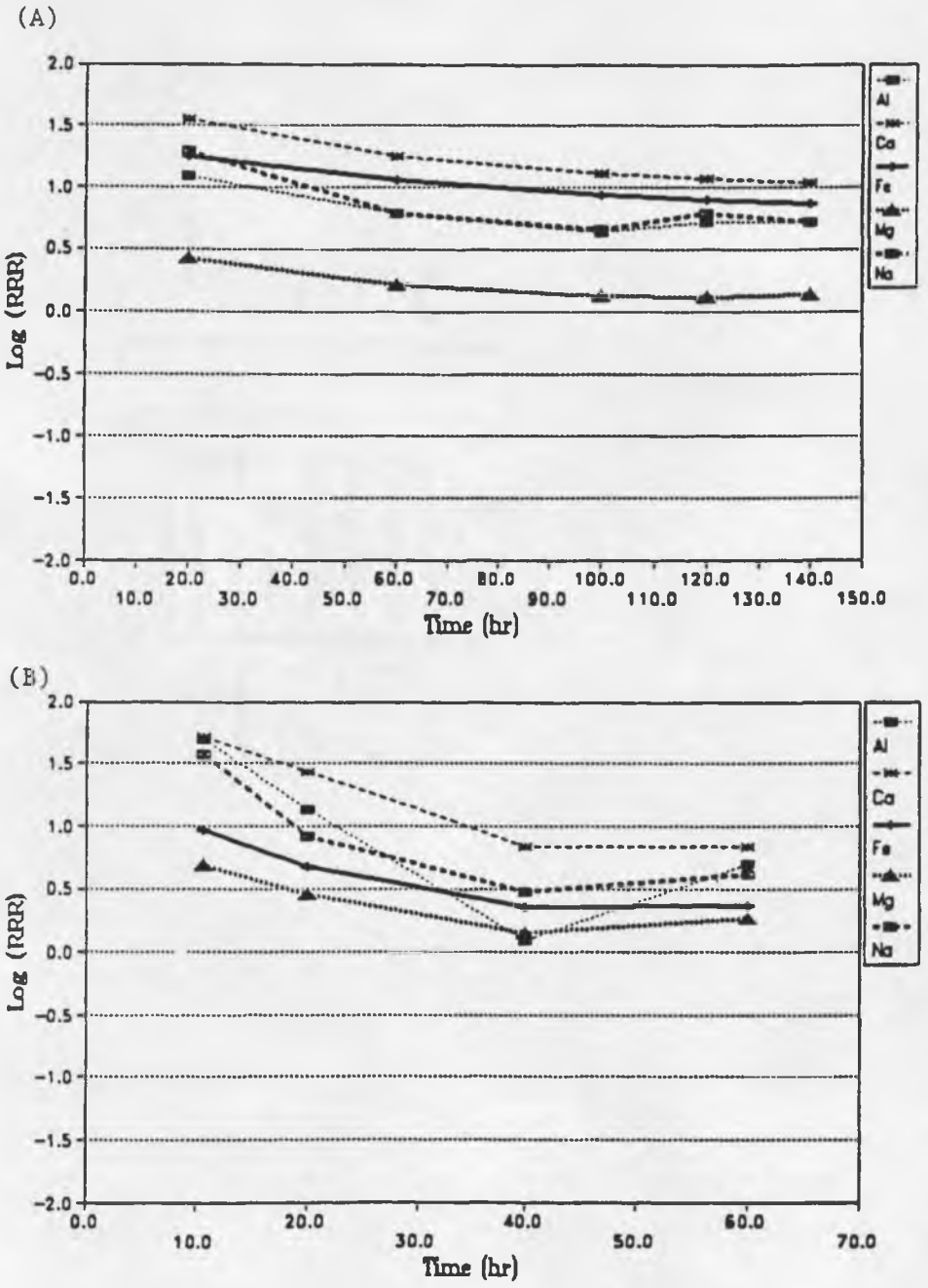

Figure 3.5 Relative release rate curves at pH 4 for hornblende batch reactor experiments (A) BR14 and (B) BR19

Ca>Al>Na>Mg>Fe. Ca exhibited the highest preferential release, whereas both Mg and Fe were closest to stoichiometric dissolution. The Fe showed variable signs of retention (e.g., BR11); it is unknown why this did not occur in all experiments. Under the experimental conditions, Fe would be expected to be preferentially retained due to saturated concentrations. The most reasonable explanation might be that Fe concentrations were in error due to the measured solutions being close to the detection limit (10 ppb). Although only pH 4 results are presented, the same trends were observed for pH 5 and 6; all data are tabulated in Appendix 1.

Estimates of depth of leaching were done for both hornblende and tremolite FR experiments using cumulative concentrations of cations leached into solution (Table 3.4). Ca was used to estimate the molecular weight for both minerals due to: (1) it having the highest cumulative cation release (moles), (2) the number of moles of Ca per mole of mineral being fixed in both mineral formulas, and (3) Ca having one of the highest RRR for both minerals.

3.1.2 Tremolite Batch Reactor (BRT) Acid Consumption Rates

Four BR experiments were carried out using #100-200 tremolite, for durations of 80 to 90 hr. The experimental parameters are summarized in Table 3.1. Three of these experiments were carried out at pH 4 and one at pH 6. The only BRT experiment carried out at pH 6 is not discussed here

Table 3.4. Depth (Å) of Leaching Estimates[1]

(Angstrom)	Al	Ca	Fe	Mg	Si
Hornblende(HB)	22.7	36.9	2.87	1.92	2.95
Tremolite	4.41×10^4	128.0	1570	28.7	52.5

Hornblende sample calculation

hornblende formula $NaCa_2(Fe,Al,Mg)_5(Al,Si)_8O_{22}(OH)_2$

Ca Wt% from microprobe analysis = 4.686 (g/g) x 100

$$\frac{4.686 \text{ g Ca}}{100 \text{ g HB}} * \text{mole}/40.078 \text{ g Ca} = \frac{0.11692 \text{ mole Ca}}{100 \text{ g HB}}$$

$$\frac{2 \text{ mole Ca}}{\text{mole HB}} / \frac{0.11692 \text{ mole Ca}}{100 \text{ g HB}} = \frac{17.106 * 100 \text{ g HB}}{\text{mole HB}}$$

proportionality factor to multiply other elements in order to calculate HB molecular wt.

hornblende molecular wt = 1486.82 g mineral/mole mineral (using Ca)

$$\frac{1486.82 \text{ g mineral}}{\text{mole mineral}} * \frac{\text{mole mineral}}{2 \text{ mole Ca}} * \frac{\text{cm}^3}{3.2 \text{g}} * \left(\frac{\text{m}}{100 \text{cm}}\right)^3 \left(\frac{\text{g}}{1.278 \text{m}^2}\right) *$$

$$\left(\frac{1}{4.0 \text{g HB}}\right) * (8.12 \times 10^{-5} \text{ mole } Ca_{aq}) = 3.69 \times 10^{-9} \text{ m}$$

hornblende density = 3.2 g/cc
#100-200 hornblende surface area = 1.278 m^2/g

[1] Blank corrected FR concentrations were used to calculate leached layer

due to its excessive pH variability (>0.5 pH units) during the experiment and absence of replicate experiments (to validate the results), but the data are documented in Appendix 2.

Acid consumption rates for BRT experiments (BR26 and 27) at pH 4 are illustrated in Figure 3.6. In this figure, both the acid consumption rates display good reproducibility and linear behavior after 10-20 hours. All the BRT acid consumption rates are summarized in Table 3.5.

BR25 (also done at pH 4) results were not included in Figure 3.6 because no acid addition was necessary to maintain pH for this experiment. The experiment was started at an initial pH of 3.92 instead of pH 4.00, and the pH did not rise quickly enough and sufficiently (i.e., it did not reach >4.05 pH units) to prompt the titrator to add acid. The pH (for this experiment) after sampling usually dropped about 0.05 pH units, which was not enough to necessitate the addition of acid. This set of conditions was not experienced with any other experiment, although a small drop in pH was typical for all experiments after each sampling. It is not known why this occurred. There was found to be no bias due to sorption of acid anions on the sampling tube and plastic syringe from the acid washing procedure. Acid anion sorption was checked by alternating the use of acid washed and non-acid washed sampling tube and plastic syringe.

3.1.2.1 Tremolite batch reactor dissolution rates (BRT). Cation release rates for BRT experiments at pH 4 are displayed

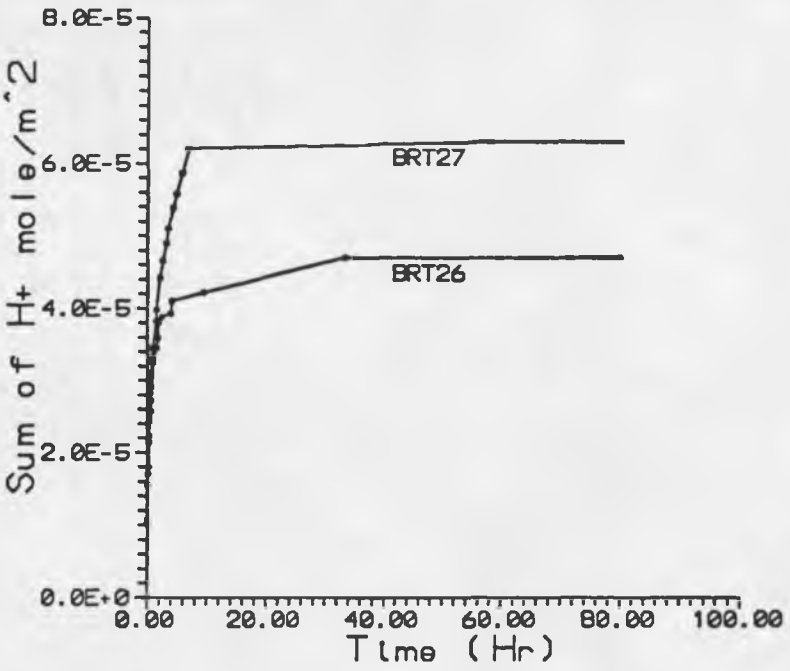

Figure 3.6 Tremolite batch reactor experiment acid consumption rates for pH 4

Table 3.5. Tremolite Average Acid Consumption Rates (mole/(m^2*sec))

pH	This study (Mean) ± (90% CI)	Hopkins (1989)
4	$2.13 \pm 8.74 \times 10^{-12}$	8.07×10^{-9}

in Figures 3.7-3.9. In these figures, all the cations exhibit linear behavior after 20 hr. except for Na, which displays non-linear behavior even after 40 hr. The Na non-linear behavior was due to measured concentrations being at the detection limit (<50 ppb), brought about by the 1+4 sample dilutions. This was also reflected in the scatter in the data. The dilutions were done due to restrictions made on sample extraction size. BR experiments did not allow much sample volume to be extracted in time. In addition to Na, the BRT Fe experimental concentrations were also at the detection limit (10 ppb).

Al was the only BRT cation which displayed a negative release rate, although computer model results predicted Al phases were not saturated under the experimental conditions. BRT cation release rates are summarized in Table 3.6.

3.1.2.2 BR tremolite stoichiometric ratio. The BRT cations measured at pH 4 all converged to stoichiometric dissolution in this order Al>Na>Fe>Ca>Mg (from slowest to fastest convergence). The cation RRR results are illustrated in Figures 3.10 and 3.11, and calculated cation release rates are documented in Table 3.6.

The Ca was released at a slower rate than Fe despite the more soluble Ca nature. One explanation for this difference is that the Fe concentrations were close to the detection limit (10 ppb), putting the relative order of release for Ca versus Fe in question.

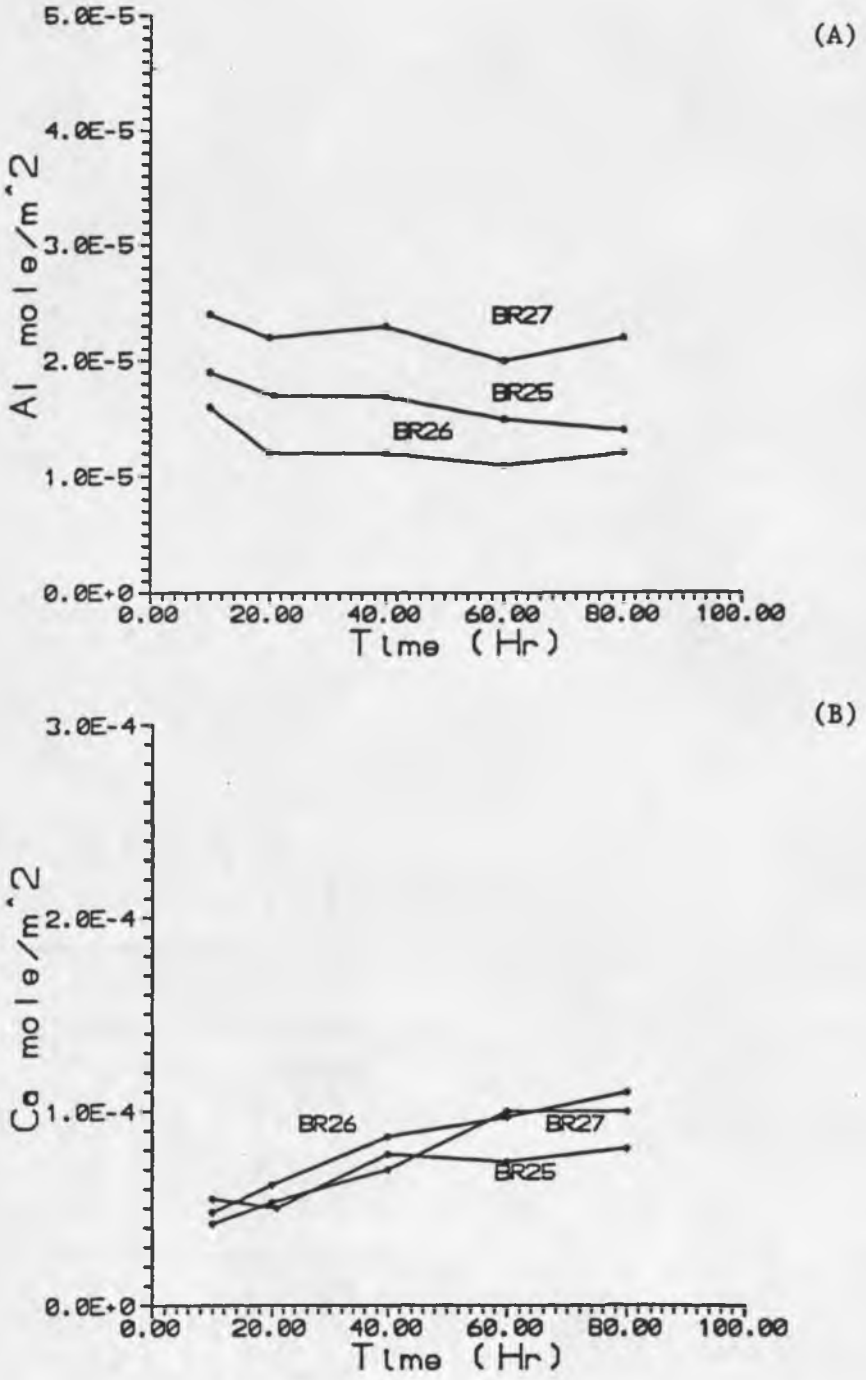

Figure 3.7 Tremolite batch reactor dissolution rates for (A) Al and (B) Ca at pH 4

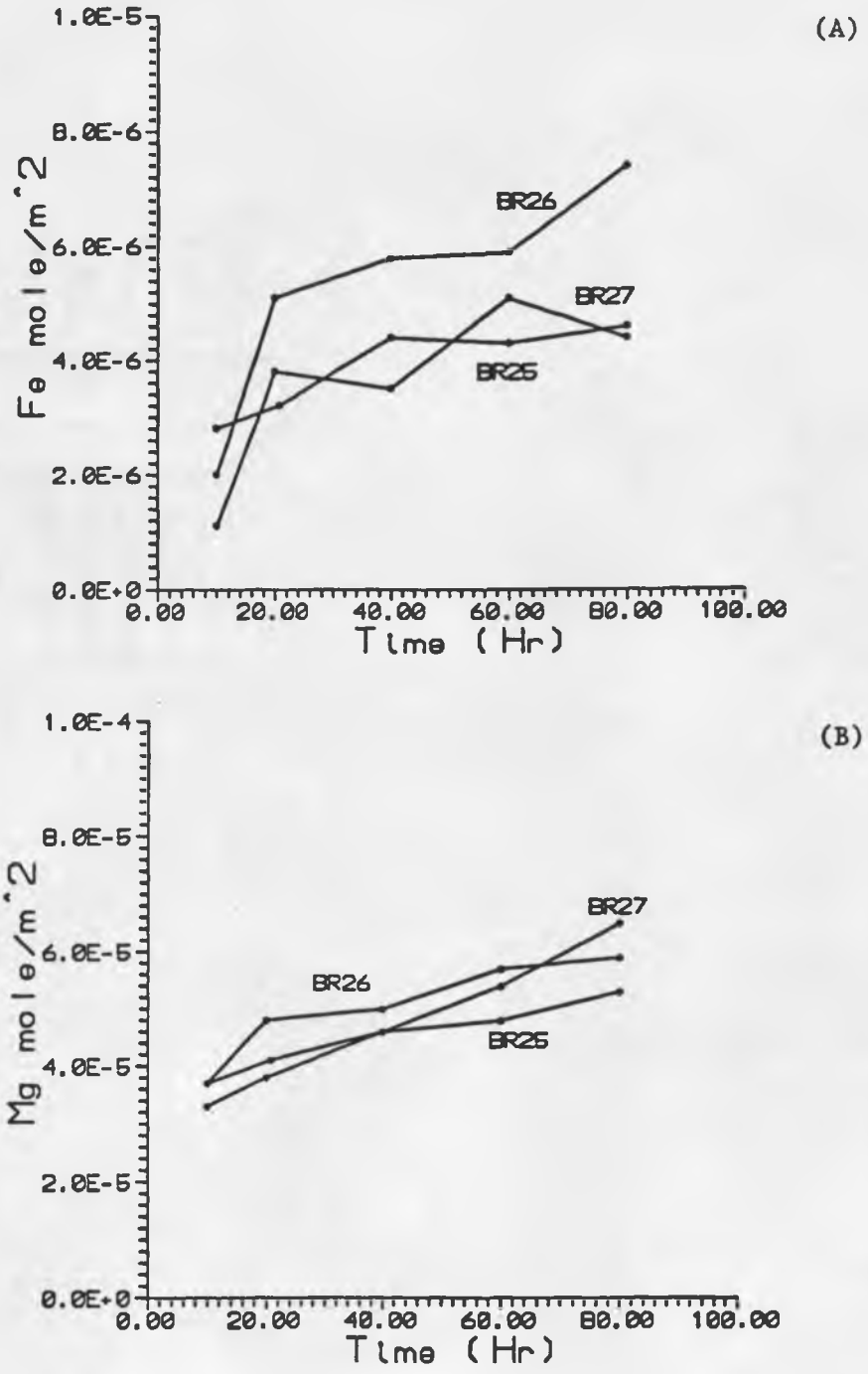

Figure 3.8 Tremolite batch reactor dissolution rates for (A) Fe and (B) Mg at pH 4

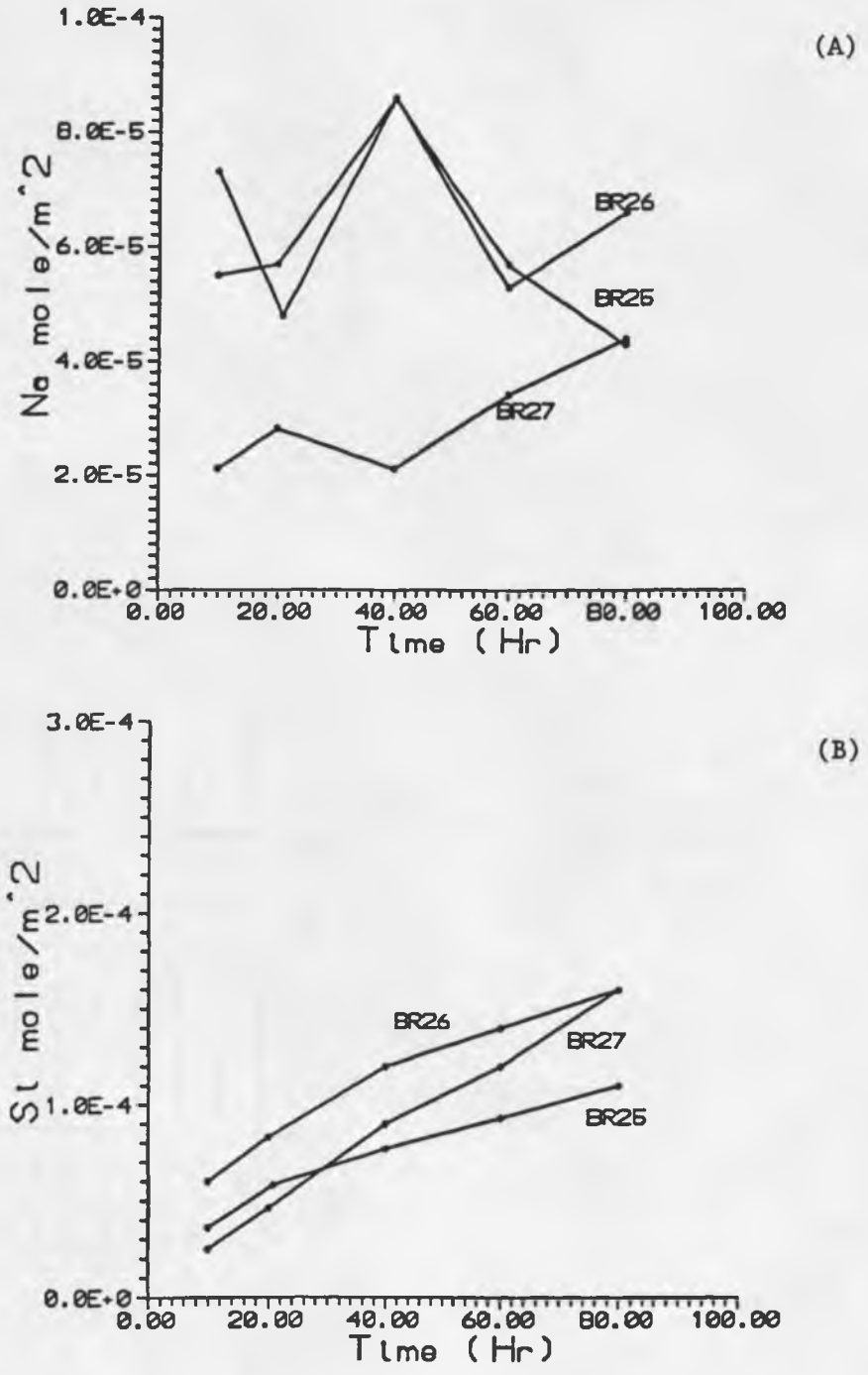

Figure 3.9 Tremolite batch reactor dissolution rates for (A) Na and (B) Si at pH 4

Table 3.6. Tremolite BR Cation Release Rate for pH 4 (mole/(m^2*sec))

	This study[1] (Mean) ± (90% CI)	Hopkins (1989)
Al	$-1.30 \pm 3.06 \times 10^{-11}$	--
Ca	$1.66 \pm 3.30 \times 10^{-10}$	--
Fe	$9.72 \pm -- \times 10^{-12}$	--
Mg	$5.76 \pm 1.30 \times 10^{-11}$	--
Na	$8.08 \pm -- \times 10^{-11}$	--
Si	$3.13 \pm 2.24 \times 10^{-10}$	3.93×10^{-10}

[1] 90% CI could not be calculated for cations with only one data set which passes the t-test

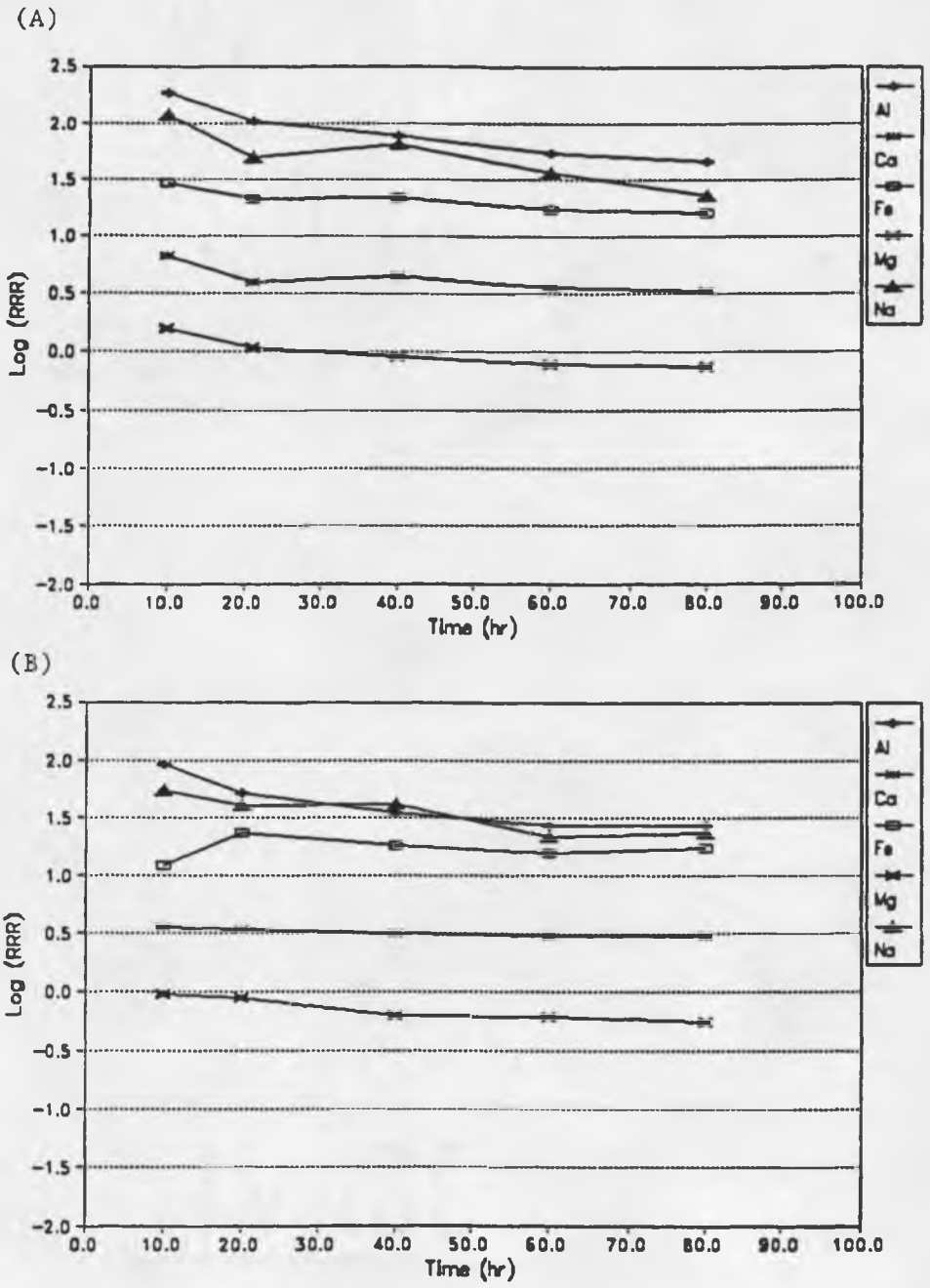

Figure 3.10 Relative release rate curves at pH 4 for tremolite batch reactor experiments (A) BR25 and (B) BR26

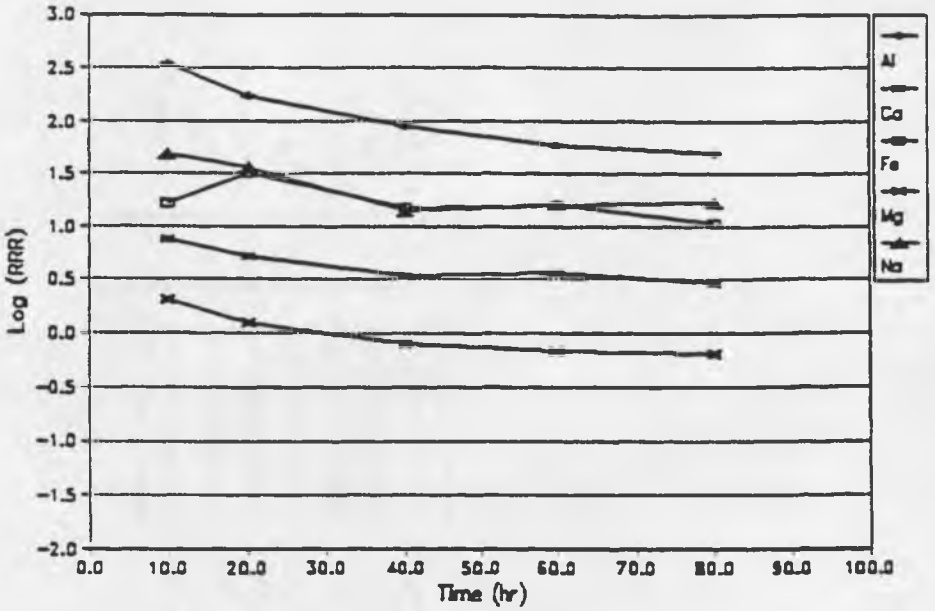

Figure 3.11 Relative release rate curves at pH 4 for tremolite batch reactor experiment BR27

Based on the RRR results, if dissolution is congruent, Mg is a possible rate limiting cation for tremolite dissolution at pH 4. Mg concentrations usually were at stoichiometric dissolution for the first 10-20 hours. However, over the span of the experiments, Si eventually became preferentially released from the mineral surface. This trend for Mg occurred in all three BRT experiments.

3.2 Flow-Through Reactor (FR)

One FR experiment was run for hornblende and one for tremolite for 78 days each. For both minerals, experimental parameters included pH, the sequence of change in pH, and presence of organic ligands. A chronology for FR experiments is documented in Table 3.7.

3.2.1 FR Hornblende (FRH) Results

The FRH (hornblende) cation release (mole/(m^2*sec)) for the cations studied as a function of time are illustrated in Figures 3.12 to 3.14. Na was the only exception due to high background concentrations caused by the use of sodium oxalate and sodium azide. The general trends observed in these plots are summarized in Table 3.8.

3.2.1.1 FR hornblende (FRH) pH trends. Fe and Mg were the only cations which exhibited slight pH enhancement in response to decreases in pH, and then only for the pH change from 9 to 7 (Figure 3.13). The Fe results, however, turned

Table 3.7. Flow-Through Reactor Experiment Schedule

DAY	SUMMARY
	FRH
1-3	pH 9 used 5 mM boric acid and 5 mM sodium azide; calibrate pump flow
4-36	pH 9 used 5 mM boric acid and 5 mM sodium azide; added 4.0006 g #100-200 hornblende to reactor
37-41	pH 7 used 1 mM sodium azide and 5 mM HEPES
42-50	pH 7 used 5 mM HEPES, 1 mM sodium oxalate and 1 mM sodium azide
51-55	pH 7 used 1 mM sodium azide and 5 mM HEPES
56-62	pH 7 used 1 mM sodium oxalate, 5 mM HEPES and 1 mM sodium azide
63-69	pH 7 used 1 mM sodium azide and 5 mM HEPES
70-78	pH 6 used 1 mM sodium azide and 5 mM MES
	FRT
1-24	pH 9 used 5 mM boric acid and 1 mM potassium cyanide; added 4.0024 g #100-200 tremolite
25-37	pH 7 used 5 mM HEPES and 1 mM potassium cyanide
38-48	pH 7 used 5 mM HEPES, 5 ppm HS and 1 mM potassium cyanide
49-52	pH 7 used 5 mM HEPES and 1 mM potassium cyanide
53-58	pH 7 used 5 mM HEPES, 5 ppm HS and 1 mM potassium cyanide
59-68	pH 7 used 5 mM HEPES and 1 mM potassium cyanide
69-78	pH 6 used 5 mM MES and 1 mM potassium cyanide

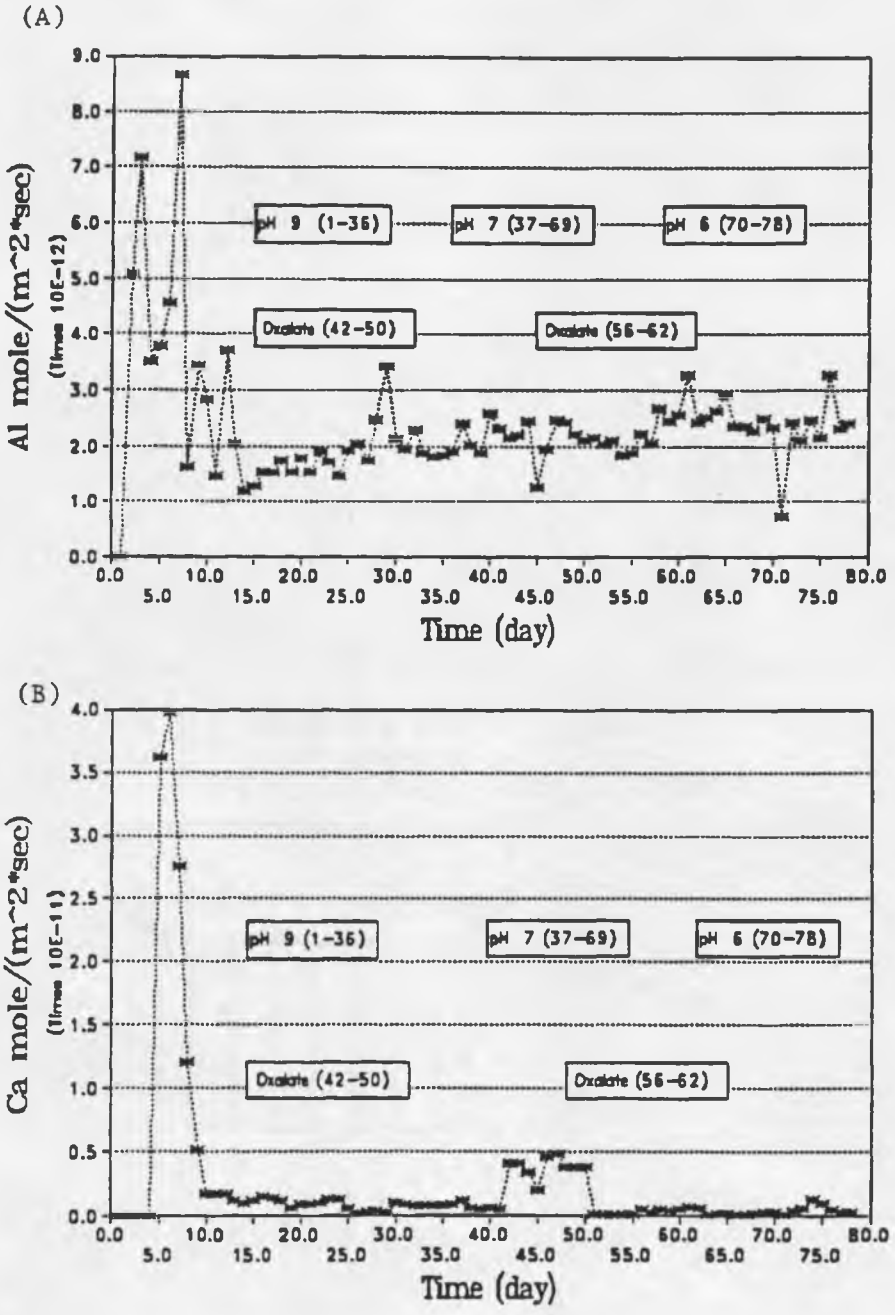

Figure 3.12 Hornblende flow-through bed reactor (A) Al and (B) Ca dissolution rates

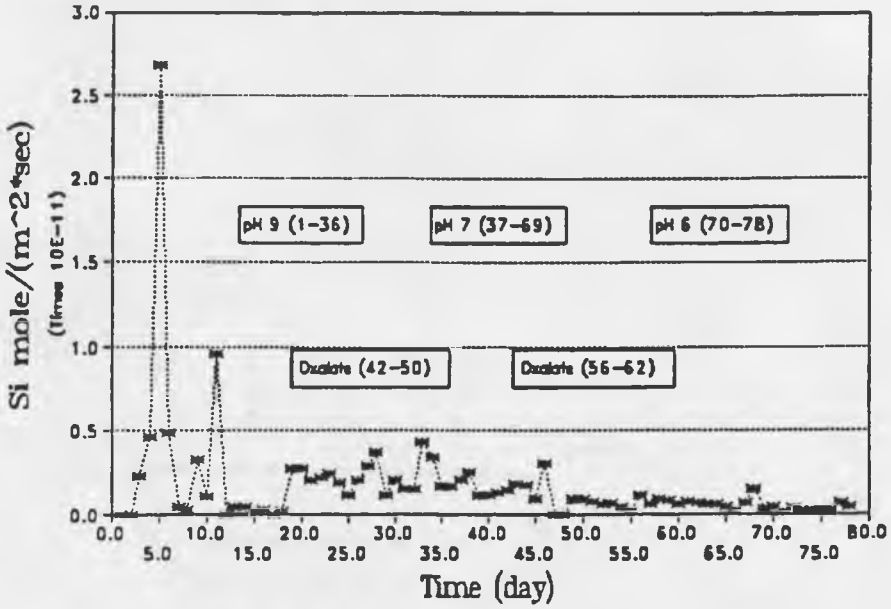

Figure 3.14 Si dissolution rates for hornblende flow-through bed reactor experiment

Table 3.8. Flow-through Bed Reactor Enhancement Results

Cation	pH enhancement	Organic Ligand enhancement
	FRH (#100-200 Hornblende with oxalate)	
Al	No enhancement	No enhancement
Ca	No enhancement	Partial enhancement(1st)
Fe	Partial enhancement(9-7)	Enhancement
Mg	Partial enhancement(9-7)	Partial enhancement(1st)
Na	Data of no use	Data of no use
Si	No enhancement	No enhancement
	FRT (#100-200 Tremolite with HS)	
Al	Partial enhancement(7to6)	Inconclusive
Ca	Partial enhancement(7to6)	Partial enhancement(1st)
Fe	Inconclusive	Enhancement
Mg	Partial enhancement(9to7)	Partial Enhancement(1st)
Na	No enhancement	Partial enhancement(1st)
Si	No enhancement	Enhancement
	Mast and Drever Experiment for Anthophyllite	
Mg	Partial enhancement	No enhancement
Si	Partial enhancement	No enhancement

out to be the least reliable, as the concentrations measured were close to the detection limit (10 ppb). For the whole experiment, Mg dissolution rate appeared to decrease with pH exhibiting rates of $4.0x10^{-13}$ mole/(m^2*sec) at pH 9, $3.0x10^{-13}$ mole/(m^2*sec) at pH 7, and $2.0x10^{-13}$ mole/(m^2*sec) at pH 6. Mg trends for pH 9 were questionable due to the cation release rate still decreasing during this period (pH 9); i.e., it never stabilized.

The FRH Al dissolution rate appeared to be independent of pH, with rates of $1.9x10^{-12}$ mole/(m^2*sec) at pH 9, $2.2x10^{-12}$ mole/(m^2*sec) at pH 7, and $2.4x10^{-12}$ mole/(m^2*sec) at pH 6. In contrast, the Si dissolution rate appeared to decrease with pH, although concentrations were close to zero $2.5x10^{-12}$ mole/(m^2*sec) for pH 9, $1.0x10^{-12}$ mole/(m^2*sec) for pH 7, and nondetectable at pH 6. Dissolution rates could not be determined for Ca and Fe, both of which had concentrations at zero. In general, there did not appear to be pH trends for any cation release; the similar effect was observed in the BR experimental results.

3.2.1.2 FR hornblende (FRH) ligand effects. FRH dissolution rates for Ca, Fe, and Mg exhibited varying degrees of enhancement in response to the introduction of organic ligands. In this segment of the FRH experiment, the introduction of oxalate was carried out during two separate intervals. This alternating of oxalate was to see if any artifacts such as ultra-fines were present, which would display enhancement

in the initial exposure but not in the second one. Only the Fe appeared to exhibit release enhancement for both periods of oxalate introduction. Ca and Mg displayed enhancement of release only during the first oxalate exposure. The results are summarized in Table 3.8.

3.2.1.3 FR hornblende stoichiometric ratio. FRH Al, Ca, and Mg standard RRR results are illustrated in Figures 3.15 to 3.16. These figures represent individual data points and are the standard method of representing relative release rates. In this study, these figures are of little use due to the noise and gaps between data points. The gaps in the figures represent zero concentrations which cannot be represented by log graphs (Fe and Na results were inconclusive). Figure 3.15a illustrates the Al RRR curve which exhibited a preferential release of Al with respect to Si in time. This is in contrast to both the Ca and Mg RRR, which exhibited behavior close to congruent dissolution. Mg was the only cation which was observed to have an initial period of retention with respect to Si followed by stoichiometric dissolution.

Figures 3.17 to 3.18 represent the cumulative FRH Log(RRR) curves and are included to help augment the standard Log(RRR) results (individual data points). All the cumulative Log(RRR) curves were done using uncorrected concentrations due to noise and some of the data exhibiting zero concentrations.

The cumulative Log(RRR) results for Al are displayed in Figure 3.17a. Al exhibited a consistently positive preferen-

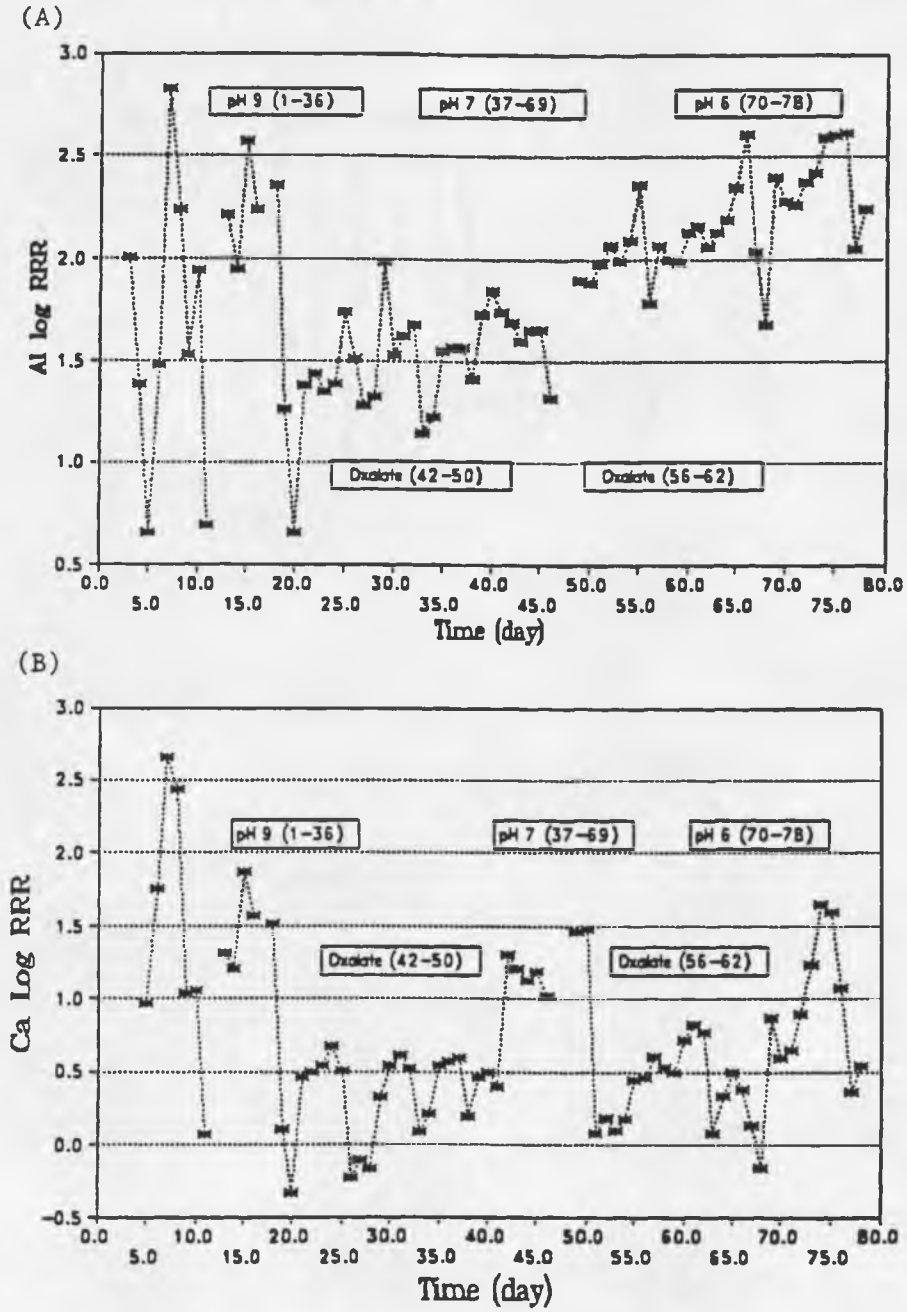

Figure 3.15 Hornblende flow-through bed reactor experiment standard relative release rate curves for (A) Al and (B) Ca

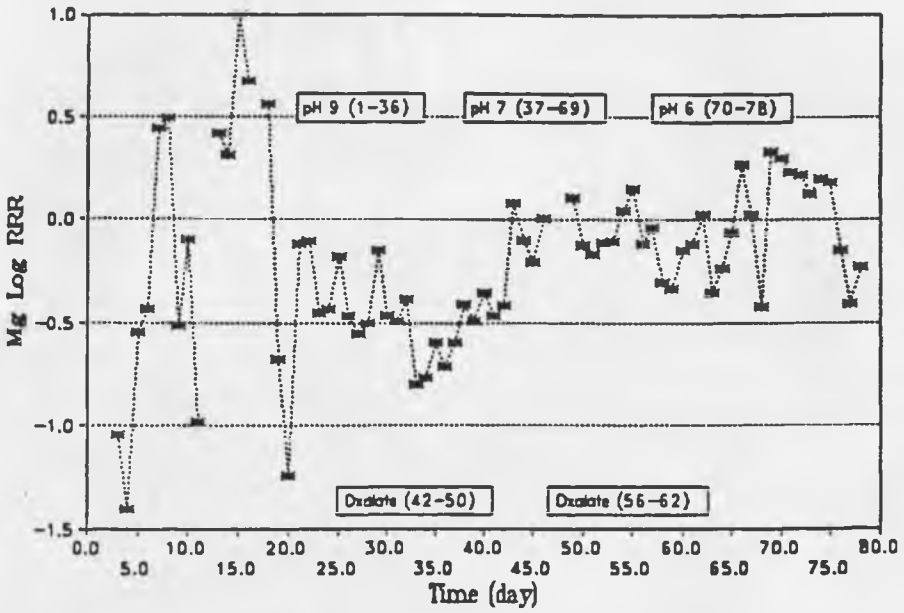

Figure 3.16 Hornblende flow-through bed reactor experiment standard relative release rate curve for Mg

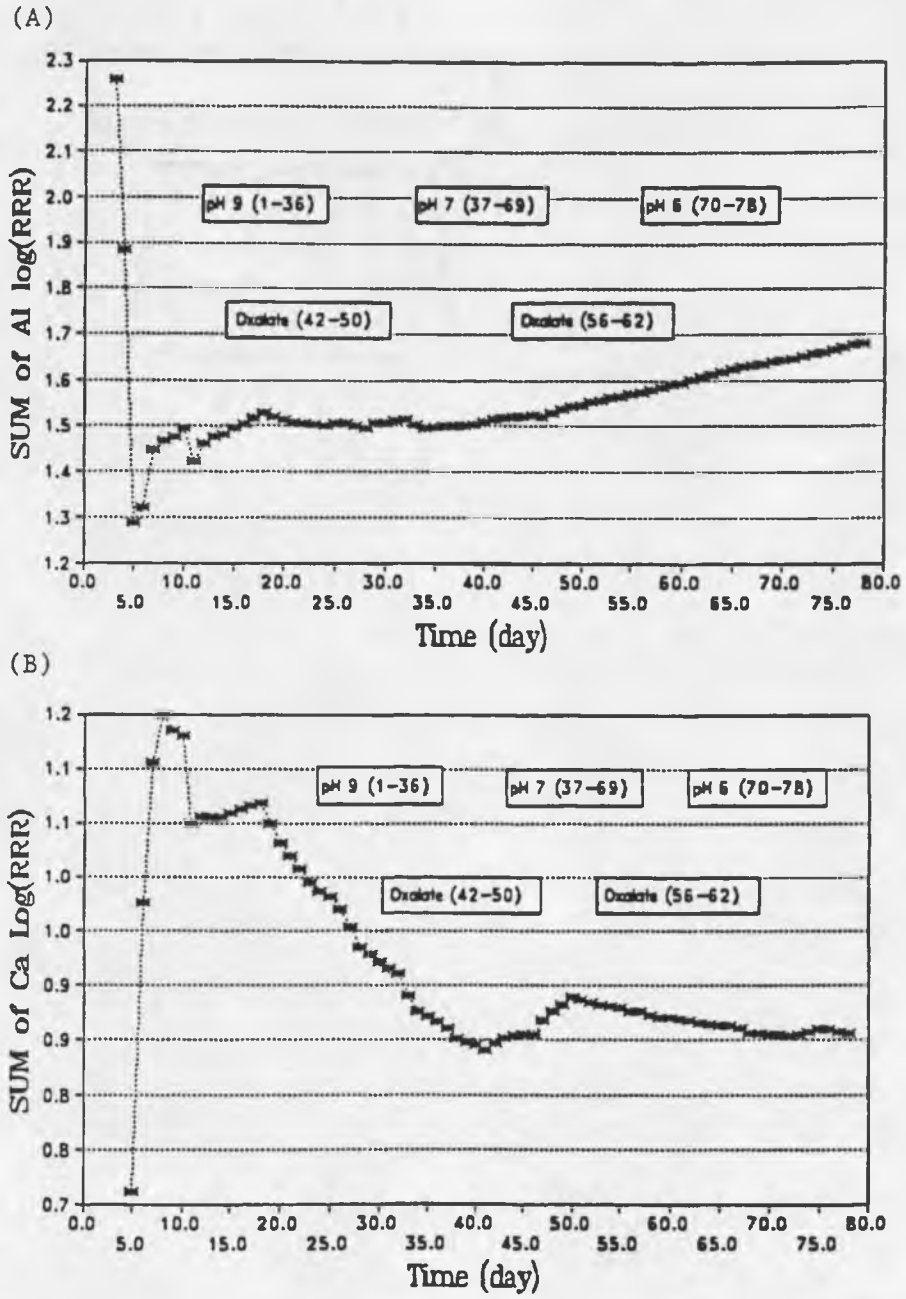

Figure 3.17 Hornblende flow-through bed reactor experiment cumulative relative release rates for (A) Al and (B) Ca

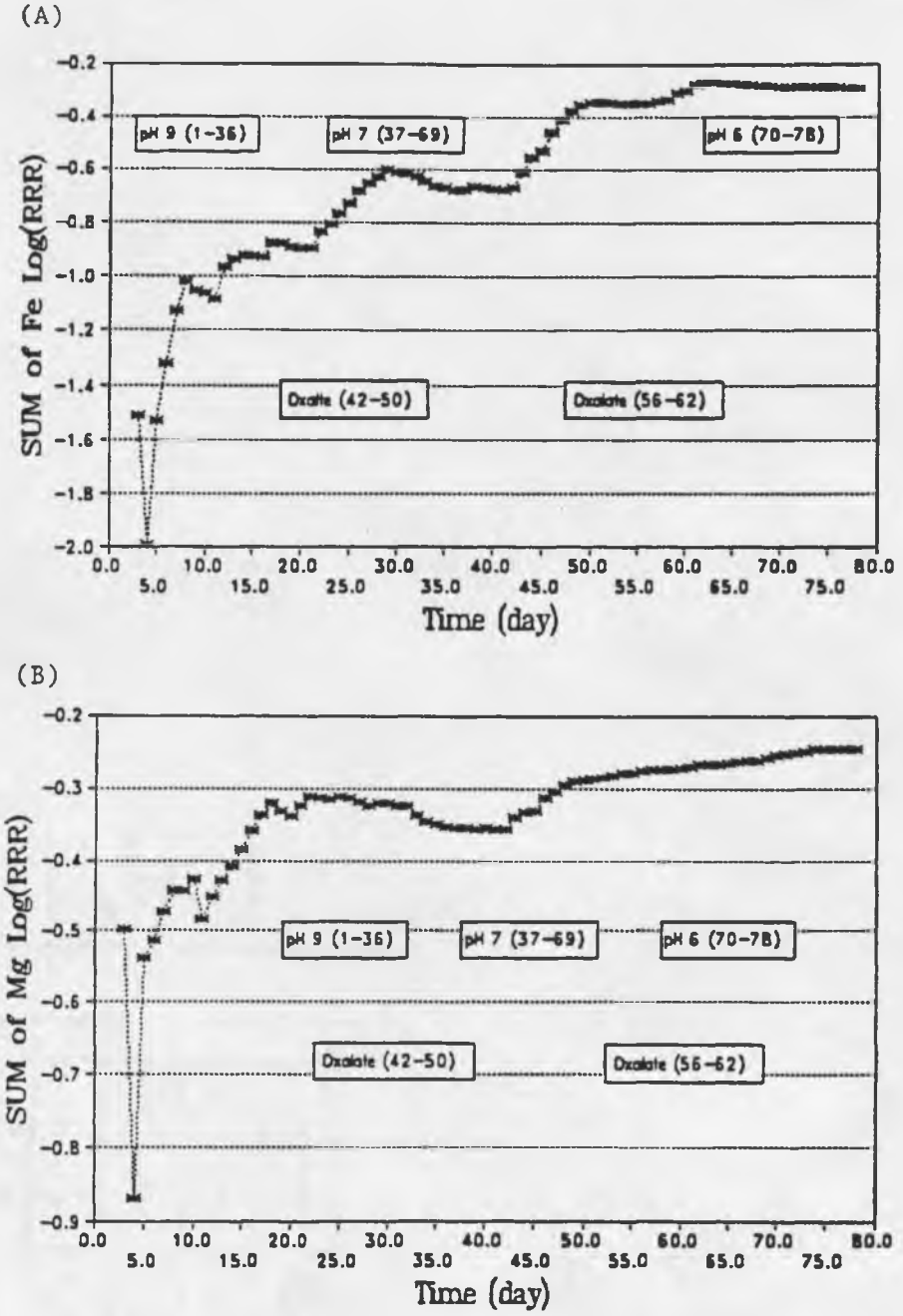

Figure 3.18 Hornblende flow-through bed reactor experiment cumulative relative release rates for (A) Fe and (B) Mg

tial release relative to Si. The RRR value for Al stabilized at a constant Log(RRR) of 1.5 for the period between 18-40 days and then displayed continued enhanced release with no effect of pH or second oxalate introduction being observed. One explanation for the continued enhancement is that the oxalate sorbed to the mineral surface promoting preferential Al release.

The cumulative Ca RRR (Figure 3.17b) exhibited a steady approach to congruent dissolution after an initial period of preferential release during the first 10 days. This initial period of preferential release probably resulted from the presence of ultra-fines--an effect also seen in the acid consumption rate curves in the BR experiments. The trend toward congruent dissolution continued until the first oxalate introduction, which promoted preferential release of Ca until the oxalate flow was discontinued. Ca cumulative RRR then decreased, only to reach a constant rate of 0.85 after about 68 days. No effect due to change in pH or to the second oxalate exposure can be seen.

Fe and Mg (cumulative RRR) were initially preferentially retained in the mineral relative to Si, although both did eventually approach stoichiometric (zero) dissolution (Figure 3.18). The Fe cumulative RRR exhibited no effect due to changes in pH, although ligand enhancement is apparent. The cumulative Fe RRR curve reached a plateau after the second ligand introduction at -0.28. Mg cumulative RRR, however,

seemed to decrease slightly after the 20th day and reached a plateau for a short time after the first pH change (pH 9 to 7). Cumulative Mg RRR then continued to approach stoichiometric dissolution at a steady rate after the first oxalate exposure. In addition, the Mg did not experience any enhancement for the second oxalate introduction or decrease from pH 7 to pH 6.

3.2.1.4 FR hornblende cumulative release. FRH cumulative release rates were calculated and are exhibited in Figures 3.19-3.21. In these figures, the Fe exhibited the greatest effect due to both pH change and ligand introduction, with plateaus after each period. Al and Mg exhibited the steepest consistent release rates. The Al values appeared linear after the 10th day and were not affected by oxalate introduction or pH change. Mg release exhibited enhancement during the first oxalate introduction but linear behavior otherwise.

The Ca also exhibited linear behavior except for an initial sharp cumulative release. The rate then slowed down after the tenth day approaching a plateau, except for a short period during the first oxalate introduction when the rate increased sharply. There was no apparent effect on Ca release from the second oxalate exposure or the second change in pH. After an initial period of accelerated dissolution, the Si displayed a linear increase in release rate until the first oxalate introduction. The Si dissolution rate then started to

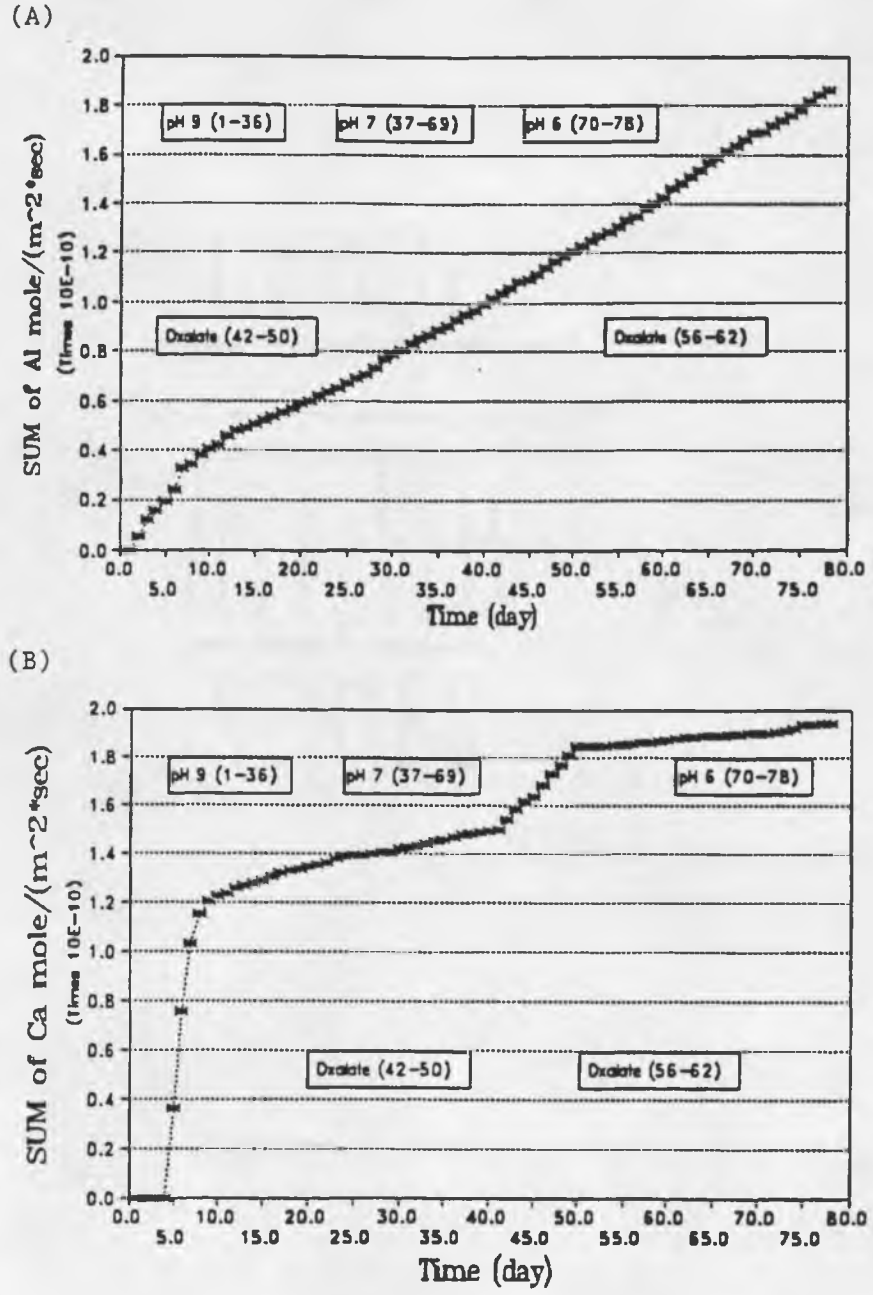

Figure 3.19 Hornblende flow-through bed reactor experiment cumulative release rates for (A) Al and (B) Ca

(A)

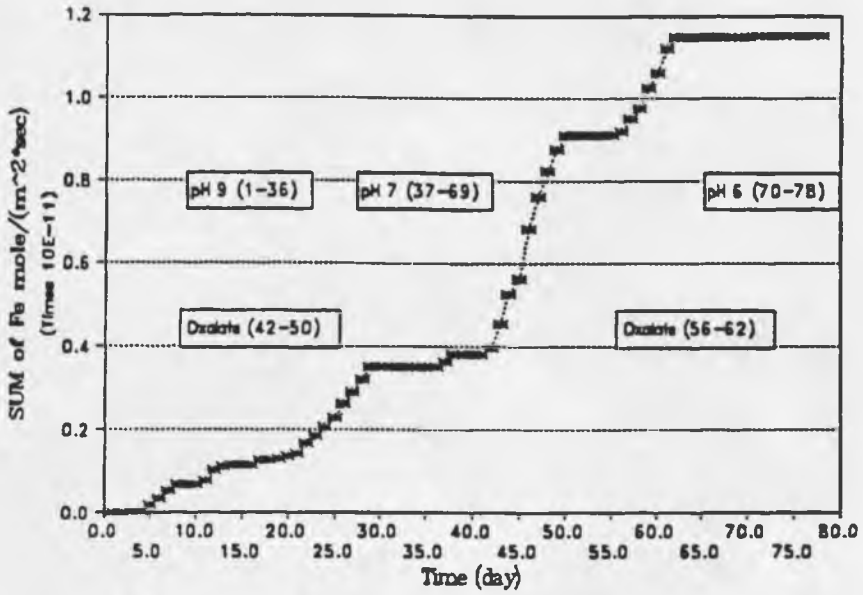

(B)

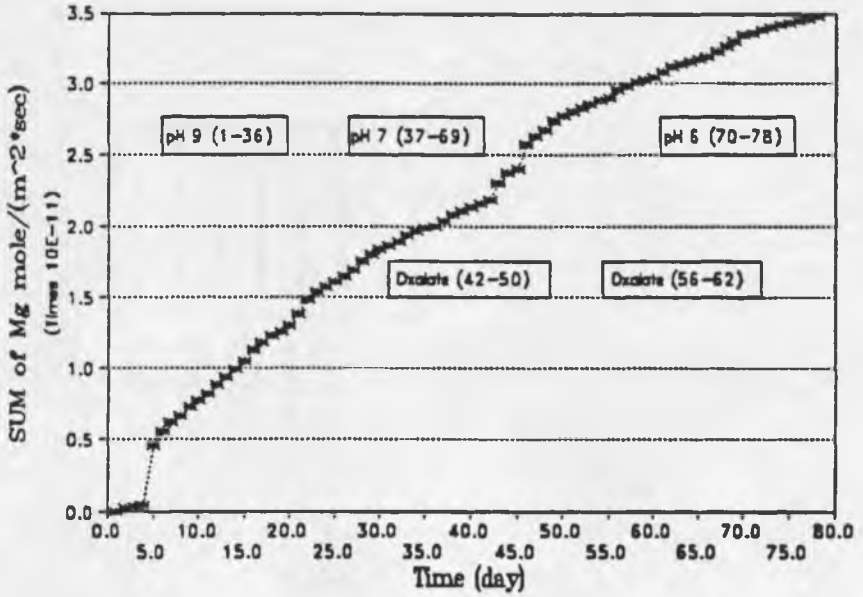

Figure 3.20 Hornblende flow-through bed reactor experiment cumulative release rates for (A) Fe and (B) Mg

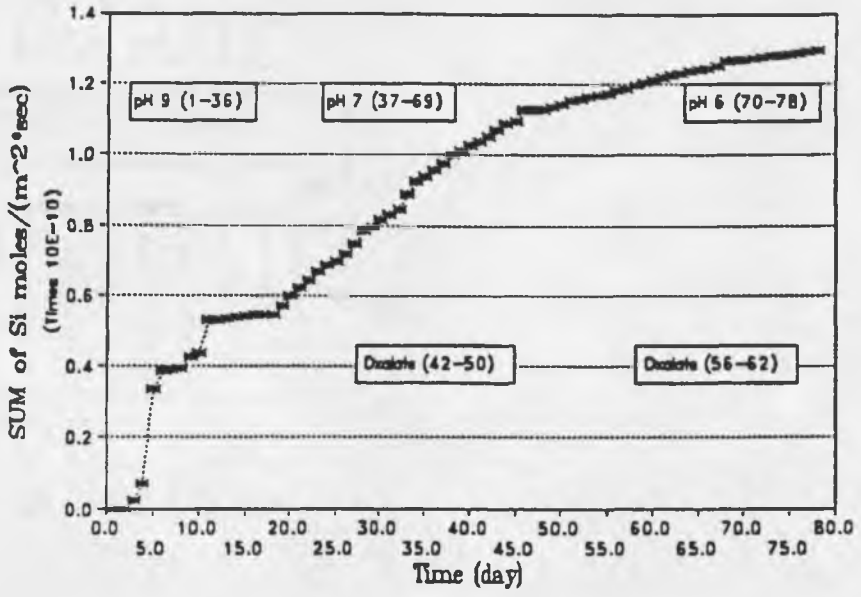

Figure 3.21 Si cumulative release rate for hornblende flow-through bed reactor experiment

taper off, possibly approaching a plateau. No effects on Si dissolution from either oxalate or pH change are apparent.

3.2.2 FR Tremolite Results (FRT)

Figures 3.22-3.24 illustrate FRT cation dissolution rates as a function of time (mole/(m^2*sec)) with enhancement results summarized in Table 3.8.

3.2.2.1 FR tremolite (FRT) in trends. In this study, only the Ca, Fe, and Mg experienced a partial enhancement due to change in pH, i.e., not for both changes in pH. Ca and Fe enhancement occurred only at the second decrease in pH (pH 7 to 6), and the Mg enhancement occurred from pH 9 to 7.

Although Al and Fe exhibited varying degrees of elevated rates in the approximate regions of the first pH change, both displayed too much noise to determine if any enhancement occurred. The Al exhibited dissolution independent of pH, $1.6x10^{-12}$ mole/(m^2*sec) at pH 9, $1.2x10^{-12}$ mole/(m^2*sec) at pH 7, and $1.8x10^{-12}$ mole/(m^2*sec) at pH 6 (Figure 3.22a). Na dissolution was independent of pH: $4.8x10^{-12}$ mole/(m^2*sec) at pH 9, $3.2x10^{-12}$ mole/(m^2*sec) at pH 7, and $5.5x10^{-12}$ mole/(m^2*sec) at pH 6 (Figure 3.24a).

3.2.2.2 FR tremolite (FRT) ligand effects. Five ppm humic substances (HS) were used as an organic ligand for pH 7 in this segment of the experiment. All the cations except Al displayed varying degrees of release enhancement. Figures 3.22 to 3.24 and Table 3.8 provide a summary of ligand

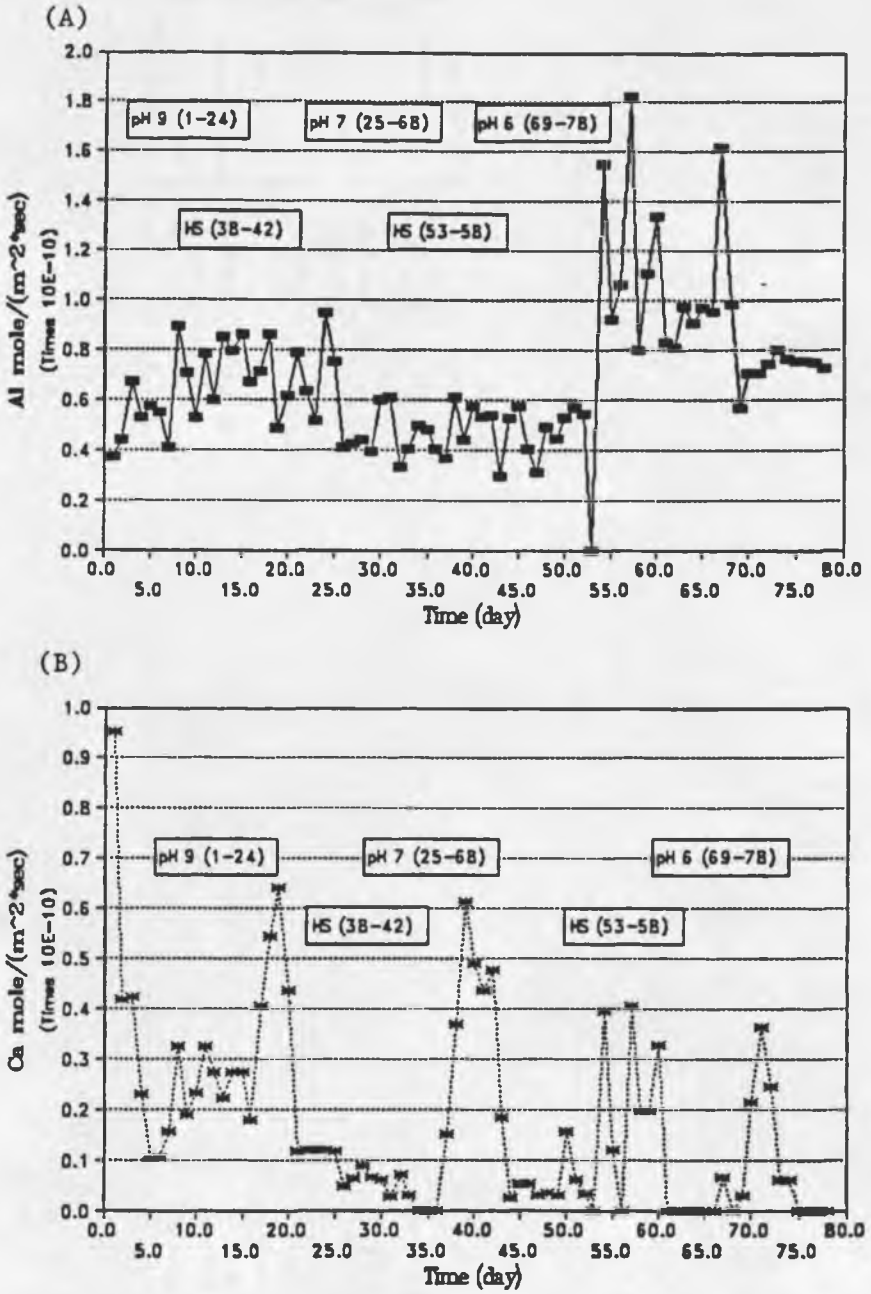

Figure 3.22 Tremolite flow-through bed reactor (A) Al and (B) Ca dissolution rates

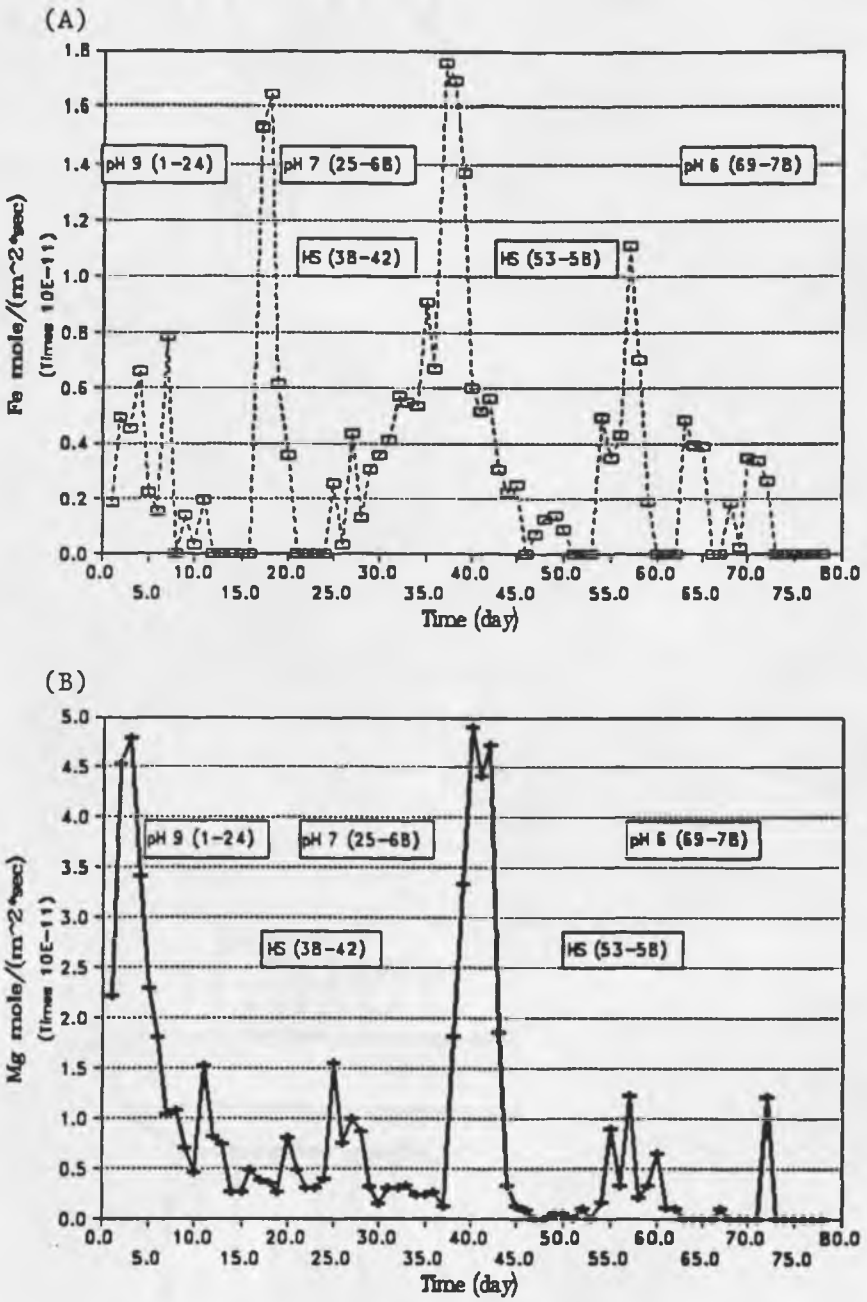

Figure 3.23 Tremolite flow-through bed reactor
(A) Fe and (B) Mg dissolution rates

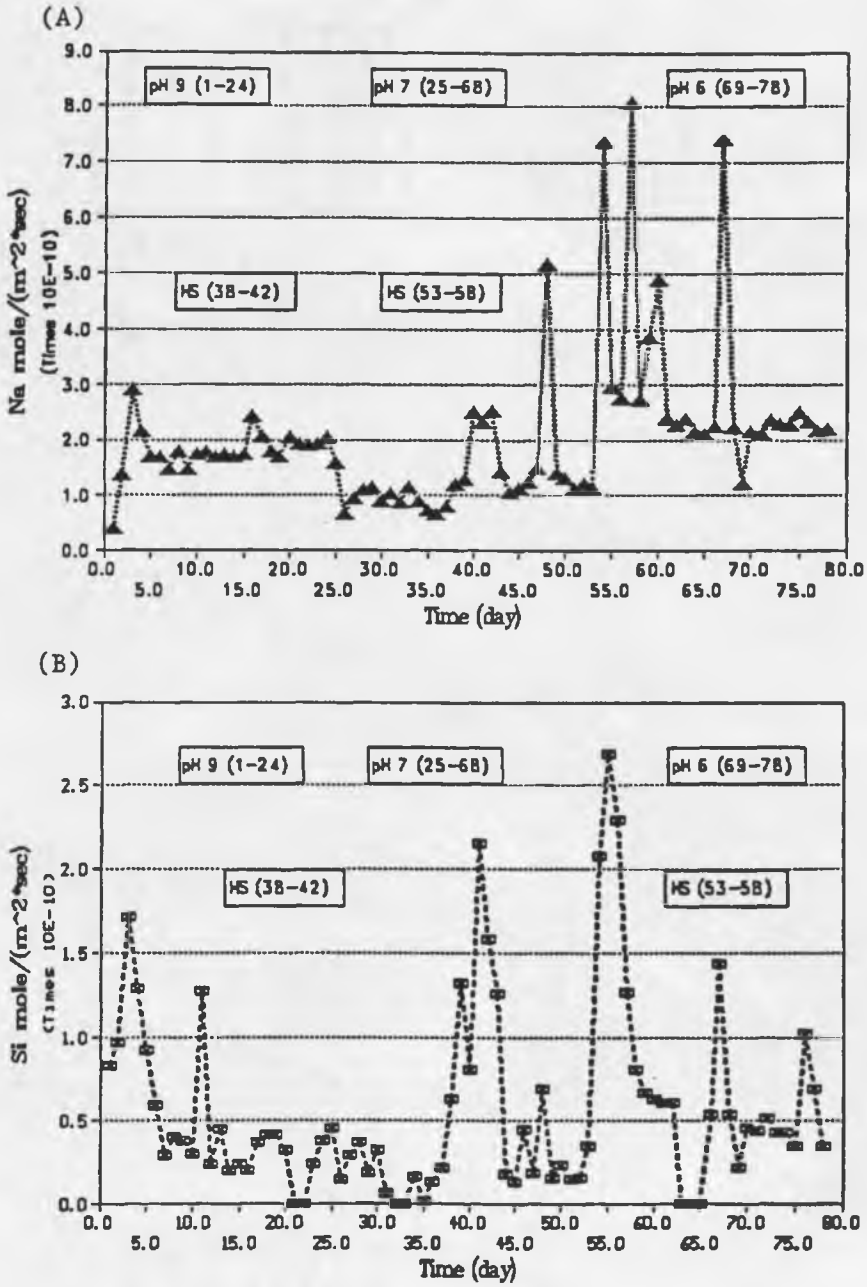

Figure 3.24 Tremolite flow-through bed reactor
(A) Na and (B) Si dissolution rates

enhancement results. It should be noted that the data for the second period of HS (53-58 days) are unreliable due to a change of the slow pump leads and a re-calibration of the pump flow. These changes may be responsible for the observed elevated, noisy concentrations of all the cations during this period.

3.2.2.3 FR tremolite stoichiometric ratio. The Al, Ca, Mg, and Na FRT standard RRR results are displayed in Figures 3.25 and 3.26. Both the Al and Na RRR results did not display much variability for this experiment (2.7 and 2.5, respectively). In contrast, Ca RRR was the only cation which displayed congruent behavior, whereas Mg RRR was the only cation which displayed incongruent dissolution, although it is difficult to say anything conclusive due to the gaps in the data. The trend indicates that Mg started being preferentially retained and, with time, the RRR curve moved consistently further away from zero.

FRT cumulative relative release results (RRR) were calculated using the same approach as the FRH cumulative RRR calculations, i.e., by using uncorrected cumulative concentrations. All the cations were preferentially released relative to Si except Mg, which was retained in the mineral. This agrees with the standard Mg RRR results (individual data). In this experiment, cumulative Ca and Fe were the only cations which seemed to approach congruent dissolution. Figures 3.27 to 3.29 illustrate the behavior of cumulative Log (RRR) versus

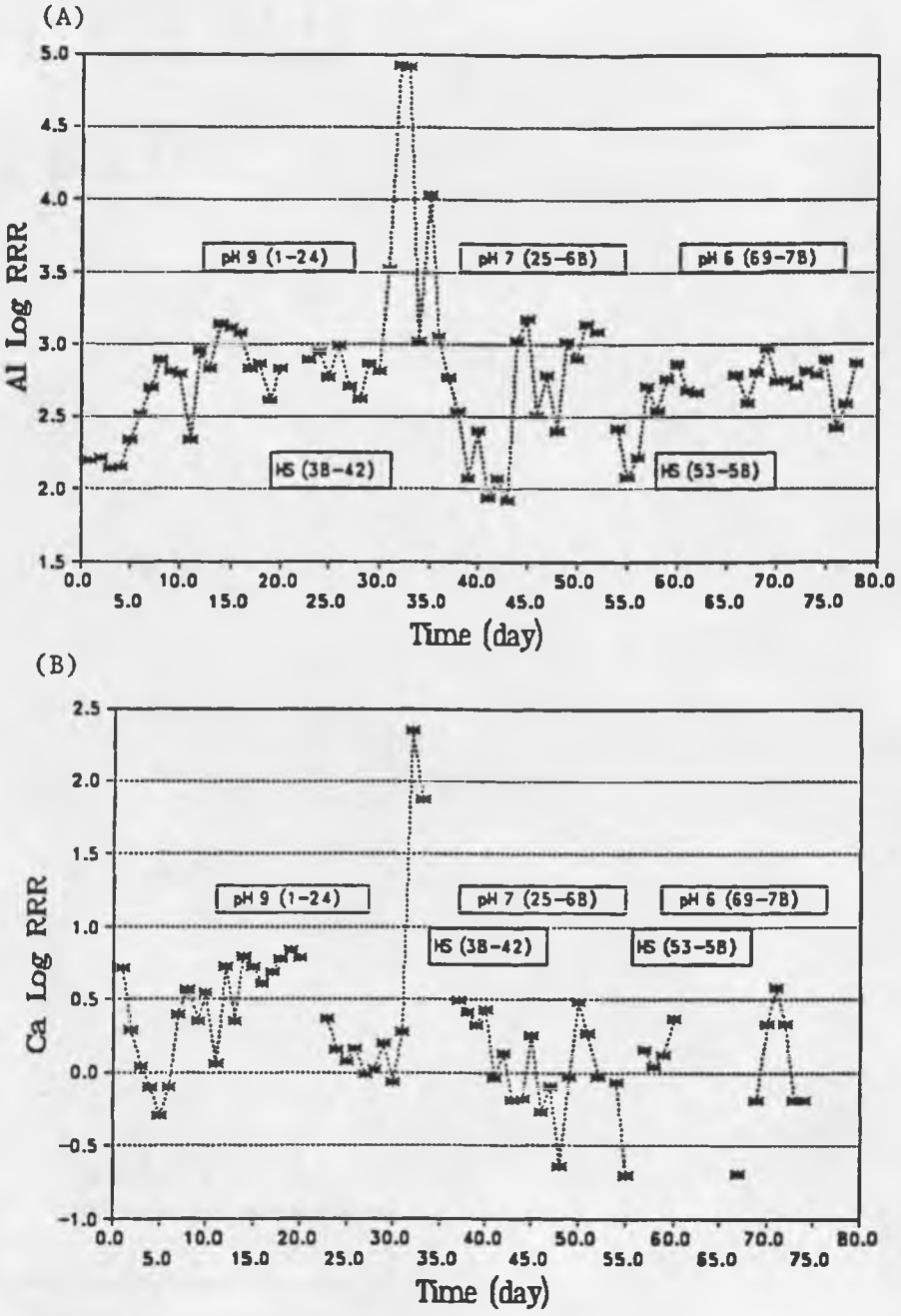

Figure 3.25 Tremolite flow-through bed reactor experiment standard relative release rate curves for (A) Al and (B) Ca

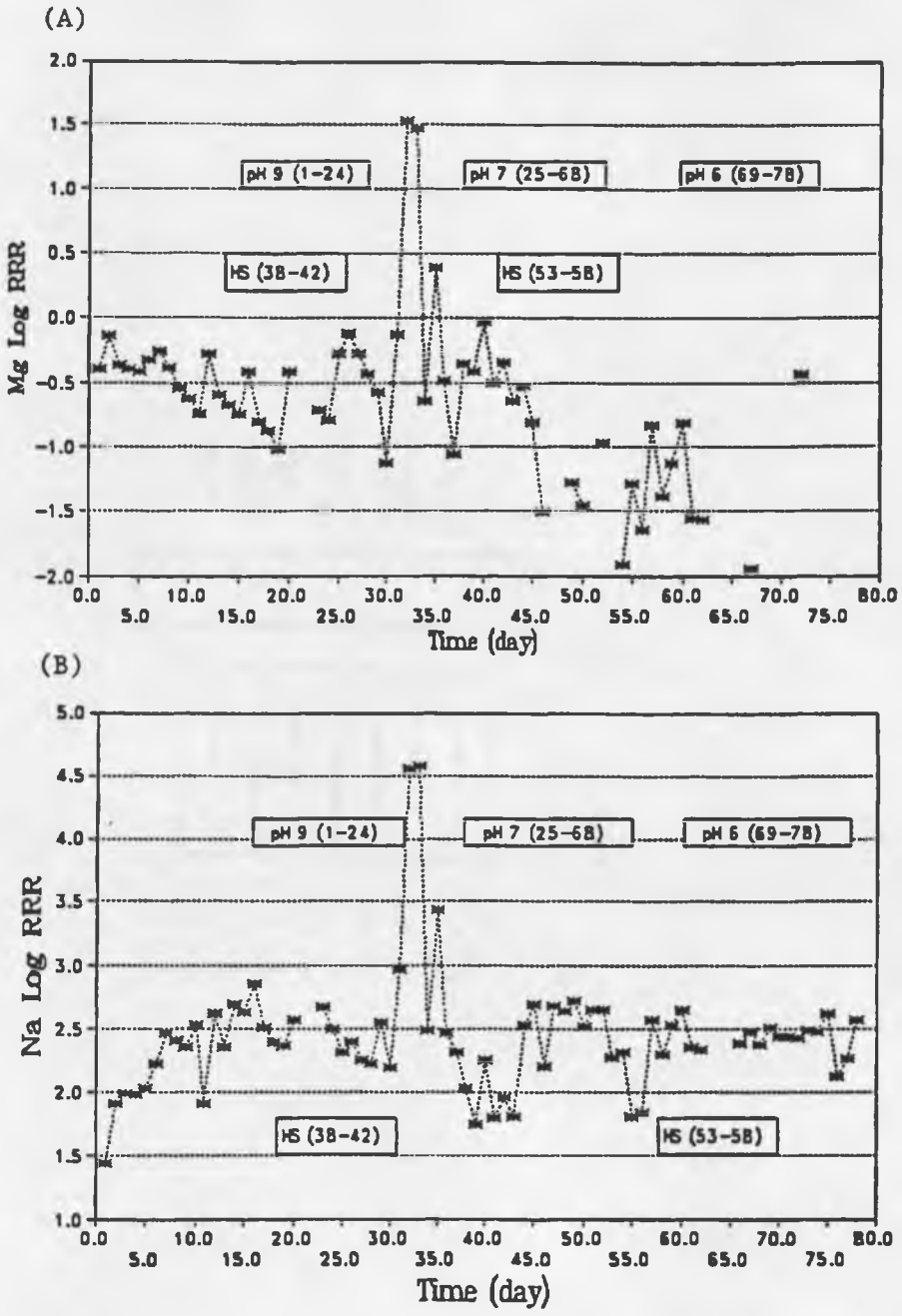

Figure 3.26 Tremolite flow-through bed reactor experiment standard relative release rate curves for (A) Mg and (B) Na

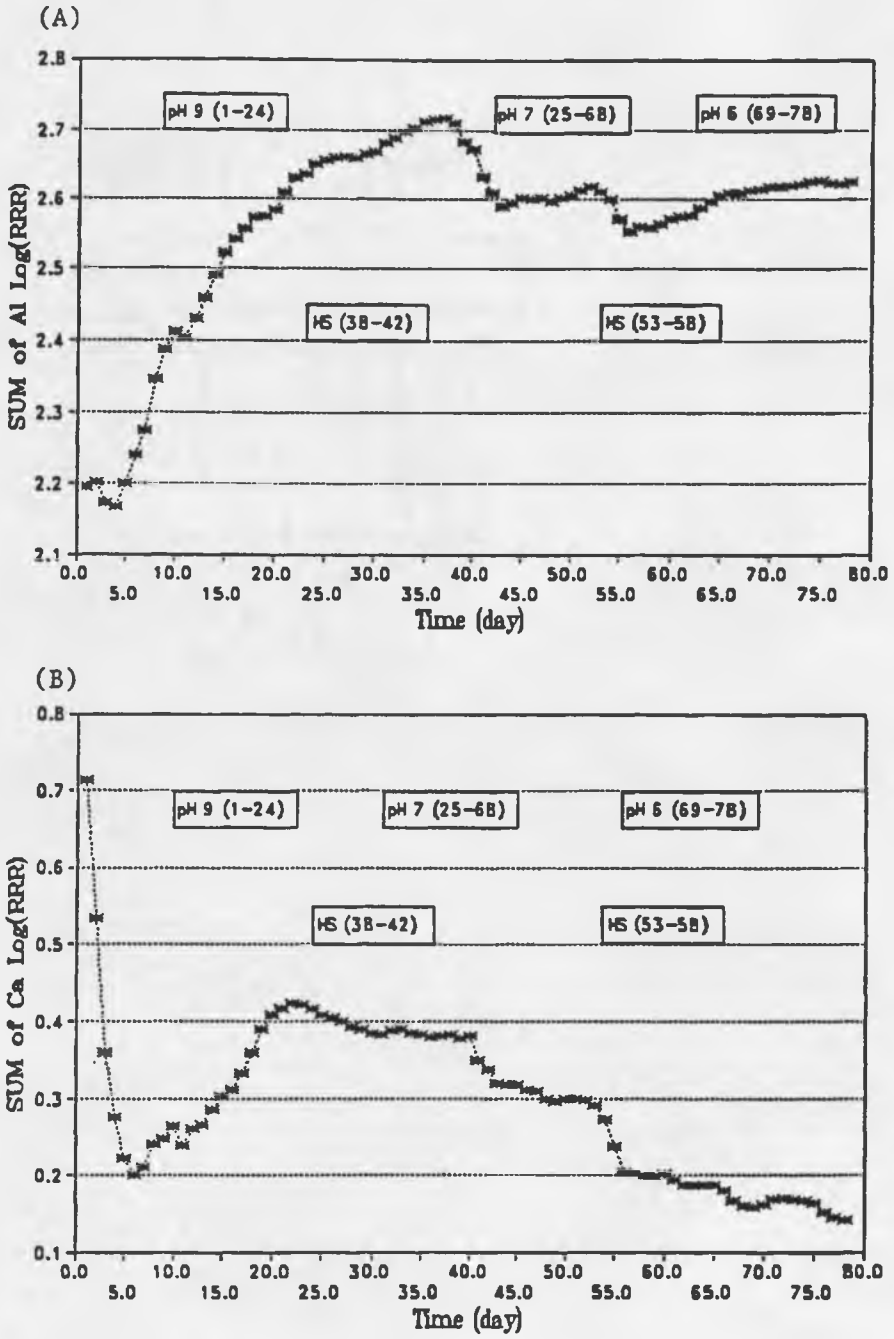

Figure 3.27 Tremolite flow-through bed reactor experiment cumulative relative release rate curves for (A) Al and (B) Ca

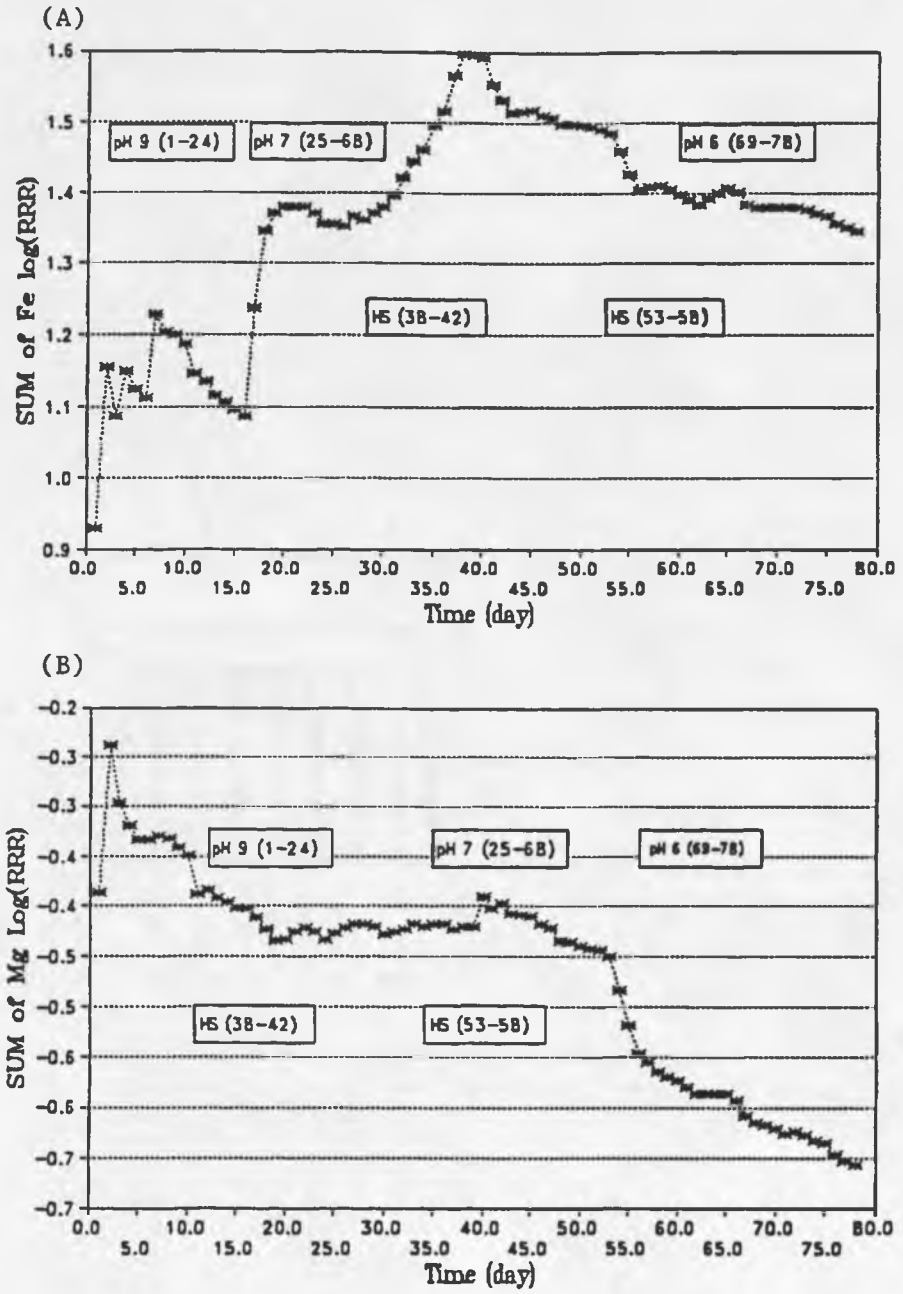

Figure 3.28 Tremolite flow-through bed reactor experiment cumulative relative release rate curves for (A) Fe and (B) Mg

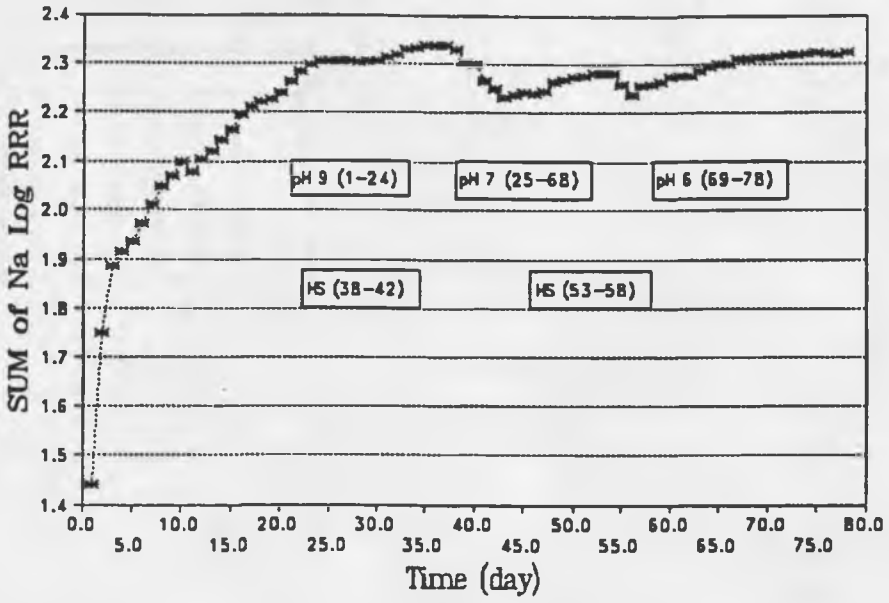

Figure 3.29 Na tremolite flow-through bed reactor experiment cumulative relative release rate curve

time for Al, Ca, Fe, Mg, and Na. Figure 3.27a illustrates that the Al (cumulative RRR) experienced a consistent preferential release relative to Si, but it started to decrease toward stoichiometric dissolution during both HS introductions. The Al started to slowly increase again after the HS was discontinued. Figure 3.27a depicts the cumulative Ca RRR curve, which shows a consistent preferential release for pH 9. After pH 9, the Ca RRR decreased toward stoichiometric (congruent) dissolution. The HS introduction appeared to increase the rate of movement toward stoichiometric dissolution for Ca. In Figure 3.28a, the cumulative Fe RRR approaches stoichiometric dissolution for pH 9, except for a sharp reversal of the trend at 17 days. The reverse in trend was due to problems in maintaining the correct level in the FR reservoir. It is believed that the overall trends displayed in Figures 3.27-3.29 should not be adversely affected by these results due to the use of cumulative concentrations. Only the Fe cumulative RRR exhibited deviations in this area. The cumulative Fe RRR experienced a consistent preferential release from the pH 9 to 7 change until the first HS introduction. Fe thereafter approached stoichiometric dissolution. Figure 3.28b illustrates that Mg (cumulative RRR) started to be preferentially retained in the mineral matrix relative to Si. The cumulative Mg RRR did plateau for the period from 17-40 days, after which it then proceeded to drift further from stoichiometric dissolution. It did appear not to be affected

by change in pH, but exhibited a steep negative trend during the second HS exposure.

The cumulative Na RRR curve (Figure 3.29) illustrates that Na was preferentially released until the first decrease in pH (pH 9 to 7), at which time the curve reached a plateau. During the first HS introduction, the Na curve (cumulative RRR) approached stoichiometric dissolution. After the first HS period, the rate seemed to again plateau (at Log(RRR) = 2.3), although a small dip in the curve is apparent during the second HS introduction.

3.2.2.4 FR tremolite cumulative release. Figures 3.30 to 3.32 illustrate the FRT cumulative release rates for the cations studied. Al, Na, and Si were the only cations that displayed a consistent increase with time. Al exhibited the most consistent behavior until the time of the second HS introduction. At this time, the slope of the Al release rate changed to a much steeper one and continued for the duration of the experiment, unaffected by the second decrease in pH (pH 7 to 6). The Na exhibited consistent increase with changes in slope at both change in pH and HS introductions. The Si cumulative release rate, however, illustrated an increase with time and steep releases due both to change in pH and to HS introductions. The cumulative release of the other cations reached plateaus, except during periods of pH change and HS introduction. During these periods, they exhibited varying degrees of release enhancement.

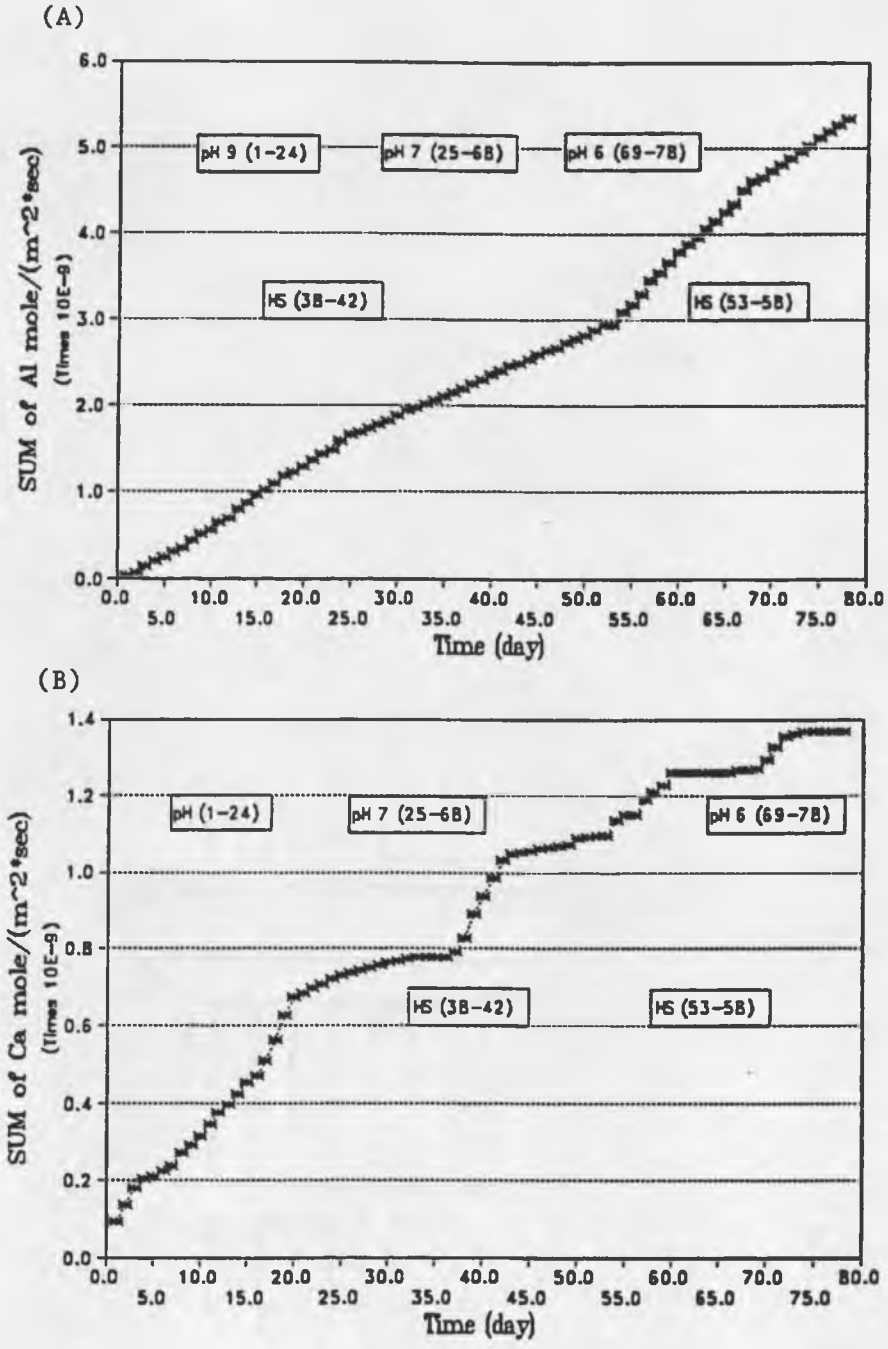

Figure 3.30 Tremolite flow-through bed reactor experiment cumulative release rates for (A) Al and (B) Ca

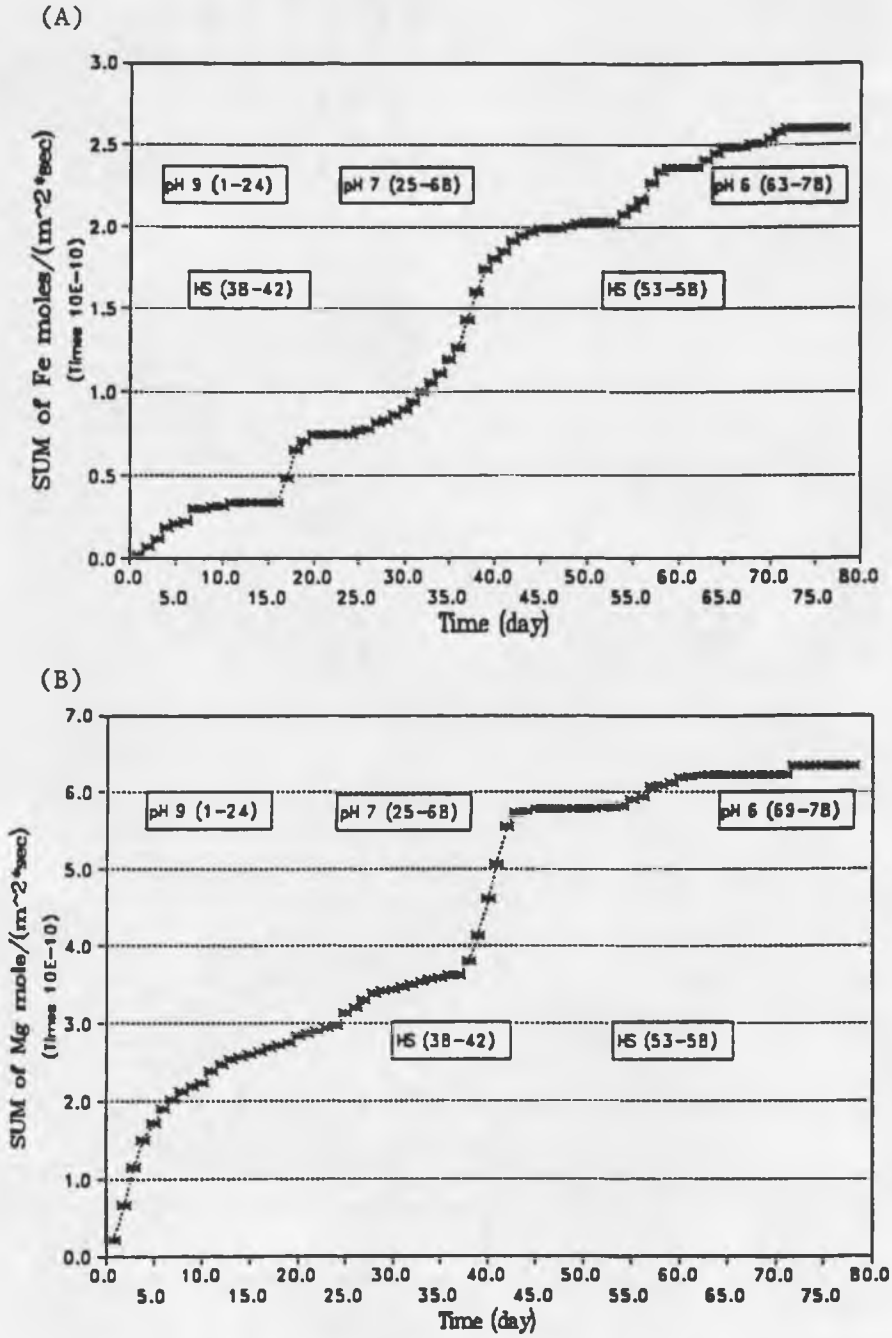

Figure 3.31 Tremolite flow-through bed reactor experiment cumulative release rates for (A) Fe and (B) Mg

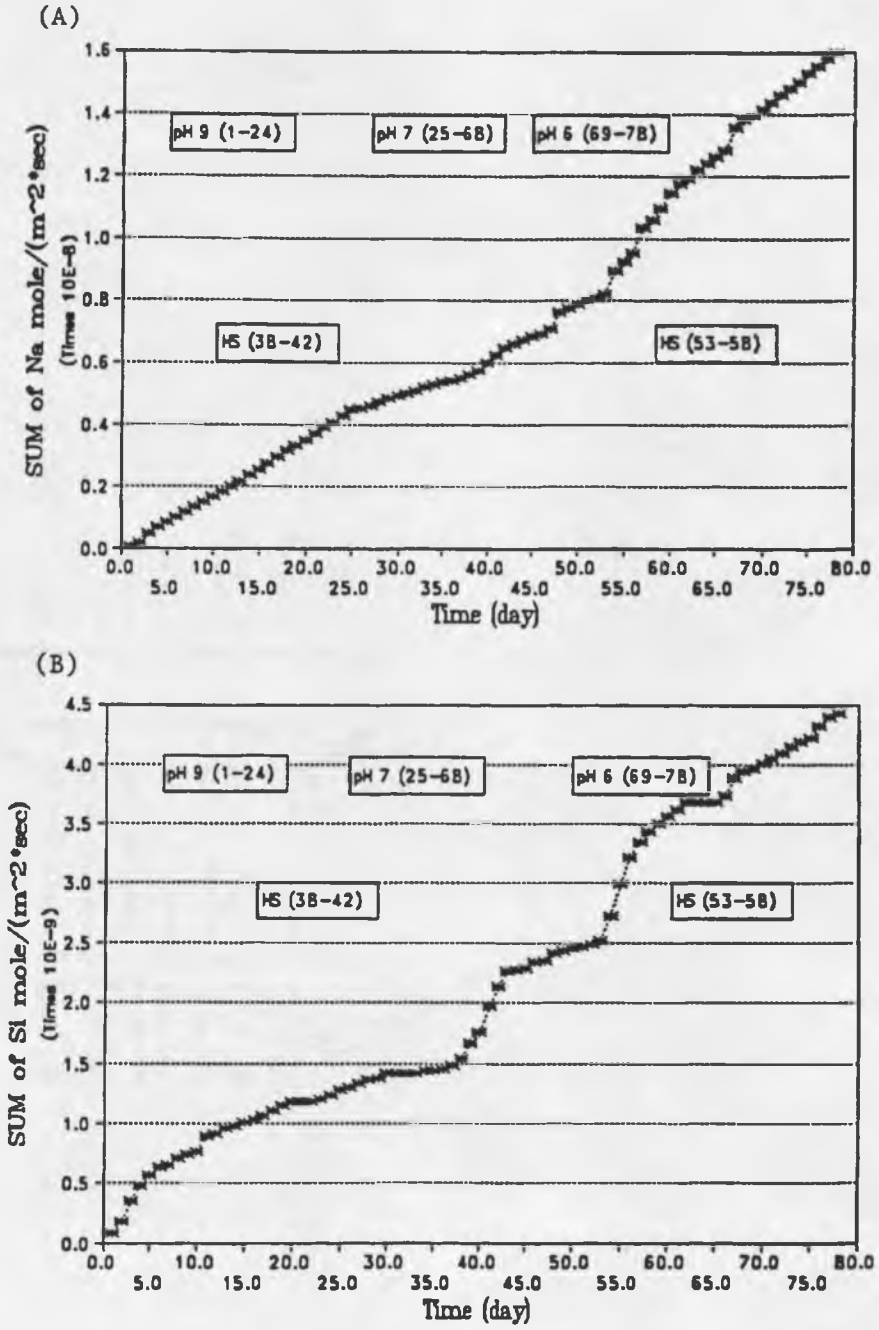

Figure 3.32 Tremolite flow-through bed reactor experiment cumulative release rates for (A) Na and (B) Si

3.3 Computer Models

SURFEQL (Westall et al., 1976) and WATEQ4F version 2.0 (Ball and Nordstrom, 1991) computer models were used in an effort to determine whether saturated conditions existed for both FR and BR experiments. pH and organic ligands were varied in the input files. Actual experimental concentrations of both batch and flow-through reactors (tabulated in Appendix 4) were used to determine whether saturated conditions existed. $Al(OH)_x^{(3-x)}$ and $Fe(OH)_x^{(3-x)}$ complexes were included as solid species in the models to determine whether secondary precipitates would form. Solubility constants used for the models were based on the WATEQ4F database, and a partial list is included in Table 3.9; examples of input data are given in Appendix 4.

Results from computer models (Table 3.10) indicated that some $Al(OH)_x^{(3-x)}$ complexes (diaspore, kaolinite, halloysite, and gibbsite) were saturated in the BR and FR experiments, with the exception of BR experiments at pH 4. For the constants used, some $Fe(OH)_x^{(3-x)}$ complexes (goethite and ferrihydrite) were saturated at the experimental concentrations for both types of experiments.

The BR and FR $Al(OH)_x^{(3-x)}$ experimental concentrations were higher than solubility limits. These concentrations may be due to rate limitations where the precipitation of $Al(OH)_x^{(3-x)}$ was slow to occur. In this study, equilibrium computer models were used. Both of the FR cumulative Al release curves

Table 3.9. Thermodynamic Data[1]

Temperature 25°C

Components[2]

AL^{+3} Ca^{+2} Fe^{+2} Mg^{+2} Na^{+} Si^{+4} H^{+} Cl^{-} OH^{-} Humate

Complexes[3]	Reactions	Log K
$CaOH^{+}$	$Ca^{2+} + H_2O = CaOH^{+} + H^{+}$	-12.78
$MgOH$	$Mg^{2+} + H_2O = MgOH^{+} + H^{+}$	-11.44
Fe^{3+}	$Fe^{3+} = Fe^{3+} e^{-}$	-13.02
$FeOH^{2+}$	$Fe^{3+} + H_2O = FeOH^{2+} + H^{+}$	-2.19
$FeOH^{+}$	$Fe^{2+} + H_2O = FeOH^{+} + H^{+}$	-9.5
$Fe(OH)_3^{-}$	$Fe^{3+} + 3H_2O = Fe(OH)_3^{-} + 3H^{+}$	-31.0
$Fe(OH)_2$	$Fe^{3+} + 2H_2O = Fe(OH)_2 + 2H^{+}$	-5.67
$Fe(OH)_3(aq)$	$Fe^{3+} + 3H_2O = Fe(OH)_3 + 3H^{+}$	-12.56
$Fe(OH)_4$	$Fe^{3+} 4H_2O = Fe(OH)_4^{-} + 4H^{+}$	-21.6
$Fe(OH)_2(aq)$	$Fe^{2+} + 2H_2O = Fe(OH)_2 + 2H^{+}$	-20.5
Magnetite	$Fe_3O_4 + 8H^{+} = 2Fe^{3+} + Fe^{2+} 4H_2O$	3.737
Hematite	$Fe_2O_3 6H^{+} = 2Fe^{3+} + 3H_2O$	-4.008
Maghemite	$Fe_2O_3 + 6H^{+} = 2Fe^{3+} 3H_2O$	6.386
Goethite	$FeOOH + 3H^{+} = Fe^{3+} 2H_2O$	-1.0
Ferrihydrite	$Fe(OH)_3 + 3H^{+} = Fe^{3+} + 3H_2O$	4.891
Gibbsite	$Al(OH)_3 + 3H^{+} = Al^{3+} + 3H_2O$	8.11
Boehmite	$AlOOH + 3H^{+} = Al^{3+} 2H_2O$	8.584
$kAlOH^{2+}$	$Al^{3+} + H_2O = AlOH^{2+} + H^{+}$	-5.00
$kAl(OH)_2^{+}$	$Al^{3+} + 2H_2O = Al(OH)_2^{+} + 2H^{+}$	-10.1
$kAl(OH)_4$	$Al^{3+} + 4H_2O = Al(OH)_4^{-} + 4H^{+}$	-22.7
$kAl(OH)_3(aq)$	$Al^{3+} + 3H_2O = Al(OH)_3 + 3H^{+}$	-16.9
Cristobalite	$SiO_2 + 2H_2O = H_4SiO_4$	-3.587
Silica gel	$SiO_2 + 2H_2O = H_4SiO_4$	-3.018
Quartz	$SiO_2 + 2H_2O = H_4SiO_4$	-3.018
Chalcedony	$SiO_2 + 2H_2O = H_4SiO_4$	-3.55
$SiO_2(a)$	$SiO_2 + 2H_2O = H_4SiO_4$	-2.71

[1] Cl^{-} was used to maintain charge balance
K_{so} from the WATEQ4F database was used

[2] Concentrations are tabulated in Appendix 4

Table 3.10. Computer Model Results[1]

		High concentration (mg/l)		Low concentration (mg/l)	
		Al	Fe	Al	Fe
FRH					
pH	6	Precip	Precip	Precip	Precip
	7	Precip	Precip	Precip	Precip
	9	Precip	Precip	Precip	Precip
FRT					
pH	6	Precip	Precip	Precip	Precip
	7	Precip	Precip	Precip	Precip
	9	Precip	Precip	Precip	Precip
BRH					
pH	4	Soluble	Precip	Soluble	Precip
	5	Precip	Precip	Precip	Precip
	6	Precip	Precip	Precip	Precip
BRT					
pH	4	Soluble	Precip	Soluble	Precip
	6	Precip	Precip	Precip	Precip

[1] Al and Fe phases that were tested for saturation are tabulated in Table 3.9

suggest that the aqueous Al concentrations did not plateau with time but had a linear release with time, thus suggesting that there was little precipitation of Al complexes from solution occurring. This release behavior corresponds with both BR Al relative release rate (hornblende and tremolite) curves, which suggested that the Al^{3+} had one of the highest rates of release.

The Fe (III) exhibited mixed results; only the BRH and FRH RRR curves showed varying degrees of Fe being retained in the mineral. The BRT and FRT RRR, however, did not show Fe (III) being preferentially retained in the mineral versus Si. The Fe (III) results are questionable due to the measured concentrations being near the detection limit.

CHAPTER 4

DISCUSSION

4.1 Tremolite Experiments

Three BRT experiments were completed at pH 4; the BRT cation release rate results are summarized in Table 3.6. They ranged from 10^{-12} to 10^{-10} moles/(m^2*sec) for different cations. The acid consumption rates for the BRT experiments are also depicted in Figure 3.6. The lower rate is not surprising, as the pH of the experiments was relatively low (pH 4). It can be seen from this figure that the curves become linear with time and have good reproducibility. The acid consumption rates that were measured proved to be three orders of magnitude lower than that measured by Hopkins (1989) (Table 3.5). It is believed that this discrepancy is due to artifacts in the Hopkins experiment, such as leaving the ultra-fines in her sample. The cation release rates measured in the batch reactors are similar to those measured in the flow-through reactors 10^{-11} to 10^{-13} moles/(m^2*sec), which is further evidence that Hopkins' results may be biased.

All the BRT cations that were measured displayed linear behavior and good reproducibility with the exception of Na (Figures 3.7-3.9). It is unknown why the Na displayed such poor results except that concentrations were close to the detection limit (50 ppb) brought about by 1+4 sample dilutions. In addition, the Al was the only BRT cation to exhibit negative trends (release rates). Previous studies by Lin and

Benjamin (1990) and Waite et al. (1988) have found negative Fe release rates for some of their minerals.

Results for computer simulations (SURFEQL and WATEQ4F version 2.0) for all BR and FR experiments suggest that several iron phases (goethite and ferrihydrite) were saturated and aluminum phases were unsaturated at pH 4. This is not what was observed for BR tremolite experiments, as Al exhibited a negative release rate and Fe a positive release rate. One possible explanation may be that conditions favored the measured negative trends for Al and not Fe; i.e., reactions for Fe may have been kinetically limited. This is possible as the Fe (II) must first be oxidized to Fe (III) before it can precipitate from solution. In order to keep this from occurring, oxygen concentrations were kept low in this system by bubbling N_2 through the experimental solutions. The computer models (equilibrium type) help to establish that conditions for a leached layer of aluminum hydroxide and iron hydroxide do exist but are not able to prove its existence. It is also doubtful, however, that either Al or Fe will have much effect on the mineral dissolution rate due to secondary precipitation for either mineral. The tremolite has only 0.06% atoms Al and 0.06% atoms Fe present, whereas hornblende has only 1.80% atoms Fe and 0.62% atoms Al.

Literature values of silica release rates for tremolite are tabulated in Table 4.1. In this table, it can be seen that the Si rate for this study (pH 4) is several orders of

Table 4.1. Silica Release Rates for Tremolite at pH 4*

Rate (r)$_2$ (mole/(m^2*sec))	Temperature	References
3.98 x10^{-12}	20^{0}C	Schott et al. (1981)
3.93 x10^{-10}	25^{0}C	Hopkins (1989)
3.13 x10^{-10}	25^{0}C	This study

*Data from Hopkins, 1989

magnitude greater than that of Schott et al. (1981) but comparable to that of Hopkins (1989). It is not unexpected that this study's Si release rate is similar to Hopkins due to the low SiO_2 solubility at this pH (pH 4). The cation dissolution rate for Si for the flow-through reactor (pH 6 to 9) is closer to that of Schott, ranging between 0.5 to $2x10^{-12}$ mole/(m^2*sec).

The ratio of the rate of Si release to other cations (RRR) gives information about stoichiometric dissolution and rate-limiting cations (when congruent dissolution occurs). The tremolite BR experiments done at pH 4 (Figures 3.10-3.11) showed that Al had the highest cation RRR. In addition, Mg was the only cation which appeared to be initially preferentially released and with time be retained in the mineral with respect to Si. (The figures which depict cumulative data (cumulative RRR and cumulative cation concentrations) have the inherent property of incorporating cumulative error into each successive data point). This may be an indicator that Mg or Si may be rate-limiting cations (Table 4.2). Although the tremolite study by Schott et al. (1981) found similar results as this study, i.e., both Ca and Mg had an initial period of incongruent release followed by congruent dissolution, they did not note any retention of Mg with time in the mineral. They speculated that a thin surface layer on the mineral was formed which was depleted in Mg that could serve as cation-limiting. Both the FRT (tremolite) Mg standard and cumulative

Table 4.2. Summary of Reasons for Mg or Si Retention

	Al	Ca	Fe	Mg	Na	Si
	FRH Hornblende					
Cumulative release Fig. 3.19-3.21	linear increase	plateau	plateau	increase	--	slow increase
Cumulative RRR for each cation Fig. 3.17-3.18	increase Positive away from zero	positive decrease to zero	negative plateau	negative increase to zero	--	--
Depth of leaching (Å) Table 3.6	23	37	2.9	1.9	--	3.0
	Batch Reactor (Hornblende)					
Order of RRR release[1]	2	1	5	4	3	--
	FRT Tremolite					
Cumulative release Fig 3.30-3.32	linear increase	plateau	plateau	plateau	increase	increase
Cumulative RRR for each cation Fig 3.27-3.29	positive plateau	positive decrease to zero	positive decrease after HS to zero	negative decrease away from zero	positive plateau	--
Depth of leaching (Å) Table 3.6	4.4×10^4	130	1600	29	--	52
	Batch Reactor (Tremolite)					
Order of RRR release	1	4	3	5	2	--

[1] 1=Highest and 5=Lowest

RRR curves (Figures 3.26a and 3.28b) illustrate that Mg appears to be retained in the mineral relative to Si, but this has to be qualified due to the poor Mg data for the latter part of the experiment. This helps to corroborate the Mg BRT RRR results. In addition, the cumulative Si release is much greater than the cumulative Mg release curves (FRT).

The use of the microprobe for the elemental analysis of the minerals has an intrinsic problem of error for lighter elements such as Al and Si. But an error up to 25% should have relatively little effect on the RRR results when these are expressed as logarithms.

An estimate for the depth of leaching for each cation was calculated as shown in Table 3.4, with Mg being the cation that was most retained. In all the previous literature on Mg-silicate dissolution studies, however, there does not seem to be any cases in which Mg is cited as a rate-limiting cation. This could be due to the studies using acidic solutions instead of basic solutions (Mast, personal communication, 1992). In Table 4.2, observations of RRR, cumulative release rates and depth of the leached layer are presented. Here, the Mg appears to be retained relative to the other cations.

In this study, the dissolution experiments by Mast and Drever (1987) were chosen as an analogue for the FR portion. Unfortunately, the mineral that they studied was anthophyllite, not tremolite, as described in their journal article (Mast, personal communication, 1992). Anthophyllite

$(Mg,Fe)_7Si_8O_{22}(OH)_2$ is a Ca-poor mafic or ultra-mafic rock rich in Mg (Blackburn and Dennen, 1988). The difference in composition between tremolite and anthophyllite can be most distinctly seen in Table 2.2. This should be kept in mind as analogies to their work are drawn.

Although no previous study was found which cited Mg as rate-limiting, there appears to be some evidence of this in previous studies done by Mast and Drever (1987) and Hopkins (1989). Some Hopkins (1989) RRR rates do reflect a slight negative trend for Mg at pH 4 and 6 using hornblende. In addition, in the article by Mast and Drever (1987), although Mg was not cited as being preferentially retained, one of their figures (Figure 11) does depict negative retention of Mg relative to Si at pH 4 and 5. Mast also noted Mg as rate-limiting in one of her flow-through experiments, done at basic pH, that is unpublished at this time (Mast, personal communication, 1992).

The RRR results depend on both Mg and Si release so it can also be hypothesized, as many researchers in the past have done, that Si is rate-limiting. Unfortunately, the results of this study cannot conclusively prove which cation controls dissolution, if rate-limiting cations do exist for hornblende or tremolite.

Part of the Mg bias in this study can be attributed to the manner in which the relative release rate curves were plotted, i.e., using cumulative values which reflect an

overall trend for the entire experiment. Using this technique, experimental errors are also accumulated. This might be very important for the tremolite experiments, where Mg was close to detection levels. Both standard Log(RRR) and cumulative Log(RRR) were used in this study to elucidate trends. Cumulative rates were helpful for cases where concentrations were at the detection limit (e.g., for Fe and Mg). The results for Mg (Figure 3.26a) are a good example; standard Log(RRR) for Mg could not be calculated after the 62nd day, as Mg concentrations were at the detection limit. Before day 62, however, the negative RRR is obvious. This is emphasized in Figure 3.28b for the Mg cumulative Log(RRR) curve.

The FR study of organic ligand enhancement showed Mg, Ca, Fe, and Na to be positively affected although not consistently in both mineral experiments (Table 3.8). One explanation for the Ca, Fe, and Mg behavior is that ultra-fines or preferential sites of dissolution, such as etch pits, are responsible for the initial enhancement (Mast and Drever, 1987). In contrast, Mast and Drever (1987) did not note any ligand enhancement for anthophyllite. Their experimental conditions differed from this study, not only in the mineral used, but the change in pH effects was studied in a separate experiment than the oxalate, which was done at constant pH.

No obvious dependence of release rates on pH was found in this study. This is in contrast to Mast and Drever (1987) who

found that, as pH increased, significant amounts of Si, but not Mg, were released, whereas, as pH decreased, significant levels of both Si and Mg were released. One difference in the experimental protocol between this study and Mast and Drever (1987) is that their equilibrium times were larger, and that only pH changes or additional ligand was added per flow-through reactor experiment. It is not obvious that this difference in protocol should have biased the results of this study.

4.2 Hornblende Experiments

For hornblende, pH and organic ligand effects were studied as well as the effect of surface area and dissolution rate by using three different size fractions. The relationship of surface area and reaction rate can be expressed as (Holdren and Speyer, 1985; Stumm and Wollast, 1990; Zinder et al., 1986; Hopkins, 1989):

$$\frac{dM_i}{dt} = fsk(T)n$$

where:

M_i = mass of dissolved solute i;

t = time;

k(T) = rate constant for dissolution reaction (a function of temperature);

s = surface area of the reactant;

f = ratio of effective total surface area of the reactant; and

n = stoichiometric coefficient i released by dissolution of one mole of reactant.

Three size fractions were examined in this study, > #30, #30-40 and #100-200. Although initial rates were different for the > #30 and for #30-40 and #100-200 size fractions, the linear dissolution rates were the same. One explanation for this lack of surface area dependence is the presence of micro-fractures or ultra-fines in the larger size ranges. The BET isotherm results indicated that the #30-40 size fraction had a larger surface area than the #100-200 size range, suggesting the presence of micro-fractures or ultra-fines. This observation suggests that the coarser size fractions (> #30) of hornblende should be studied. Holdren and Speyer (1985) measured dissolution rates for five size fractions of alkali feldspar and found different results. They found in their study that, with coarse minerals (everything > #200-400), dissolution rates are proportional to surface area. Holdren and Speyer (1985) also suggested that, for their mineral, dissolution rate was controlled more by reactions at crystal defects than by bulk surface area. The results from this study's hornblende BR experiments with different size fractions help reinforce this hypothesis.

When extrapolating results derived in the laboratory to the field, one must consider the major differences between the two types of studies. All the minerals used in this study were composed of freshly ground samples. It is believed that, except for ultra-fines, the influence of freshly ground mineral versus that of weathered material should not influence the results obtained as long as secondary precipitates do not control dissolution rates. Drever and Swoboda-Colberg (1989) showed no difference between dissolution rates of weathered and unweathered mineral in a study they did at Bear Brook, Maine.

Solubility calculations indicate that several Al and Fe phases were saturated for experiments run at pH 5-9 (Section 3.3); however, Al concentrations were below saturation for pH 4. Existence of an inhibiting layer on the BR hornblende mineral surface could not be proven at this time, although according to BRH cation relative release rates, Fe appears to be preferentially retained in the mineral matrix. The Fe cation release rates, however, could not corroborate these results due to there being only one negative release rate at pH 5 (Table 3.3). This may be due to kinetics limitations in the oxidation of Fe (II) to Fe (III) because of low oxygen content of the reactors. In addition, the Al was not found to remain behind in the mineral matrix; in fact, Al had one of the highest rates of relative release (RRR) for pH 4, 5, and

6. However, the Al did exhibit negative cation release rates at pH 5 and 6, which may suggest reprecipitation (Table 3.6).

In this study, the BR hornblende exhibited these RRR results, in order of highest release to lowest, Ca > Al > Na > Mg > Fe. Hopkins (1989) cited similar results with Ca and Na having the most pronounced RRR. She only did one experiment (hornblende at pH 5) which tested Al concentrations, the result of which showed non-linear behavior with time due to concentrations being at the detection limit.

In the BRH experiment, it was found that Mg was at or approached stoichiometric dissolution more quickly than any other cation for the pH used (4, 5, 6). In support of this, the Hopkins (1989) study also noted similar results. She found that Mg and Fe had a more rapid approach to stoichiometric dissolution than Ca and Na.

The acid consumption rates for the (pH 4) BR hornblende and tremolite are very close, 4.51×10^{-12} and 2.13×10^{-12} mole/(m^2*sec), respectively (Tables 3.2 and 3.5). The similar rates suggest that the dissolution process is similar for both minerals. One explanation is that the quantity of Fe present in both minerals is very small (Table 2.1 and 2.2) (even though tremolite has 1/30 the amount of Fe present in hornblende). The low Fe content and the similar dissolution rates suggest that Fe did not form a secondary precipitate layer in this study.

This study could not prove any pH dependence. One reason for not finding any pH dependence was due to drift at pH 6 which ranged up to 0.1 or 0.2 pH units. The Dosimat 665, which leaked acid, was a factor which may have had a detrimental effect on results. BR11-16 were affected by this problem, although the cation release rates for these experiments did not exhibit any gross variations from other experimental results.

The Si results of several previous dissolution studies done at pH 5 are summarized in Table 4.3. This list is only a partial listing and is in no way intended to make any pretense for being complete. Here, it can be seen that dissolution rates differ not only from mineral to mineral but study to study. For example, refer to hornblende which illustrates a difference in magnitude of two between this study's results versus that of Hopkins (1989). The differences can be attributed to such things as apparatus, temperature, and amount of effective surface area present.

This study's results implicate either Mg or Si as the best choice for the rate-limiting cations for both minerals in either apparatus (BR and FR) for the pH studied (Table 4.2). Mg contradicts the hypothesis posed by Mast and Drever (1987) that detachment of Si rather than Mg was involved in the rate-limiting step. The evidence for Mg retention in hornblende includes the FRH results of cation cumulative release (Figures 3.19-3.21). Cumulative cation release can compound errors,

Table 4.3. Tabulated Silica Release Rate at pH 5 and 25°C*

Mineral	Rate (r) (mole/(m^2*sec))	References
Quartz	4.1×10^{-14}	Rimstadt and Barnes (1980)
Muscovite	2.56×10^{-13}	Lin and Clemency (1981)
Forsterite	1.20×10^{-12}	Grandstaff (1980)
K-feldspar	1.67×10^{-12}	Busenberg and Clemency (1976)
Albite	1.19×10^{-11}	Holdren and Berner (1979)
Enstatite	1.0×10^{-10}	Schott et al. (1981)
Diopside	1.40×10^{-10}	" "
Hornblende	2.51×10^{-10}	Hopkins (1989)
Hornblende	4.84×10^{-12}	This study
Tremolite	2.81×10^{-10}	Hopkins (1989)
Anorthite	5.60×10^{-9}	Fleer (1982)

*Data from Hopkins, 1989

however, and the standard RRR curves do not show the same retention (Figure 3.16). The FRH and FRT Al cumulative mole curves did not plateau as did Fe (Figures 3.19-3.21 and 3.30-3.32) as would be expected for less soluble elements. In addition, the FRH cumulative RRR (Figures 3.17-3.18) indicated that Fe was retained in the mineral. Mg was also implicated as being retained in the mineral in the depth of leaching calculations as being the least soluble (Table 3.4). However, the BRH RRR curves are not as conclusive; they indicated Fe as being preferentially retained, whereas Mg was close to stoichiometric dissolution. The relative error for Fe and Mg analysis, respectively, was 0.30 and 0.08.

The FRT (tremolite) evidence for Mg as rate-limiting is based on both the standard and cumulative RRR results; however, the lack of data for the last part in the experiment complicates analysis. The FRT cumulative RRR results (Figures 3.28-3.30) show that Mg was the only cation which was preferentially retained in the mineral relative to Si, both of which are significant constituents of tremolite, respectively 13.5% and 20.8% atoms. The cumulative Mg RRR curve is influenced by dissolution behavior of Mg and Si. In this case, the cumulative release rate curves (Figures 3.31b and 3.32b) show that Si had a distinct pronounced release with time, while Mg had a lower release rate. In addition, Mg had the least amount leached out of the mineral according to the depth of leaching calculation. The BRT RRR results also add support for Mg as

a rate-limiting cation (Figures 3.10-3.11). They depict the Mg as being preferentially retained. The FRT cation cumulative release ratios (Figures 3.30-3.32) do not contradict this hypothesis. In these figures, only Al, Na, and Si exhibited significant increases in release rate with time.

CHAPTER 5

CONCLUSIONS

Mineral dissolution is the major process of neutralizing acid deposition over time (Mast and Drever, 1987). However, the immediate amount of ANC provided by amphibole minerals over short time scales (hours to days) provides small amounts of buffering. In this study, the hornblende and tremolite dissolution rates were in the range obtained for other minerals, but still can be very slow (Tables 3.2 and 3.5) compared to residence time of surface water in a watershed.

In alpine regions in the western United States, such as the Sierra Nevada, many watersheds contain little soil. The rate of mineral weathering is highly dependent on mineral contact time. This suggests that one of the most important parameters in evaluating acid rain sensitivity in alpine regions is the mineral-water contact time as well as mineral soil distribution.

A hypothetical example of the potential buffering capacity found in a watershed can be estimated if certain parameters are known. Important initial conditions that would be required include contact time, effective surface area, pH of solution, and soil composition. In the Sierra Nevada, Emerald Lake (EML) has been the subject of numerous scientific studies which have focused on characterizing the area (e.g., Wolford, 1992). An estimate of buffering capacity attributed to hornblende in EML has been done for that location. The

parameters for the soil surface area (1.2 m^2/g) and soil mass ($202x10^6$ kg) for EML (Wolford, 1992) have been used. In addition, acid consumption rates for hornblende (Table 3.2) have been used in the calculations. Using the acid consumptions measured in this study for pH 4, 5, and 6, the acid consumption rate for hornblende is:

$$H^+ \frac{mole}{yr} =$$

$$\left(H^+ rate \frac{mole}{m^2 * sec}\right)\left(3600 \frac{sec}{hr}\right)\left(24 \frac{hr}{day}\right)\left(365 \frac{day}{yr}\right)\left(1.2 \frac{m^2}{g}\right) 202 * 10^6 kg)$$

To determine the acid consumption rate for a soil that is only partially composed of hornblende, the following equation was used:

$$\left(H^+ \frac{mole}{yr}\right) (\% \text{ hornblende composition}) = H^+ \frac{mole}{yr} \text{ hornblende}$$

For these estimates, soil with a 0.1% hornblende composition was assumed. The results indicated that hornblende can be an important source of acid neutralizing capacity at soil concentrations $\geq$ 0.1% (pH 4 $3.44x10^4$ H^+ mole/yr hornblende). This can be compared to the average wet deposition of $1.5x10^5$ mole/yr (Bales, 1993). These results show that further research on hornblende is warranted.

One important area of research that needs to be investigated is the applicability of laboratory measured dissolution rates to field situations. These laboratory rates could be significantly higher than dissolution rates for in-situ

minerals. Mineral dissolution rates measured in the laboratory can be up to three orders of magnitude higher than that measured in the field (Velbel, 1990; Drever and Swoboda-Colberg, 1989). The reasons for this overestimation include temperature differences and, more importantly, effective surface area. Surface area affected by contacting solutions is considered to be the main parameter responsible for the discrepancy between laboratory and field estimates in mineral dissolution rates (Velbel, 1990; Drever and Swoboda-Colberg, 1989). Because of these reasons, more work needs to be done to characterize hornblende so that the dissolution rates obtained can be extrapolated into the field. The surface area anomaly (particle size difference) noted earlier in this paper for hornblende should be investigated to determine if this is consistent for the mineral. Temperature effects as well as a more in-depth investigation of pH behavior also need to be studied.

APPENDIX 1

HORNBLENDE BATCH REACTOR CONCENTRATIONS

APPENDIX 1

HORNBLENDE BATCH REACTOR CONCENTRATIONS

pH 4

1/9/92 Hornblende (mg/l)
2.5004 g Gilmont > #30
BR6 (500 ml reactor & large stirrer)

Sample#	Time (Hr)	Al	Ca	Fe	Mg	Na	Si	Sample Size (ml)
1	1.00	0.36	5.05	0.79	0.63	0.88	1.00	5.0
2	10.07	0.70	5.95	1.10	1.44	1.17	1.38	5.0
3	45.00	0.63	6.30	1.06	1.50	1.80	1.37	5.0
4	70.00	3.79	6.45	1.15	2.39	1.81	7.15	4.8
5	90.00	0.87	6.20	0.70	1.83	1.25	3.11	5.0

1/17/92 Hornblende (mg/l)
5.003 g Gilmont > #30
BR7 (500 ml reactor & large stirrer)

Sample#	Time (Hr)	Al	Ca	Fe	Mg	Na	Si	Sample Size (ml)
1	0.97	0.15	3.75	0.23	0.68	1.09	0.55	5.0
2	20.00	0.03	4.85	1.07	1.04	1.18	1.78	5.0
3	45.00	0.17	5.60	1.28	1.38	1.34	3.04	5.0
4	70.00	0.18	5.65	1.39	1.42	1.46	3.74	5.0
5	90.25	0.31	6.15	1.47	1.87	2.02	4.24	5.0

APPENDIX 1 (continued)

pH 4

4/9/92 Hornblende (mg/l)
2.5001 g Dosimat #30-40
BR11 (500 ml reactor & large stirrer)

Sample#	Time (Hr)	Al	Ca	Fe	Mg	Na	Si	Sample Size (ml)
1	20.00	0.49	0.24	0.12	0.25	0.66	0.16	5.0
2	40.00	0.13	0.21	0.15	0.31	0.51	0.40	5.0
3	60.00	0.22	0.37	0.35	0.63	0.96	0.92	5.0
4	80.00	0.16	0.44	0.22	0.63	0.79	1.02	5.0
5	100.00	0.20	0.55	0.31	0.79	1.22	1.40	5.0
6	120.00	0.25	0.85	0.37	0.95	1.55	1.63	5.0
7	140.00	0.26	1.28	0.50	1.27	1.66	2.29	5.0

5/2/92 Hornblende (mg/l)
2.5001 g Dosimat #100-200
BR14 (500 ml reactor & large stirrer)

Sample#	Time (Hr)	Al	Ca	Fe	Mg	Na	Si	Sample Size (ml)
1	20.00	0.22	4.75	2.37	0.39	1.32	0.37	5.0
2	60.00	0.22	4.65	2.96	0.48	0.83	0.73	5.0
3	100.00	0.21	4.70	3.19	0.54	0.84	1.01	5.0
4	120.00	0.27	4.65	3.15	0.57	1.23	1.09	5.0
5	140.00	0.32	4.95	3.36	0.69	1.23	1.27	5.0

APPENDIX 1 (continued)

pH 4

6/12/92 Hornblende (mg/l)
4.9998 g Gilmont #30-40
BR19 (500 ml reactor & large stirrer)

Sample#	Time (Hr)	Al	Ca	Fe	Mg	Na	Si	Sample Size (ml)
1	10.67	0.27	2.15	0.39	0.23	0.81	0.12	5.0
2	20.00	0.19	2.85	0.50	0.34	0.45	0.29	5.0
3	40.00	0.05	2.05	0.68	0.47	0.46	0.83	5.0
4	60.00	0.20	2.10	0.71	0.63	0.65	0.85	5.0

6/16/92 Hornblende (mg/l)
2.4998 g Gilmont #100-200
BR20 (500 ml reactor & large stirrer)

Sample#	Time (Hr)	Al	Ca	Fe	Mg	Na	Si	Sample Size (ml)
1	10.00	0.21	5.25	1.65	0.31	0.21	0.52	5.0
2	20.00	0.12	5.50	2.39	0.35	0.19	0.60	5.0
3	40.00	0.17	5.50	2.67	0.39	0.43	0.73	5.0
4	60.00	0.08	5.25	2.30	0.41	0.51	0.92	5.0
5	80.00	0.24	5.75	2.62	0.48	0.45	0.86	5.0
6	91.00	0.38	6.90	2.72	0.53	0.47	0.95	5.0

APPENDIX 1 (continued)

pH 5

1/21/92 Hornblende (mg/l)
2.5004 g Gilmont > #30
BR8 (500 ml reactor & large stirrer)

Sample#	Time (Hr)	Al	Ca	Fe	Mg	Na	Si	Sample Size (ml)
1	1.03	1.10	3.30	0.13	0.65	2.44	2.30	5.0
2	21.07	1.06	4.65	0.66	1.18	1.41	3.77	5.0
3	42.78	1.09	5.00	0.95	1.28	1.02	7.40	5.0
4	70.10	1.10	5.35	1.07	1.49	1.37	4.66	5.0
5	90.53	1.10	5.45	1.02	1.68	1.28	5.82	5.0

2/2/92 Hornblende (mg/l)
2.5004 g Gilmont > #30
BR9 (500 ml reactor & large stirrer)

Sample#	Time (Hr)	Al	Ca	Fe	Mg	Na	Si	Sample Size (ml)
1	1.05	1.26	4.90	0.09	0.61	1.01	0.60	5.0
2	20.00	1.24	5.00	0.49	1.00	1.51	1.01	5.0
3	45.00	1.34	5.50	0.72	1.25	1.05	1.57	5.0
4	70.00	1.29	5.40	0.89	1.34	1.16	1.68	5.0
5	90.00	1.34	5.85	0.91	1.56	1.27	2.32	5.0

APPENDIX 1 (continued)

pH 5

4/17/92 Hornblende (mg/l)
2.4999 g Dosimat #30-40
BR12 (500 ml reactor & large stirrer)

Sample#	Time (Hr)	Al	Ca	Fe	Mg	Na	Si	Sample Size (ml)
1	20.33	0.32	1.35	0.11	0.33	0.57	0.93	5.0
2	40.58	0.19	1.50	0.18	0.44	1.33	1.14	5.0
3	60.00	0.24	2.10	0.21	0.64	0.88	1.54	5.0
4	80.00	0.22	1.60	0.17	0.71	0.90	1.87	5.0
5	100.00	0.23	2.25	0.25	0.83	0.92	2.33	5.0
6	120.00	0.20	1.80	0.25	0.85	0.88	2.47	5.0
7	140.00	0.20	1.65	0.23	0.94	0.94	2.85	5.0

4/17/92 Hornblende (mg/l)
2.5000 g Dosimat #100-200
BR15 (500 ml reactor & large stirrer)

Sample#	Time (Hr)	Al	Ca	Fe	Mg	Na	Si	Sample Size (ml)
1	20.00	0.26	4.85	0.74	0.30	0.45	0.13	5.0
2	40.00	0.25	4.20	1.27	0.29	0.57	0.21	5.0
3	60.00	0.28	5.00	1.70	0.42	0.52	0.44	6.0
4	80.00	0.29	4.80	1.69	0.40	0.70	0.57	5.0
5	100.00	0.27	5.35	1.71	0.49	1.16	0.72	5.0
6	120.00	0.27	5.10	1.75	0.48	1.18	0.88	5.0
7	140.00	0.24	5.00	1.72	0.49	0.87	0.94	5.0

APPENDIX 1 (continued)

pH 5

6/23/92 Hornblende (mg/l)
4.9997 g Gilmont #100-200
BR21 (500 ml reactor & large stirrer)

Sample#	Time (Hr)	Al	Ca	Fe	Mg	Na	Si	Sample Size (ml)
1	10.00	0.14	6.20	0.85	0.43	0.42	0.16	5.0
2	-	-	-	-	-	-	-	-
3	40.00	0.10	6.80	2.13	0.55	0.47	0.97	5.0
4	60.00	0.26	8.10	2.68	0.69	0.89	1.00	5.0
5	80.00	0.24	7.05	2.72	0.73	0.82	1.03	5.0

6/27/92 Hornblende (mg/l)
2.5000 g Gilmont #100-200
BR22 (500 ml reactor & large stirrer)

Sample#	Time (Hr)	Al	Ca	Fe	Mg	Na	Si	Sample Size (ml)
1	10.00	0.29	5.35	0.84	0.26	0.33	0.21	5.0
2	20.00	0.16	7.40	1.06	0.32	0.17	0.31	5.0
3	40.00	0.02	7.10	1.44	0.35	0.19	0.83	5.0
4	60.00	0.07	7.35	1.86	0.38	0.26	0.65	5.0
5	80.00	0.04	7.20	2.05	0.40	0.45	0.72	5.0

APPENDIX 1 (continued)

pH 6

9/17/91 Hornblende (mg/l)
Gilmont > #30
BR2 (250 ml reactor & stir plate)

Sample#	Time (Hr)	Al	Ca	Fe	Mg	Na	Si	Sample Size (ml)
1	5.08	0.83	1.10	0.09	0.99	1.39	5.25	5.0
2	10.00	0.07	1.60	0.55	0.50	0.00	-	5.0
3	20.25	0.41	1.60	0.61	0.60	0.00	1.80	5.0
4	30.00	0.36	1.80	0.84	0.60	0.09	3.06	5.0
5	45.17	0.45	1.80	0.66	0.70	2.70	-	5.0
6	60.00	0.30	2.00	0.29	0.90	1.39	5.21	7.0
7	81.00	0.41	2.40	0.44	1.10	4.14	6.65	7.0

10/30/91 Hornblende (mg/l)
2.4999 g Gilmont > #30
BR4 (500 ml reactor & large stirrer)

Sample#	Time (Hr)	Al	Ca	Fe	Mg	Na	Si	Sample Size (ml)
1	5.05	0.23	5.07	0.02	0.65	1.80	0.79	9.8
2	9.98	0.13	5.43	0.49	0.96	2.70	1.23	8.8
3	20.03	0.10	5.79	0.46	1.07	3.20	1.69	9.0
4	39.97	0.07	5.97	0.44	1.20	1.80	2.66	8.8
5	54.98	0.39	5.97	0.37	0.94	1.30	1.86	8.7
6	70.50	0.43	6.33	0.47	1.29	1.30	2.40	8.6
7	90.50	-	5.43	0.47	1.20	1.80	2.80	8.8

APPENDIX 1 (continued)

pH 6

2/11/92 Hornblende (mg/l)
2.5004 g Gilmont > #30
BR10 (500 ml reactor & large stirrer)

Sample#	Time (Hr)	Al	Ca	Fe	Mg	Na	Si	Sample Size (ml)
1	10.50	0.13	6.85	0.26	1.11	2.08	0.00	5.0
2	22.50	0.24	7.15	1.11	1.38	1.51	1.11	5.0
3	34.00	0.25	6.30	0.94	1.43	0.91	0.94	5.0
4	53.25	0.16	5.20	0.53	1.04	0.95	0.53	5.0
5	70.50	0.11	5.45	0.54	1.16	0.84	0.54	5.0
6	96.65	0.13	5.00	0.52	1.15	1.03	0.52	5.0

4/25/92 Hornblende (mg/l)
2.5001 g Dosimat #30-40
BR13 (500 ml reactor & large stirrer)

Sample#	Time (Hr)	Al	Ca	Fe	Mg	Na	Si	Sample Size (ml)
1	20.00	0.18	1.10	0.05	0.32	0.55	0.91	5.0
2	40.00	0.19	1.55	0.04	0.48	0.79	1.60	5.0
3	60.00	0.14	1.50	0.05	0.57	0.69	2.01	6.0
4	80.00	0.14	2.85	0.07	0.88	1.39	3.42	5.0
5	100.00	0.18	1.70	0.07	1.12	0.80	4.48	5.0
6	120.00	0.23	2.65	0.12	1.51	1.58	6.13	5.0
7	140.00	0.19	4.00	0.21	2.05	2.60	8.30	5.0

APPENDIX 1 (continued)

pH 6

7/1/92 Hornblende (mg/l)
2.4996 g Gilmont #100-200
BR23 (500 ml reactor & large stirrer)

Sample#	Time (Hr)	Al	Ca	Fe	Mg	Na	Si	Sample Size (ml)
1	10.00	0.31	4.65	0.33	0.24	0.55	0.83	9.0
2	21.67	0.00	21.45	0.39	0.33	0.56	0.98	5.0
3	40.00	0.17	5.85	0.81	0.31	0.33	1.34	5.0
4	60.00	0.00	5.75	1.23	0.36	0.32	1.41	5.0
5	80.00	0.00	6.70	1.45	0.42	0.35	1.67	5.0

APPENDIX 1 (continued)

HORNBLENDE H^+ VERSUS TIME DATA

BR6 pH 4 (2.5004 g)

Elapsed Time (hr)	Volume H^+ (ml)	Mole/m^2 H^+
0.0	0.0000	0.00×10^{0}
5.0	0.9649	9.44×10^{-5}
10.0	1.0535	1.03×10^{-4}
20.0	1.1355	1.11×10^{-4}
30.0	1.1385	1.11×10^{-4}
40.0	1.2048	1.18×10^{-4}
50.0	1.2048	1.18×10^{-4}
60.0	1.2048	1.18×10^{-4}
70.0	1.2395	1.21×10^{-4}
80.0	1.2395	1.21×10^{-4}
90.0	1.2395	1.21×10^{-4}

BR7 pH 4 (5.003 g)

Elapsed Time (hr)	Volume H^+ (ml)	Mole/m^2 H^+
0.0	0.0000	0.00×10^{0}
5.0	1.0005	4.89×10^{-5}
10.0	1.0955	5.35×10^{-5}
20.0	1.1640	5.69×10^{-5}
30.0	1.1918	5.82×10^{-5}
40.0	1.2255	5.99×10^{-5}
50.0	1.2370	6.05×10^{-5}
60.0	1.2370	6.05×10^{-5}
70.0	1.2400	6.06×10^{-5}
80.0	1.2400	6.06×10^{-5}
90.0	1.2500	6.11×10^{-5}

APPENDIX 1 (continued)

BR19 pH 4 (4.9998 g)

Elapsed Time (hr)	Volume H^+ (ml)	Mole/m^2 H^+
0.0	0.0000	0.00×10^{0}
1.0	0.0060	6.56×10^{-8}
5.0	0.0210	2.29×10^{-7}
10.0	0.0320	3.50×10^{-7}
15.0	0.0410	4.48×10^{-7}
20.0	0.0520	5.68×10^{-7}
30.0	0.0560	6.12×10^{-7}
40.0	0.0860	9.40×10^{-7}
50.1	0.0860	9.40×10^{-7}
59.4	0.0920	1.01×10^{-6}

BR20 pH 4 (2.4998 g)

Elapsed Time (hr)	Volume H^+ (ml)	Mole/m^2 H^+
0.0	0.0000	0.00×10^{0}
0.5	0.1710	5.40×10^{-7}
1.0	0.2530	7.92×10^{-7}
5.0	0.5690	1.78×10^{-6}
10.0	0.6620	2.07×10^{-6}
15.0	0.6750	2.11×10^{-6}
20.0	0.6950	2.18×10^{-6}
30.1	0.6950	2.18×10^{-6}
40.1	0.6950	2.18×10^{-6}
50.1	0.7090	2.22×10^{-6}
60.1	0.7370	2.31×10^{-6}
70.1	0.7450	2.33×10^{-6}
80.9	0.7450	2.33×10^{-6}
91.0	0.7450	2.33×10^{-6}
100.8	0.7450	2.33×10^{-6}

APPENDIX 1 (continued)

BR8 pH 5 (2.5004 g)

Elapsed Time (hr)	Volume H^+ (ml)	Mole/m^2 H^+
0.0	0.0000	0.00×10^{0}
5.0	0.5248	5.13×10^{-5}
10.0	0.6299	6.16×10^{-5}
20.0	0.7010	6.85×10^{-5}
30.0	0.7323	7.16×10^{-5}
40.0	0.7585	7.42×10^{-5}
50.0	0.7635	7.47×10^{-5}
60.0	0.7635	7.47×10^{-5}
70.0	0.7645	7.48×10^{-5}
80.0	0.7645	7.48×10^{-5}
90.0	0.7645	7.48×10^{-5}

BR9 pH 5 (2.5003 g)

Elapsed Time (hr)	Volume H^+ (ml)	Mole/m^2 H^+
0.0	0.0000	0.00×10^{0}
1.2	0.6375	6.23×10^{-5}
15.8	0.8850	8.65×10^{-5}
18.3	0.9140	8.94×10^{-5}
41.3	0.9425	9.22×10^{-5}
68.1	0.9565	9.35×10^{-5}
88.9	0.9565	9.35×10^{-5}

APPENDIX 1 (continued)

BR15 pH 5 (2.5000 g)

Elapsed Time (hr)	Volume H^+ (ml)	Mole/m^2 H^+
1.0	0.0000	0.00×10^{0}
5.0	0.0150	4.70×10^{-8}
10.0	0.0400	1.25×10^{-7}
19.0	0.0600	1.88×10^{-7}
49.0	0.0950	2.97×10^{-7}
99.0	0.1350	4.23×10^{-7}

BR21 pH 5 (2.4998 g)

Elapsed Time (hr)	Volume H^+ (ml)	Mole/m^2 H^+
0.0	0.0000	0.00×10^{0}
0.5	0.0226	3.53×10^{-8}
1.0	0.0379	5.93×10^{-8}
5.0	0.2023	3.17×10^{-7}
10.0	0.2885	4.52×10^{-7}
20.0	0.3288	5.15×10^{-7}
30.0	0.3377	5.29×10^{-7}
40.1	0.3409	5.34×10^{-7}
50.1	0.3409	5.34×10^{-7}
60.1	0.3409	5.34×10^{-7}
71.0	0.3409	5.34×10^{-7}
79.6	0.3409	5.34×10^{-7}

APPENDIX 1 (continued)

BR22 pH 5 (2.5000 g)

Elapsed Time (hr)	Volume H^+ (ml)	Mole/m^2 H^+
0.0	0.0000	0.00×10^{0}
1.0	0.1080	3.38×10^{-7}
2.0	0.1580	4.95×10^{-7}
5.0	0.3340	1.05×10^{-6}
7.0	0.4330	1.36×10^{-6}
10.0	0.5410	1.69×10^{-6}
15.0	0.6395	2.00×10^{-6}
20.0	0.6885	2.16×10^{-6}
25.0	0.7110	2.23×10^{-6}
30.1	0.7265	2.27×10^{-6}
40.1	0.7525	2.36×10^{-6}
50.1	0.7775	2.43×10^{-6}
60.1	0.7990	2.50×10^{-6}
69.9	0.8095	2.53×10^{-6}
80.0	0.8185	2.56×10^{-6}

BR2 pH 6 (2.5000 g)

Elapsed Time (hr)	Volume H^+ (ml)	Mole/m^2 H^+
0.0	0.0000	0.00×10^{0}
5.0	1.7749	1.74×10^{-5}
10.0	2.1300	2.08×10^{-5}
20.0	2.5680	2.51×10^{-5}
30.0	3.0750	3.01×10^{-5}
40.0	3.4810	3.40×10^{-5}
50.0	3.8310	3.75×10^{-5}
60.0	4.9162	4.81×10^{-5}
70.0	5.8380	5.71×10^{-5}

APPENDIX 1 (continued)

BR4 pH 6 (2.4999 g)

Elapsed Time (hr)	Volume H^+ (ml)	Mole/m^2 H^+
0.0	0.0000	0.00×10^{0}
5.0	0.5805	5.68×10^{-5}
10.0	0.6450	6.31×10^{-5}
20.0	0.7085	6.93×10^{-5}
30.0	0.7280	7.12×10^{-5}
40.0	0.7495	7.33×10^{-5}
50.0	0.7625	7.46×10^{-5}
60.0	0.7655	7.49×10^{-5}
70.0	0.7763	7.59×10^{-5}
80.0	0.7800	7.63×10^{-5}
90.0	0.7855	7.68×10^{-5}

BR10 pH 6 (2.5004 g)

Elapsed Time (hr)	Volume H^+ (ml)	Mole/m^2 H^+
0.0	0.0000	0.00×10^{0}
5.0	0.6963	6.81×10^{-5}
10.0	0.7813	7.64×10^{-5}
20.0	0.8600	8.41×10^{-5}
30.0	0.8913	8.71×10^{-5}
40.0	0.9138	8.94×10^{-5}
50.0	0.9313	9.11×10^{-5}
60.0	0.9363	9.16×10^{-5}
70.0	0.9543	9.33×10^{-5}
80.0	0.9688	9.47×10^{-5}
90.0	0.9850	9.63×10^{-5}
96.5	0.9918	9.70×10^{-5}

APPENDIX 1 (continued)

BR13 pH 6 (2.5001 g)

Elapsed Time (hr)	Volume H^+ (ml)	Mole/m^2 H^+
0.0	0.0000	0.00×10^{0}
0.5	0.0160	3.50×10^{-8}
1.0	0.0220	4.81×10^{-8}
5.2	0.0500	1.09×10^{-7}
8.0	0.0680	1.49×10^{-7}
11.0	0.0820	1.79×10^{-7}
19.1	0.1200	2.62×10^{-7}
26.2	0.1440	3.15×10^{-7}
29.1	0.1540	3.37×10^{-7}
37.0	0.1860	4.06×10^{-7}
39.7	0.1960	4.28×10^{-7}
45.1	0.2120	4.63×10^{-7}
54.3	0.2420	5.29×10^{-7}
61.8	0.2620	5.73×10^{-7}
67.9	0.2880	6.29×10^{-7}
74.1	0.3100	6.77×10^{-7}
80.1	0.3380	7.39×10^{-7}
89.0	0.3800	8.30×10^{-7}
98.0	0.4320	9.44×10^{-7}
100.0	0.4440	9.70×10^{-7}
106.1	0.5140	1.12×10^{-6}
110.0	0.5680	1.24×10^{-6}

BR23 pH 6 (2.4999 g)

Elapsed Time (hr)	Volume H^+ (ml)	Mole/m^2 H^+
0.0	0.0000	0.00×10^{0}
0.5	0.0070	2.19×10^{-8}
1.0	0.0385	1.21×10^{-7}
5.0	0.1710	5.35×10^{-7}
10.0	0.2975	9.32×10^{-7}
20.0	0.3430	1.07×10^{-6}
30.0	0.3430	1.07×10^{-6}
40.0	0.3430	1.07×10^{-6}
50.1	0.3430	1.07×10^{-6}
60.1	0.3430	1.07×10^{-6}
70.1	0.3430	1.07×10^{-6}
79.9	0.3430	1.07×10^{-6}

APPENDIX 2

TREMOLITE BATCH REACTOR CONCENTRATIONS

APPENDIX 2

TREMOLITE BATCH REACTOR CONCENTRATIONS

pH 6

6/3/92 Tremolite (mg/l)
2.4999 g Gilmont #100-200
BR18 (500 ml reactor & large stirrer)

Sample#	Time (Hr)	Al	Ca	Fe	Mg	Na	Si	Sample Size (ml)
1	10.25	0.22	0.70	0.04	0.42	0.37	1.62	5.0
2	20.00	0.24	1.15	0.07	0.50	0.64	2.07	5.0
3	40.00	0.20	0.95	0.11	0.56	0.61	2.72	5.0
4	60.00	0.06	0.90	0.46	0.61	0.67	2.80	5.0
5	80.00	0.09	0.85	0.10	0.60	0.70	3.07	5.0
6	90.00	0.02	2.60	0.06	0.63	0.80	2.89	5.0

pH 4

7/15/92 Tremolite (mg/l)
2.4999 g Gilmont #100-200
BR25 (500 ml reactor & large stirrer)

Sample#	Time (Hr)	Al	Ca	Fe	Mg	Na	Si	Sample Size (ml)
1	10.00	0.21	0.90	0.07	0.38	0.69	0.42	5.0
2	20.83	0.19	0.85	0.08	0.42	0.47	0.68	5.0
3	40.00	0.19	1.35	0.11	0.48	0.85	0.93	5.0
4	60.00	0.17	1.30	0.11	0.52	0.58	1.14	5.0
5	80.00	0.17	1.45	0.12	0.58	0.45	1.37	5.0

APPENDIX 2 (continued)

pH 4

7/21/92 Tremolite (mg/l)
2.4996 g Gilmont #100-200
BR26 (500 ml reactor & large stirrer)

Sample#	Time (Hr)	Al	Ca	Fe	Mg	Na	Si	Sample Size (ml)
1	10.00	0.17	0.80	0.05	0.38	0.53	0.69	5.0
2	20.00	0.14	1.05	0.12	0.49	0.55	0.98	5.0
3	40.00	0.14	1.50	0.14	0.52	0.85	1.48	5.0
4	60.00	0.13	1.70	0.15	0.61	0.53	1.77	5.0
5	80.00	0.15	1.95	0.19	0.65	0.68	2.06	5.0

7/24/92 Tremolite (mg/l)
2.5001 g Gilmont #100-200
BR27 (500 ml reactor & large stirrer)

Sample#	Time (Hr)	Al	Ca	Fe	Mg	Na	Si	Sample Size (ml)
1	10.00	0.27	0.70	0.03	0.34	0.20	0.29	5.0
2	20.08	0.25	0.90	0.09	0.39	0.28	0.55	5.0
3	40.05	0.26	1.20	0.09	0.49	0.21	1.09	5.0
4	60.00	0.24	1.80	0.13	0.58	0.34	1.52	5.0
5	80.00	0.26	1.80	0.11	0.71	0.46	1.95	5.0

APPENDIX 2 (continued)

TREMOLITE H^+ VERSUS TIME DATA

BR18 pH 6 (2.4999 g)

Elapsed Time (hr)	Volume H^+ (ml)	Mole/m^2 H^+
0.0	0.0000	0.00×10^{0}
0.6	0.0310	3.01×10^{-6}
1.1	0.0390	3.79×10^{-6}
5.4	0.0640	6.21×10^{-6}
9.9	0.0700	6.80×10^{-6}
33.0	0.0730	7.09×10^{-6}
40.2	0.1430	1.39×10^{-5}
48.1	0.1470	1.43×10^{-5}
57.8	0.1500	1.46×10^{-5}
79.9	0.1510	1.47×10^{-5}
89.9	0.1930	1.87×10^{-5}

BR26 pH 4 (2.4996 g)

Elapsed Time (hr)	Volume H^+ (ml)	Mole/m^2 H^+
0.0	0.0000	0.00×10^{0}
0.5	0.0250	2.43×10^{-5}
1.0	0.0335	3.25×10^{-5}
4.1	0.0425	4.13×10^{-5}
9.5	0.0435	4.22×10^{-5}
33.4	0.0485	4.71×10^{-5}
80.0	0.0485	4.71×10^{-5}

APPENDIX 2 (continued)

BR27 pH 4 (2.5001 g)

Elapsed Time (hr)	Volume H^+ (ml)	Mole/m^2 H^+
0.0	0.0000	$0.00x10^{0}$
0.5	0.0280	$2.72x10^{-5}$
0.9	0.0370	$3.59x10^{-5}$
1.5	0.0410	$3.98x10^{-5}$
2.1	0.0455	$4.42x10^{-5}$
3.2	0.0510	$4.95x10^{-5}$
4.9	0.0575	$5.58x10^{-5}$
5.8	0.0605	$5.87x10^{-5}$
6.9	0.0640	$6.21x10^{-5}$
58.2	0.0650	$6.31x10^{-5}$
80.1	0.0650	$6.31x10^{-5}$

APPENDIX 3

FIRST FLOW-THROUGH REACTOR CONCENTRATIONS

APPENDIX 3
FIRST FLOW-THROUGH REACTOR CONCENTRATIONS

(mg/l) Sample#	Al	Ca	Fe	Mg	Na	Si	Vol (L)
1	0.219	0.000	0.000	0.006	45.4	0.000	0.300
2	0.199	0.000	0.000	0.008	95.8	0.000	0.335
3	0.284	0.000	0.001	0.004	85.3	0.093	0.278
4	0.118	0.000	0.000	0.003	60.0	0.161	0.328
5	0.148	2.100	0.013	0.146	70.4	1.090	0.315
6	0.179	2.300	0.012	0.034	64.8	0.196	0.269
7	0.339	1.600	0.015	0.022	71.8	0.017	0.305
8	0.064	0.700	0.012	0.018	73.0	0.012	0.305
9	0.134	0.300	0.000	0.019	75.7	0.132	0.297
10	0.112	0.100	0.000	0.016	67.3	0.042	0.319
11	0.060	0.100	0.009	0.020	80.5	0.406	0.302
12	0.145	0.100	0.019	0.022	83.0	0.000	0.281
13	0.080	0.070	0.007	0.020	90.8	0.016	0.302
14	0.055	0.070	0.004	0.020	82.2	0.021	0.277
15	0.050	0.090	0.000	0.021	82.8	0.005	0.317
16	0.060	0.090	0.000	0.026	76.3	0.012	0.266
17	0.060	0.080	0.011	0.020	68.3	0.012	0.326
18	0.070	0.070	0.000	0.018	64.6	0.010	0.289
19	0.060	0.030	0.002	0.011	66.7	0.111	0.302
20	0.070	0.050	0.004	0.014	64.0	0.518	0.310
21	0.060	0.050	0.004	0.030	67.7	0.084	0.318
22	0.076	0.060	0.022	0.034	67.0	0.093	0.327
23	0.064	0.070	0.014	0.016	60.9	0.096	0.342
24	0.059	0.080	0.018	0.014	65.9	0.081	0.267
25	0.074	0.030	0.019	0.014	68.6	0.045	0.308
26	0.078	0.010	0.026	0.013	70.4	0.081	0.318
27	0.070	0.020	0.023	0.016	76.6	0.122	0.272
28	0.090	0.020	0.025	0.021	81.9	0.142	0.365
29	0.130	0.020	0.023	0.015	99.0	0.045	0.266
30	0.082	0.059	0.000	0.013	107.0	0.081	0.324
31	0.074	0.050	0.000	0.009	97.2	0.059	0.326
32	0.089	0.043	0.000	0.012	98.1	0.062	0.290
33	0.073	0.045	0.000	0.013	98.5	0.174	0.312
34	0.068	0.046	0.001	0.011	99.5	0.136	0.288
35	0.071	0.048	0.000	0.008	97.1	0.067	0.332
36	0.073	0.051	0.000	0.006	96.8	0.066	0.336
37	0.093	0.069	0.008	0.010	31.0	0.084	0.282
38	0.075	0.032	0.015	0.018	16.9	0.097	0.320
39	0.074	0.028	0.000	0.007	16.5	0.046	0.323
40	0.102	0.031	0.000	0.010	16.4	0.048	0.275
41	0.083	0.026	0.000	0.008	16.8	0.050	0.334
42	0.081	0.232	0.012	0.012	17.8	0.055	0.307
43	0.082	0.230	0.045	0.039	57.1	0.069	0.386

APPENDIX 3 (continued)
FIRST FLOW-THROUGH REACTOR CONCENTRATIONS
(continued)

(mg/l) Sample #	Al	Ca	Fe	Mg	Na	Si	Vol (L)
44	0.093	0.191	0.056	0.026	60.8	0.069	0.258
45	0.098	0.233	0.065	0.021	56.9	0.072	0.150
46	0.077	0.275	0.098	0.060	60.8	0.125	0.296
47	0.085	0.245	0.054	0.018	60.4	--	0.367
48	0.094	0.217	0.051	0.016	63.6	--	0.297
49	0.083	0.212	0.040	0.021	63.0	0.035	0.348
50	0.078	0.215	0.024	0.012	62.9	0.034	0.345
51	0.080	0.007	0.002	0.009	19.8	0.028	0.257
52	0.077	0.007	0.000	0.008	12.3	0.022	0.337
53	0.079	0.007	0.000	0.010	12.2	0.027	0.317
54	0.070	0.006	0.000	0.010	12.6	0.019	0.375
55	0.083	0.007	0.000	0.008	14.6	0.012	0.246
56	0.086	0.028	0.008	0.017	57.0	0.047	0.355
57	0.081	0.019	0.024	0.010	60.1	0.023	0.336
58	0.101	0.024	0.018	0.008	59.5	0.034	0.274
59	0.093	0.021	0.040	0.007	58.8	0.032	0.300
60	0.097	0.026	0.029	0.008	58.8	0.024	0.305
61	0.122	0.039	0.046	0.010	58.1	0.028	0.337
62	0.089	0.032	0.022	0.013	56.7	0.026	0.300
63	0.097	0.006	0.000	0.005	18.8	0.024	0.346
64	0.102	0.010	0.000	0.006	14.0	0.022	0.348
65	0.114	0.011	0.000	0.007	12.6	0.017	0.233
66	0.097	0.004	0.000	0.007	14.8	0.008	0.350
67	0.091	0.008	0.000	0.014	13.7	0.028	0.225
68	0.089	0.009	0.000	0.011	13.2	0.062	0.330
69	0.098	0.020	0.000	0.013	12.9	0.013	0.268
70	0.091	0.013	0.000	0.015	14.4	0.016	0.346
71	0.082	0.014	0.001	0.012	13.2	0.015	0.092
72	0.099	0.023	0.000	0.011	12.7	0.014	0.282
73	0.086	0.039	0.000	0.007	12.0	0.011	0.352
74	0.093	0.074	0.000	0.006	13.9	0.008	0.315
75	0.084	0.057	0.000	0.005	13.1	0.007	0.375
76	0.110	0.022	0.000	0.003	12.4	0.009	0.262
77	0.091	0.013	0.000	0.005	12.0	0.027	0.315
78	0.094	0.013	0.001	0.005	12.0	0.018	0.157

APPENDIX 3 (continued)
SECOND FLOW-THROUGH REACTOR CONCENTRATIONS

(mg/l) Sample #	Al	Ca	Fe	Mg	Na	Si	Vol (L)
1	0.058	0.220	0.006	0.031	0.052	0.134	0.260
2	0.078	0.110	0.018	0.072	0.202	0.178	0.260
3	0.086	0.080	0.012	0.055	0.316	0.228	0.275
4	0.062	0.040	0.016	0.036	0.214	0.157	0.262
5	0.075	0.020	0.006	0.027	0.188	0.126	0.287
6	0.071	0.020	0.004	0.021	0.185	0.080	0.338
7	0.071	0.040	0.028	0.016	0.214	0.051	0.202
8	0.111	0.060	0.000	0.012	0.188	0.052	0.314
9	0.100	0.040	0.004	0.009	0.176	0.056	0.275
10	0.077	0.050	0.001	0.006	0.215	0.045	0.280
11	0.097	0.060	0.005	0.017	0.187	0.165	0.260
12	0.073	0.050	0.000	0.009	0.175	0.030	0.384
13	0.102	0.040	0.000	0.008	0.176	0.056	0.380
14	0.097	0.050	0.000	0.003	0.173	0.025	0.290
15	0.105	0.050	0.000	0.003	0.180	0.030	0.270
16	0.076	0.030	0.000	0.005	0.235	0.023	0.332
17	0.083	0.070	0.037	0.004	0.204	0.045	0.365
18	0.106	0.100	0.042	0.004	0.187	0.053	0.257
19	0.061	0.120	0.016	0.003	0.180	0.055	0.304
20	0.076	0.080	0.009	0.009	0.213	0.041	0.317
21	0.090	0.020	0.000	0.005	0.186	0.000	0.280
22	0.072	0.020	0.000	0.003	0.182	0.000	0.400
23	0.058	0.020	0.000	0.003	0.182	0.027	0.357
24	0.107	0.020	0.000	0.004	0.194	0.044	0.357
25	0.086	0.020	0.006	0.016	0.153	0.053	0.287
26	0.172	0.030	0.003	0.028	0.225	0.064	0.106
27	0.090	0.020	0.019	0.019	0.163	0.064	0.195
28	0.101	0.030	0.006	0.018	0.211	0.089	0.215
29	0.081	0.020	0.013	0.006	3.670	0.040	0.112
30	0.131	0.020	0.016	0.003	0.159	0.073	0.178
31	0.151	0.010	0.021	0.007	0.214	0.017	0.142
32	0.095	0.030	0.034	0.008	0.209	0.000	0.117
33	0.093	0.010	0.026	0.007	0.219	0.000	0.210
34	0.112	0.000	0.025	0.005	0.170	0.039	0.175
35	0.100	0.000	0.042	0.005	0.137	0.004	0.153
36	0.100	0.000	0.034	0.006	0.135	0.033	0.143
37	0.098	0.060	0.097	0.003	0.178	0.061	0.195
38	0.145	0.130	0.083	0.039	0.236	0.157	0.122
39	0.132	0.270	0.084	0.089	0.318	0.407	0.100
40	0.135	0.170	0.029	0.103	0.495	0.196	0.208
41	0.139	0.170	0.028	0.104	0.518	0.587	0.127
42	0.129	0.170	0.028	0.102	0.513	0.396	0.190
43	0.076	0.070	0.016	0.043	0.303	0.337	0.110

APPENDIX 3 (continued)
SECOND FLOW-THROUGH REACTOR CONCENTRATIONS
(continued)

(mg/l) Sample #	Al	Ca	Fe	Mg	Na	Si	Vol (L)
44	0.139	0.010	0.012	0.008	0.229	0.048	0.147
45	0.145	0.020	0.013	0.003	0.238	0.035	0.154
46	0.102	0.020	0.000	0.002	0.260	0.116	0.150
47	0.066	0.010	0.003	0.000	0.263	0.039	0.190
48	0.095	0.010	0.005	0.000	0.851	0.139	0.197
49	0.095	0.010	0.006	0.001	0.250	0.034	0.222
50	0.113	0.050	0.004	0.001	0.237	0.052	0.134
51	0.128	0.020	0.000	0.000	0.213	0.034	0.174
52	0.113	0.010	0.000	0.002	0.214	0.034	0.184
53	0.000	0.000	0.000	0.000	0.066	0.025	0.550
54	0.106	0.040	0.007	0.001	0.428	0.148	0.563
55	0.104	0.020	0.008	0.009	0.284	0.314	0.380
56	0.107	0.000	0.009	0.003	0.235	0.239	0.328
57	0.182	0.060	0.023	0.011	0.687	0.132	0.397
58	0.083	0.030	0.015	0.002	0.239	0.087	0.372
59	0.114	0.030	0.004	0.003	0.337	0.072	0.375
60	0.138	0.050	0.000	0.006	0.430	0.068	0.371
61	0.084	0.000	0.000	0.001	0.204	0.064	0.355
62	0.084	0.000	0.000	0.001	0.201	0.066	0.375
63	0.097	0.000	0.010	0.000	0.201	0.000	0.383
64	0.090	0.000	0.008	0.000	0.180	0.000	0.398
65	0.096	0.000	0.008	0.000	0.177	0.000	0.350
66	0.099	0.000	0.000	0.000	0.198	0.059	0.400
67	0.168	0.010	0.000	0.001	0.657	0.156	0.368
68	0.103	0.000	0.004	0.000	0.196	0.059	0.370
69	0.126	0.010	0.001	0.000	0.223	0.049	0.180
70	0.089	0.040	0.009	0.000	0.229	0.059	0.298
71	0.091	0.070	0.009	0.000	0.229	0.059	0.295
72	0.082	0.040	0.006	0.012	0.220	0.059	0.353
73	0.088	0.010	0.000	0.000	0.213	0.049	0.349
74	0.083	0.010	0.000	0.000	0.209	0.049	0.355
75	0.083	0.000	0.000	0.000	0.234	0.039	0.346
76	0.083	0.000	0.000	0.000	0.219	0.117	0.350
77	0.082	0.000	0.000	0.000	0.201	0.078	0.354
78	0.079	0.000	0.000	0.000	0.203	0.039	0.367

APPENDIX 4

COMPUTER MODEL PARAMETERS

APPENDIX 4

COMPUTER MODEL PARAMETERS[1]

Temperature 25°C

Hornblende flow-through reactor concentrations (mg/l)

	pH 9		pH 7		pH 6	
	High	Low	High	Low	High	Low
Al	0.090	0.070	0.100	0.070	0.100	0.084
Ca	0.060	0.010	0.030	0.007	0.074	0.013
Fe	0.020	0.004	0.015	0.002	0.001	0.001
Mg	0.020	0.010	0.010	0.008	0.015	0.003
Na	100.0	60.0	17.0	12.0	14.4	12.0
Si	0.120	0.060	0.090	0.030	0.027	0.008

Tremolite flow-through reactor concentrations (mg/l)

	pH 9		pH 7		pH 6	
	High	Low	High	Low	High	Low
Al	0.070	0.020	0.140	0.050	0.060	0.040
Ca	0.120	0.020	0.160	0.010	0.070	0.010
Fe	0.040	0.010	0.080	0.010	0.010	0.006
Mg	0.070	0.004	0.080	0.020	0.010	0.000
Na	0.030	0.010	0.050	0.010	0.000	0.000
Si	0.150	0.020	0.070	0.020	0.040	0.060

Hornblende batch reactor concentrations (mg/l)

	pH 4		pH 5		pH 6	
	High	Low	High	Low	High	Low
Al	0.30	0.10	0.30	0.02	0.03	0.14
Ca	6.90	0.20	8.00	1.50	7.00	1.10
Fe	3.40	0.10	2.70	0.10	1.40	0.04
Mg	1.00	0.20	0.90	0.20	2.00	0.24
Na	1.50	0.40	1.30	0.50	2.60	0.35
Si	2.00	0.10	2.80	0.20	8.00	0.80

[1] Cl^- was used to maintain charge balance

APPENDIX 4 (continued)

COMPUTER MODEL PARAMETERS[1]

Temperature 25^{0}C

Tremolite batch reactor concentrations (mg/l)

	pH 4	
	High	Low
Al	0.30	0.13
Ca	2.00	0.70
Fe	0.20	0.05
Mg	0.70	0.35
Na	0.85	0.20
Si	2.00	0.40

[1] Cl^- was used to maintain charge balance

LIST OF REFERENCES

Anand, R.R., and Gilkes, R.J. (1984). Weathering of hornblende, plagioclase, and chlorite in meta-dolerite, Australia. *Geoderma*, 34, 261-280.

Bales, R.B. (1993). Personal Communication, Dept. of Hydrology and Water Resources, The University of Arizona, Tucson, Arizona.

Ball, J.W., and Nordstrom, D.K. (1991). User's Manual for WATEQ4F, with Revised Thermodynamic Data Base and Test Cases for Calculating Speciation of Major, Trace, and Redox Elements in Natural Waters, U.S. Geological Survey Open-File Report 91-183, Menlo Park, California.

Barnes, R.B. (1975). The determination of specific forms of Al in natural waters. *Chemical Geology*, 15, 177-191.

Berner, R.A., and Schott, J. (1982). Mechanism of pyroxene and amphibole weathering II. observations of soil grains. *American Journal of Science*, 282, 1214-1231.

Berner, R.A., Sjoberg, E.L., Velbel, M.A., and Krom, M.D. (1979). Dissolution of pyroxenes and amphiboles during weathering. *Science*, 207, 1205-1207.

Blackburn, W.H., and Dennen, W.H. (1988). Principles of Mineralogy. Dubuque, Iowa: Wm. C. Brown Publishers.

Breeman, V., Mulder, N.J., and Driscoll, C.T. (1986). Acidification and alkalinization of soils. In J. A. Kittrick (Ed.), Soil Mineral Weathering, 139-164. New York: Van Nostrand Reinhold.

Busenberg, E., and Clemency, C.V. (1976). The dissolution kinetics of feldspars at 25°C and 1 atm CO_2 partial pressure. *Geochimica et Cosmochimica Acta*, 40, 41-50.

Casey, W. H., and Sposito, G. (1992). On the temperature dependence of mineral dissolution rates. *Geochimica et Cosmochimica Acta*, 56, 3825-3830.

Chou, L., and Wollast, R. (1985). Steady-state kinetics and dissolution mechanisms of albite. *American Journal of Science*, 285, 963-993.

Cremeens, D. L., Norton, L. D., Darmody, R. G., and Jansen, I. J. (1988). Etch-pit measurements on scanning electron micrographs of weathered grain surfaces. *Soil Science Society of America Journal*, 52, 883-885.

De Kimpe, C. R., Miles, N., and Carson, D. (1989). Stability of Fe^{2+} bearing minerals during oxidation pretreatment for soil analysis. *Canadian Journal of Soil Science*, 69, 433-436.

Drever, J. (1988). The Geochemistry of Natural Waters, 388, Prentice-Hall Inc., Englewood Cliffs, N.J.

Drever, J. (1992). Phone communication.

Drever, J., and Swoboda-Colberg, N. (1989). Mineral weathering rates in acid-sensitive catchments: extrapolation of laboratory experiments to the field. In D. L. Miles (Ed.), Proceedings of the 6th International Symposium on Water-Rock Interaction, WRI-6, 211-214. Rotterdam/Brookfield: A.A. Balkema.

Eggleton, R.A., and Boland, J.N. (1982). The weathering of enstatite, *Clays and Clay Minerals*, 46, 240-282.

Eggleton, R.A., and Buseck, P.R. (1986). High Resolution Electron Microscopy of Feldspar Weathering. In J. A. Kittrick (Ed.), Soil Mineral Weathering, 165-175. New York: Van Nostrand Reinhold.

Fleer, U.N. (1982). The dissolution kinetics of anorthite and in aqueous solutions at temperatures below 100°C. Ph.D., Penn State University.

Franson, M.A.H. (Eds.). (1985). Standard Methods for the Examination of Water and Wastewater, 16. Washington, D.C.: American Public Health Association.

Freeze, A.R., and Cherry, J.A. (1979). Chemical properties and principles. Groundwater, 80-139. Englewood Cliffs, New Jersey: Prentice-Hall, Inc.

Furrer, G., and Stumm, W. (1986). The coordination chemistry of weathering: I. dissolution kinetics of δ-Al_2O_3 and BeO. *Geochimica et Cosmochimica Acta*, 50, 1847-1860.

Garrels, R.M. (1986). Some Free Energy Values from Geologic Relations. In J.A. Kittrick (Ed.), Soil Mineral Weathering, 176-187. New York: Van Nostrand Reinhold.

Goldstein, J.I., Newbury, D.E., Echlin, P., Joy, D.C., Fiori, C., and Lifshin, E. (1984). Scanning Electron Microscopy and X-Ray Microanalysis--A Text for Biologists, Materials Scientists, And Geologists. New York, London: Plenum Press.

Goodman, B.A., and Wilson, M.J. (1975). A Mossbauer Study of the Weathering of Hornblende. *Clay Minerals*, 11, 153-163.

Grandstaff, D.E. (1980). The dissolution rate of forsterite olivine from Hawaiian beach sand. Third Int. Symp. on Water--Rock Inter. Proceedings, 72-74. Edmonton: Alberta Res. Council.

Hem, J.D., and Roberson, C.E. (1967). Form and stability of aluminum hydroxide complexes in dilute solution. United States Geological Survey Water Supply Paper, 1827-A, 1-55.

Hendricks, S.B., and Fry, W.H. (1986). The Results of X-Ray and Microscopical Examinations of Soil Colloids. In J.A. Kittrick (Ed.), Soil Mineral Weathering, 9-29. New York: Van Nostrand Reinhold.

Henriksen, A. (1981). Susceptibility of Surface Waters to Acidification. In R. E. Johnson (Ed.), International Symposium on Acidic Precipitation and Fishery Impacts in Northeastern North America, 103-121. Cornell University, Ithaca, New York: Northeastern Division American Fisheries Society.

Hiskey, B. (1992). Personal communication.

Holdren, G.R., Jr. and Berner, R.A. (1979). Mechanisms of feldspar weathering. *Geochimica et Cosmochimica Acta*, 43, 1161-1171.

Holdren, G.R., Jr., and Speyer, P.M. (1985). Reaction rate-surface area relationships during the early stages of weathering: I. initial observations. *Geochimica et Cosmochimica Acta*, 49, 675-681.

Hopkins, E.E. (1989). Characterization of the Dissolution of Hornblende with Application to Natural Waters. M.S. Thesis, The University of Arizona.

Kenoyer, G.J., and Bowser, C.J. (1992). Groundwater Chemical Evolution in a Sandy Silicate Aquifer in Northern Wisconsin: 1. Patterns and Rates of Change. *Water Resources Research*, 28, 579-589.

Kenoyer, G.J., and Bowser, C.J. (1992). Groundwater Chemical Evolution in a Sandy Silicate Aquifer in Northern Wisconsin: 2. Reaction Modeling. *Water Resources Research*, 28, 591-600.

Kirchner, J.W., Dillon, P.J., and LaZerte, B.D. (1992). Predicted response of stream chemistry to acid loading tested in Canadian catchments. *Nature*, 358, 478-482.

Kittrick, J.A. (Eds.). (1986). Soil Mineral Weathering. New York: Van Nostrand Reinhold.

Kostov, I. (1968). Mineralogy. Edinburgh and London: Oliver and Boyd.

Lasaga, A.C. (1984). Chemical kinetics of water-rock interactions. *Journal of Geophysical Research*, 89, 4009-4025.

Lasaga, A.C., and Kirkpatrick, R.J. (Eds.). (1981). Kinetics of Geochemical Processes. Chelsea, Michigan: Mineralogical Society of America.

Lin, C.F., and Benjamin, M.M. (1990). Dissolution Kinetics of Minerals in the Presence of Sorbing and Complexing Ligands. *Environmental Science Technology*, 24, 126-134.

Lin, F., and Clemency, L.V. (1981). The kinetics of dissolution of muscovites at 25°C and 1 atm CO_2 partial pressure. *Geochimica et Cosmochimica Acta*, 45, 571-576.

Mariner, P. (1991). The effects of humic substances on transport of Cu (III) in ground water. M.S. Thesis, The University of Arizona.

Mast, A., Drever, J., and Baron, J. (1990). Chemical Weathering in the Loch Vale Watershed, Rocky Mountain National Park, Colorado. *Water Resources Research*, 26, 2971-2978.

Mast, A.M., and Drever, J. (1987). The effect of oxalate on the dissolution rates of oligoclase and tremolite. *Geochimica et Cosmochimica Acta*, 51, 2559-2568.

Murphy, W.M., and Helgeson, H.C. (1987). Thermodynamic and kinetic constraints on reaction rates among minerals and aqueous solutions. III. activated complexes and the pH-dependence of the rates of feldspar, pyroxene, wollastonite, and olivine hydrolysis. *Geochimica et Cosmochimica Acta*, 51, 3137-3153.

Norton, S.A. (1981). The Effects of Acidification on the Chemistry of Ground and Surface Waters. In R.E. Johnson (Ed.), International Symposium on Acidic Precipitation and Fishery Impacts in Northeastern North America, 93-102. Cornell University, Ithaca, New York: Northeastern Division American Fisheries Society.

Petrovich, R., (1981). Kinetics of dissolution of mechanically comminuted rock-forming oxides and silicates in the laboratory and at the Earth's surface, *Geochimica et Cosmochimica Acta*, 44, 1675-1686.

Plummer, C.C., and McGeary, D. (1983). Physical Geology (2nd ed.). Dubuque, Iowa: Wm. C. Brown Publishers.

Rashid, M.A., and Leonard, J.D. (1973). Modifications in the solubility and precipitation behavior of various metals as a result of their interaction with sedimentary humic acid. *Chemical Geology*, (11), 89-97.

Rimstadt, J.D., and Barnes, H. (1980). The kinetics of silica-water reactions. *Geochimica et Cosmochimica Acta*, 44, 1683-1699.

Roberts, W.L., Rapp, R.R., and Weber, J. (1974). Encyclopedia of Minerals. New York: Van Nostrand Reinhold.

Rosler, H.J., and Lange, H. (1972). Geochemical Tables. 273-276. New York: Elsevier Publishing Co.

Schott, J., and Berner, R. (1983). X-ray photoelectron studies of the mechanism of iron silicate dissolution during weathering. *Geochimica et Cosmochimica Acta*, 47, 2233-2240.

Schott, J., Berner, R.A., and Sjoberg, E.L. (1981). Mechanism of pyroxene and amphibole weathering: I. experimental studies of iron-free minerals. *Geochimica et Cosmochimica Acta*, 45, 2123-2135.

Siever, R., and Woodford, N. (1979). Dissolution kinetics and the weathering of mafic minerals. *Geochimica et Cosmochimica Acta*, 43, 717-724.

Spencer, H.T. (1981). Acid rain chemodynamics. In R.E. Johnson (Ed.), International Symposium on Acidic Precipitation and Fishery Impacts in Northeastern North American, 33-41. Cornell University, Ithaca, New York: Northeastern Division American Fisheries Society.

Sposito, G. (1989). The Chemistry of Soils. New York: Oxford University Press, Inc.

Sposito, G. (1989). The Environmental Chemistry of Aluminum. Boca Raton, Florida: CRC Press.

Steefel, C.I., and Cappellen, P.V. (1990). A new kinetic approach to modeling water-rock interaction: the role of nucleation, precursors, and Ostwald ripening. *Geochimica et Cosmochimica Acta*, 54, 2657-2677.

Stumm, W., and Wollast, R. (1990). Coordination chemistry of weathering: kinetics of the surface-controlled dissolution of oxide minerals. American Geophysical Union, 28, 53-69.

Sung, W., and Morgan, J.J. (1980). Kinetics and Product of Ferrous Iron Oxygenation in Aqueous Systems. *American Chemical Society*, 14, 561-568.

Swoboda-Colberg, N.G., and Drever, J.J. (1992). Mineral dissolution rates: a comparison of laboratory and field studies. In Y.K. Kharaka and A.S. Maest (Ed.), Proceedings of the 7th International Symposium on Water-Rock Interaction, WRI-7, 115-118. Rotterdam/Brookfield: A.A. Balkema.

Velbel, M. A. (1990). Influence of temperature and mineral surface characteristics on feldspar weathering rates in natural and artificial systems: a first approximation. *Water Resources Research*, 26, 3049-3053.

Waite, D.T., Wrigley, I.C., and Szymczak, R. (1988). Photo-assisted dissolution of a colloidal manganese oxide in the presence of fulvic acid. *Environmental Science and Technology*, 22, 778-785.

Westall, J.C., Zachary, J.L., and Morel, F.M. (1976). MINEQL, A Computer Program for the Calculation of the Chemical Equilibrium Composition of Aqueous Solutions, Tech. Note 18, Dept. of Civil Engineering, Massachusetts Institute of Technology, Cambridge, Massachusetts.

White, A.F., and Peterson, M.L. (1990). Role of reactive surface area characterization in geochemical models. In Melchoir, D.C., and Bassett, R.L. (Eds.). (1990). Chemical Modeling of Aqueous Systems II. Washington, DC: American Chemical Society.

Wilson, M.J. (1970). A study of weathering in a soil derived from a biotite-hornblende rock. *Clay Minerals*, 8, 291-303.

Wolford, R.A. (1992). Integrated Hydrochemical Modeling of an Alpine Watershed: Sierra Nevada, California, Dept. of Hydrology and Water Resources Publication HWR 92-040, The University of Arizona, Tucson, Arizona.

Zinder, B., Furrer, G., and Stumm, W. (1986). The coordination chemistry of weathering: II. Dissolution of Fe (III) oxides. *Geochimica et Cosmochimica Acta*, 50, 1861-1869.